THE DEVELOPMENT OF INTERMEDIATE-SCALE DISTURBANCES IN COLD AIR OUTBREAKS

by

Douglas Anthony Mansfield

Department of Meteorology
Imperial College

A Thesis submitted for the
Degree of Doctor of Philosophy
in the University of London

1972

ABSTRACT

This study of the formation of intermediate-scale disturbances in cold air outbreaks over the northeast Atlantic provides more discriminating criteria for their development than previously available.

Various mechanisms for the concentration of vorticity on this scale are investigated by considering the small amplitude phase of the disturbances. Linearised perturbation models show that only the baroclinic mechanism can explain their initial evolution.

A case study shows how two such disturbances developed in an area of low level baroclinity formed by the warming of cold air flowing over the strong gradient of sea-surface temperature north and west of Iceland. The growth-rate, wavelength and phase speed of these lows are very close to the predictions of the baroclinic theory. This baroclinity is likely to be present in all cold air outbreaks.

Surface friction is shown to have a very important effect, strong surface winds enhancing the friction and severely reducing the growth-rate. Heating from the sea-surface also reduces the growth-rate when the air flow is approximately parallel to the sea isotherms.

It is concluded that these lows will develop only when surface winds are light and where the air flow is not parallel to the sea isotherms, thus explaining their rarity compared to cold air outbreaks.

LIST OF CONTENTS

page

CHAPTER I Introduction 4

CHAPTER II Mechanisms for the concentration of vorticity

2.1 Introduction 15
2.2 Differential heating 16
2.21 Heating of a flow perpendicular to sea isotherms 17
2.22 Heating due to sea temperature anomalies 17
2.23 Heating of a flow parallel to sea isotherms 18
2.3 Horizontal shearing instability 22
2.4 Baroclinic instability 26
2.5 Orographic effects 29
2.6 The effect of the release of latent heat 33

CHAPTER III The effect of surface friction on the baroclinic motion

3.1 The unperturbed flow 36
3.2 The frictionless wave 38
3.3 The parameterisation of friction 41
3.31 The surface drag law 42
3.32 The two-layer model 49
3.4 The effect on the structure of the wave 52

CHAPTER IV The effect of surface heating

4.1 Introduction 58
4.2 A model of the heating of cold air over the sea 58
4.3 Comparison of the model with a Norwegian sea trajectory 62
4.31 Errors in estimating the warming 65
4.4 The production of the baroclinic zone 68
4.5 Heating included in the baroclinic model 71
4.6 The effect of friction and heating 75

CHAPTER V Comparison of the model with the case study of December 1967

5.1 The data 78
5.11 Upper air data 78
5.12 Surface data 79
5.13 Surface winds 79
5.14 The surface pressure field 81
5.2 The pressure perturbation 85
5.3 The time-section at OWS I 89
5.4 The mature stage 91
5.5 Some statistics of polar low formation 94
5.6 Summary 97

REFERENCES 110

ACKNOWLEDGEMENTS 112

CHAPTER I Introduction

During cold air outbreaks over the northeast Atlantic, disturbances with a wavelength of about 1000 km occasionally form and move southwards towards the British Isles. Because of their small extent they are not easily detected by the sparse network of observing stations to the north and west of Britain and by the time they are recognised as significant features they are usually already crossing the country. These disturbances are predicted only as a general likelihood of the formation of 'minor troughs', although the lows occur much less frequently than the outbreaks of cold air. Since they occur in winter months the associated precipitation is in the form of snow and the sudden onset of this often intense snowfall can cause considerable disruption, especially to transport services. Two particularly vigorous disturbances occurred in December 1967 and gave rise to some discussion. Stevenson (1968) and Harrold and Browning (1969) carried out a detailed study of the air motion and weather associated with these lows as they crossed the British Isles. In this thesis the formation stage of the disturbances is studied, including a case study of the occasion mentioned above with the object of obtaining more discriminating criteria for their development. Although the first disturbance of December 1967 was recognised as a low near OWS 'India' on a forecast issued at 1635 Z on the 7th it was not until 2235 Z that snow was forecast for Northern Ireland, Wales and central southern England, by which time it was already snowing in Northern Ireland and Wales was given only 2 hours warning of a period of snow in which 2-3 inches of snow fell in a period of about 4 hours. The previous bulletin forecast the low to move across southern Scotland and northern England and anticipated

only an increase in the frequency of showers. Application of the theory developed here would have predicted the low to move with about the 900 mb wind which is very close to the observed track and therefore at least 4 more hours warning of the onset of the snow given. Although it cannot predict exactly when a low will form the theory defines more accurately the conditions under which significant development can be expected. If special attention is paid to the data from near Iceland when these conditions are satisfied the lows could be detected earlier and hence more time would be available for the track and intensity of the lows to be established.

These disturbances are conveniently referred to as 'polar lows'. However at least two essentially different types of system have been given this name. Polar lows, as the term is used in this work, are essentially shallow disturbances growing entirely within a polar air-stream. This immediately excludes two types of system which initially appear similar on surface pressure charts. Small surface lows associated with upper air troughs have been called polar lows (e.g. Harley (1960), Suttie (1970)). (In the latter case the upper flow is not discussed but the British Daily Aerological Reports show the associated trough at 500 mb.) Small and weak depressions form in the baroclinic region marking the edge of the polar air south of Greenland and initially appear similar to polar lows but the former develop in an area of large scale baroclinity and soon are seen to extend in depth and extent as normal mid-latitude cyclones.

In Chapter II several possible mechanisms for the formation of polar lows are investigated, all of which apply to disturbances growing in the lowest 2-3 km of the atmosphere. The shallow

nature of these lows is very important because the dissipating effect of surface friction is much greater than for deep systems and we shall show that it plays a major role in determining whether or not polar lows develop. As the lows are only just resolved by the surface observations, any associated disturbance could remain unresolved at higher levels where there is less data. It is appropriate, therefore, to first establish their shallow nature.

Harrold and Browning (1969) observed a pressure perturbation up to 9 km at Pershore (central England) during the passage of the second low of December 1967, and suggested that a high level disturbance may contribute towards the growth of intense polar lows. This is likely to be true; the coincidence of the surface low and an upper cold trough would decrease the stability and enhance the convection which otherwise would be dying out over land thus explaining the abnormally large snowfall associated with the second low over southern England, and not experienced with the passage of the first low. However, the actual sequence of events shows that at least on this occasion the upper trough and the surface low had entirely separate origins. Two troughs at 500 mb which were not detectable at the surface moved southwards from Jan Mayen and OWS 'Mike' and the second of these coincided with the second polar low over southern Britain. Figs.1.1 - 1.4 show the 500 mb height field (thick lines) and the surface pressure (thin lines). The first and second surface lows and upper troughs are labelled L_1, L_2, T_1 and T_2 respectively. Fig.1.5 shows the motion of these disturbances, clearly indicating their separate origins.

An investigation of the heights of pressure surfaces above OWS I shows that in the developing stage both of the lows are

confined to heights below 3 km. Isopleths of the deviation from the average height over the period 12Z 6 Dec - 00Z 9 Dec, of each pressure surface have been plotted on a height-time section (Fig.1.6). Assuming the disturbance to be steadily advected past the station the components of the wind perpendicular to the track of the low can be used to give the gradient of the height field, assuming geostrophic balance. This is used to increase the resolution of the 12 hourly height data enabling the scale of polar lows to be resolved. Clearly the disturbances associated with the surface lows extend only to 700 mb and the upper troughs mentioned above can have played no part in the development phase of these lows.

In Chapter II models of various mechanisms for the concentration of vorticity on the scale of polar lows are developed. Because of the complexity of the processes governing the motion of the atmosphere many simplifications have to be made when developing models. While the disturbance is of small amplitude, the equations can be linearised by considering small perturbations of a mean flow. The perturbation theory is used to show that only the baroclinic mechanism is capable of describing their initial evolution and this theory predicts wavelength, growth-rates and phase speeds which agree very well with the observed systems. In Chapters III and IV the baroclinic theory is treated in more detail and the effect of surface friction and heating examined. Chapter V compares the results with the case study.

This theory of shallow baroclinic wave could also be usefully applied in other areas. Easterly waves may initially develop as waves in the shallow region of reversed N-S temperature gradient in the low latitude easterlies, friction would again be important and the effect of the release of latent heat due

to convergence and ascent would soon become important. Small but intense cyclones which develop in the Gulf of Genoa may also originate in the strongly baroclinic region formed when cold air flows over the warm Mediterranean. Again because of the warmer ocean the effect of latent heat release would be more important than in polar lows.

Figs. 1.1 - 1.4 show the 500 mb height field and surface pressure field at 12 hourly intervals. The 1st and 2nd surface lows and upper troughs are indicated by the labels L_1, L_2, T_1 and T_2 respectively.

FIG. 1.1

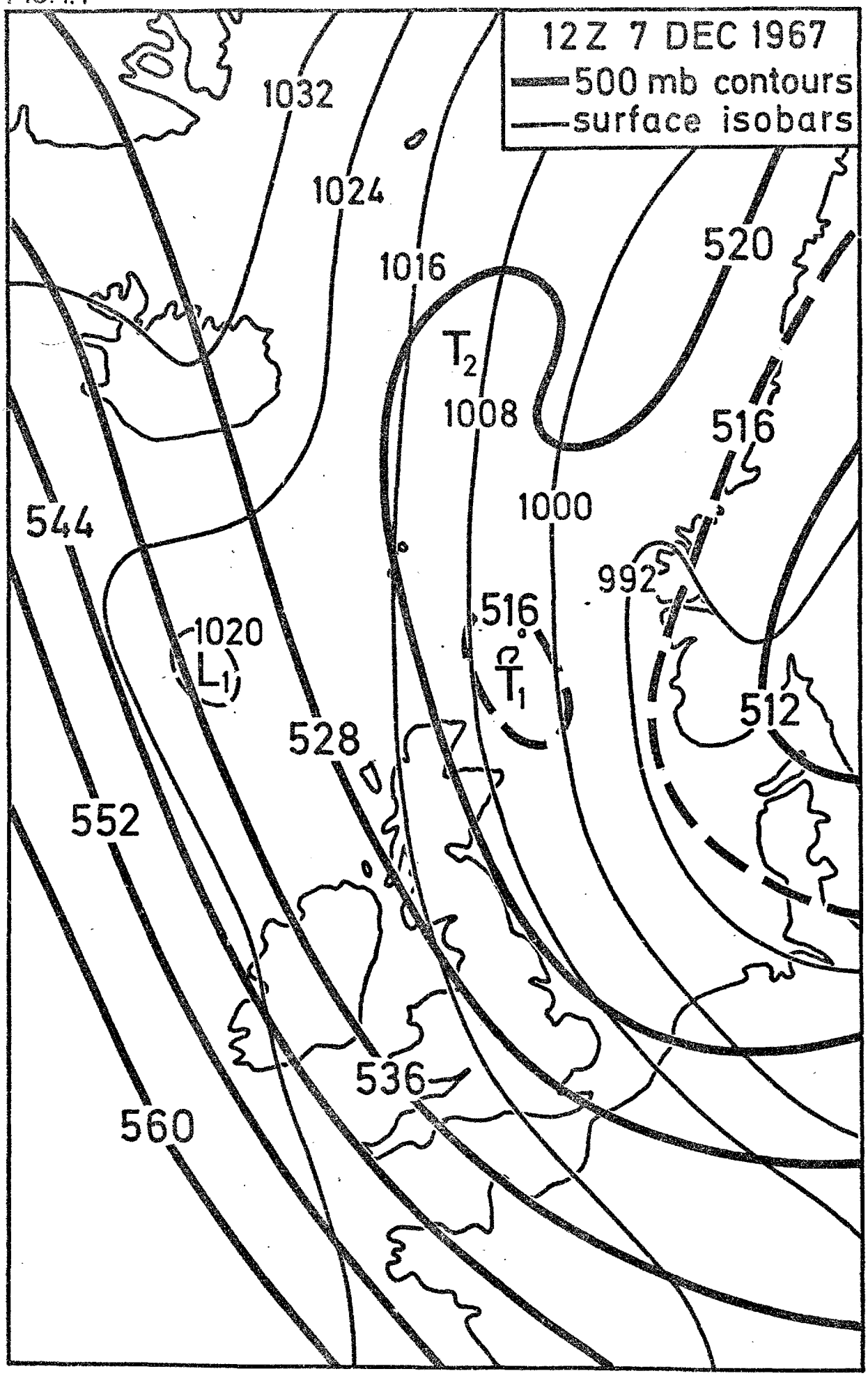

12Z 7 DEC 1967
500 mb contours
surface isobars
1032
1024
1016
1008
1000
992
520
516
516
512
544
552
528
536
560
1020
L1
T2
T1

FIG.1.2

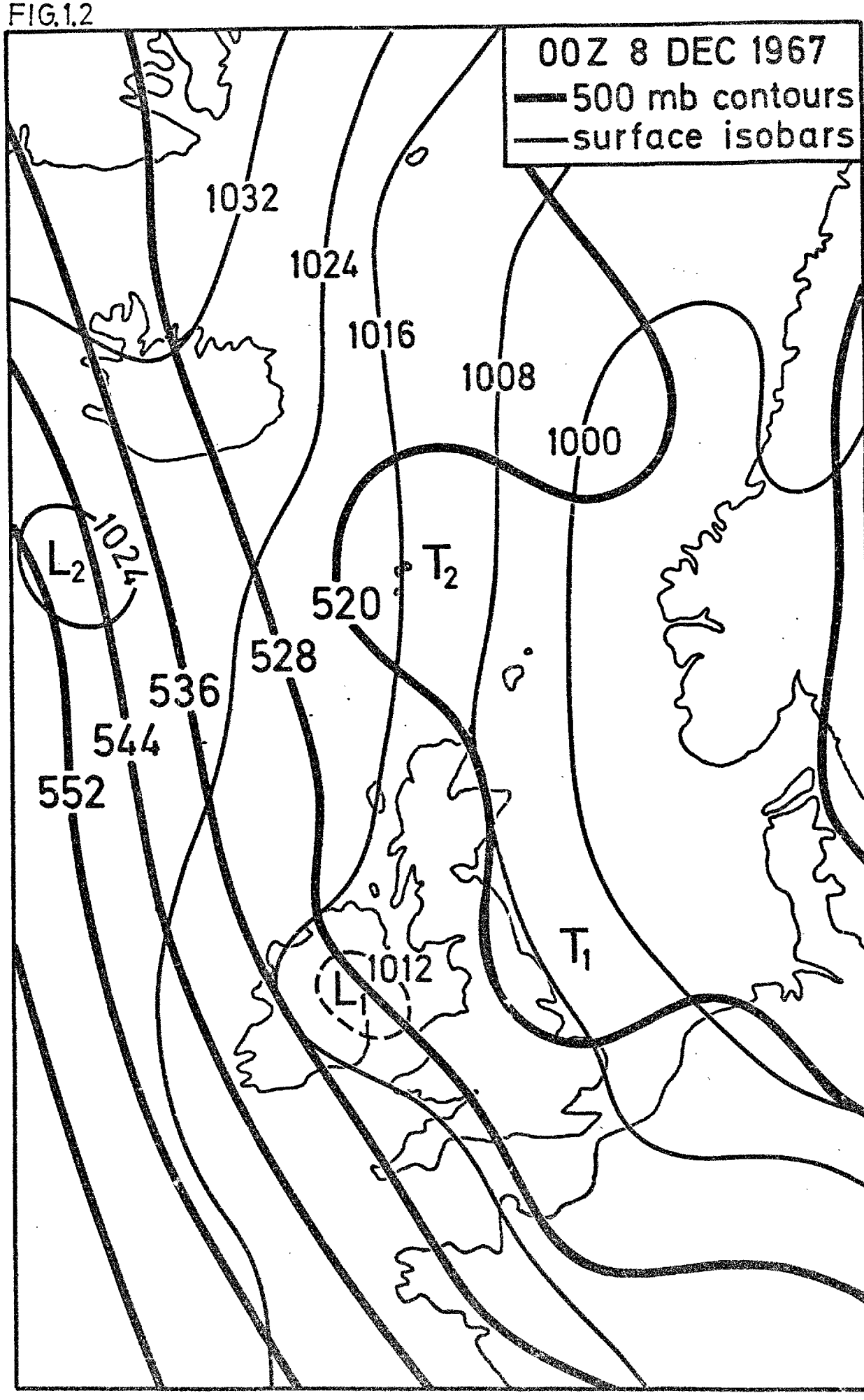

00Z 8 DEC 1967
500 mb contours
surface isobars
1032
1024
1016
1008
1000
L2
1025
520
T2
528
536
544
552
1012
L1
T1

FIG. 1.3

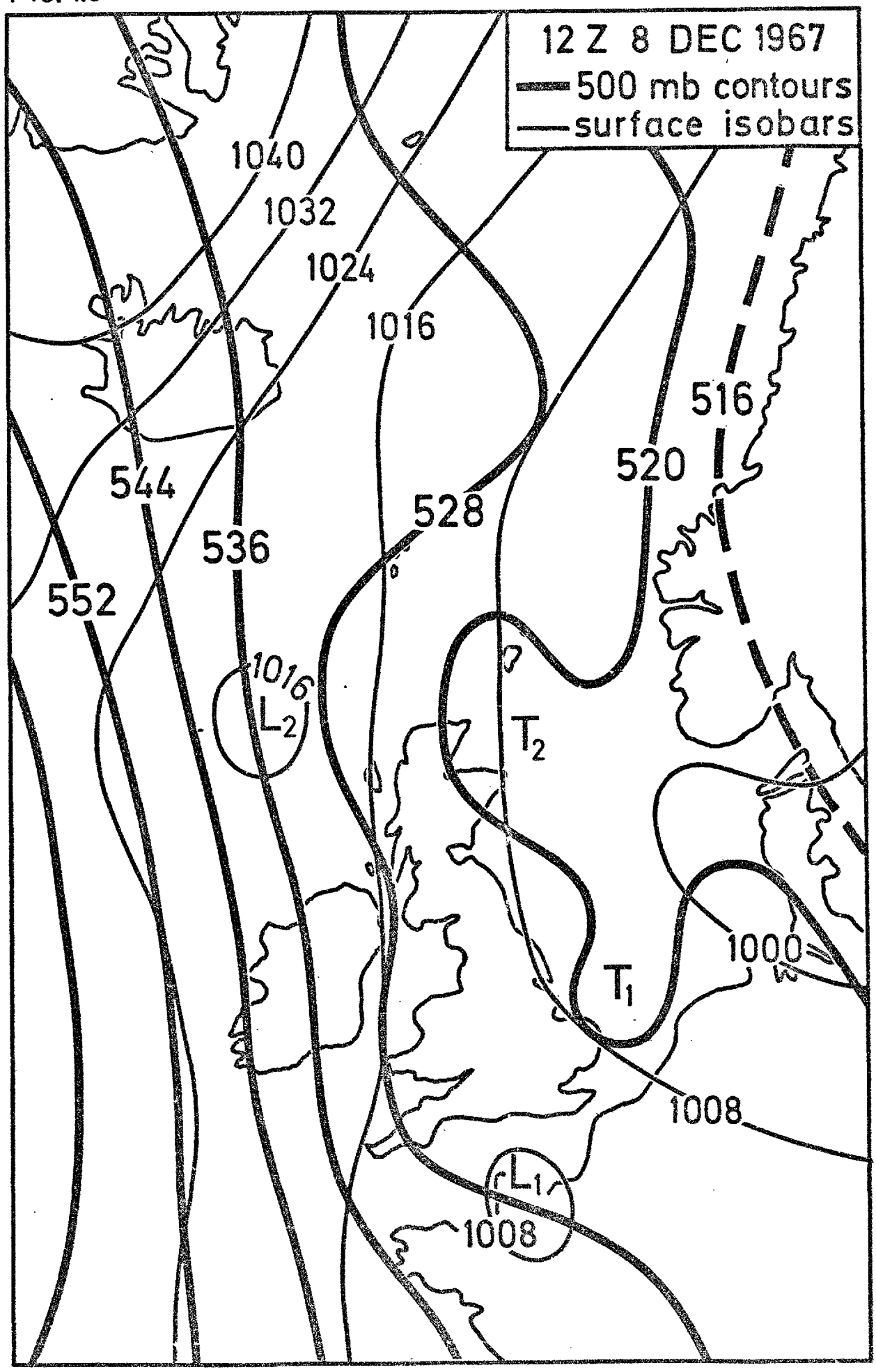
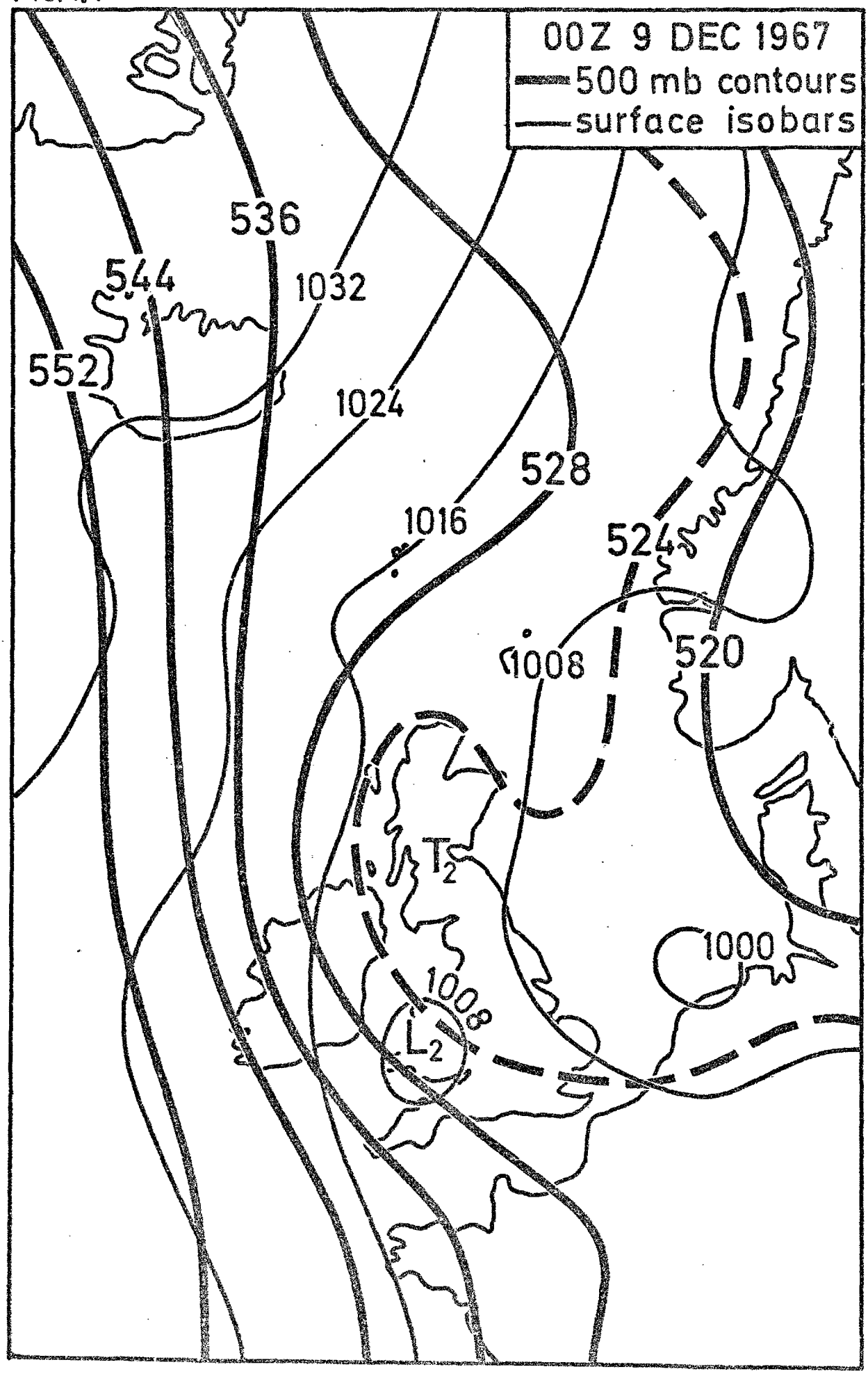

12 Z 8 DEC 1967
500 mb contours
surface isobars
1040
1032
1024
1016
516
520
544
528
536
552
1016
L2
T2
T1
1000
1008
L1
1008

FIG. 1.4


00Z 9 DEC 1967
500 mb contours
surface isobars
536
544
1032
552
1024
528
1016
524
1008
520
T_2
1000
1008
L_2

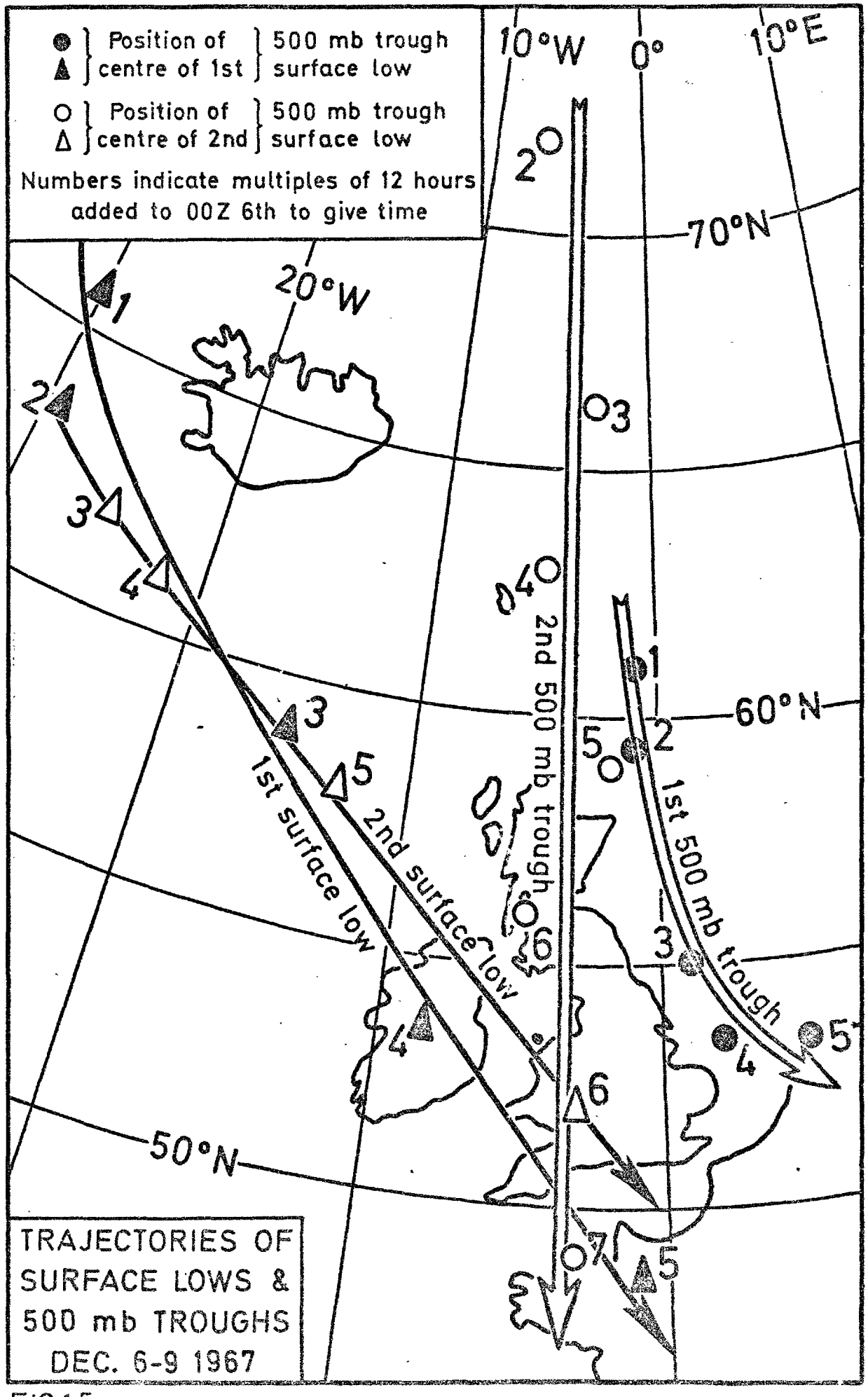
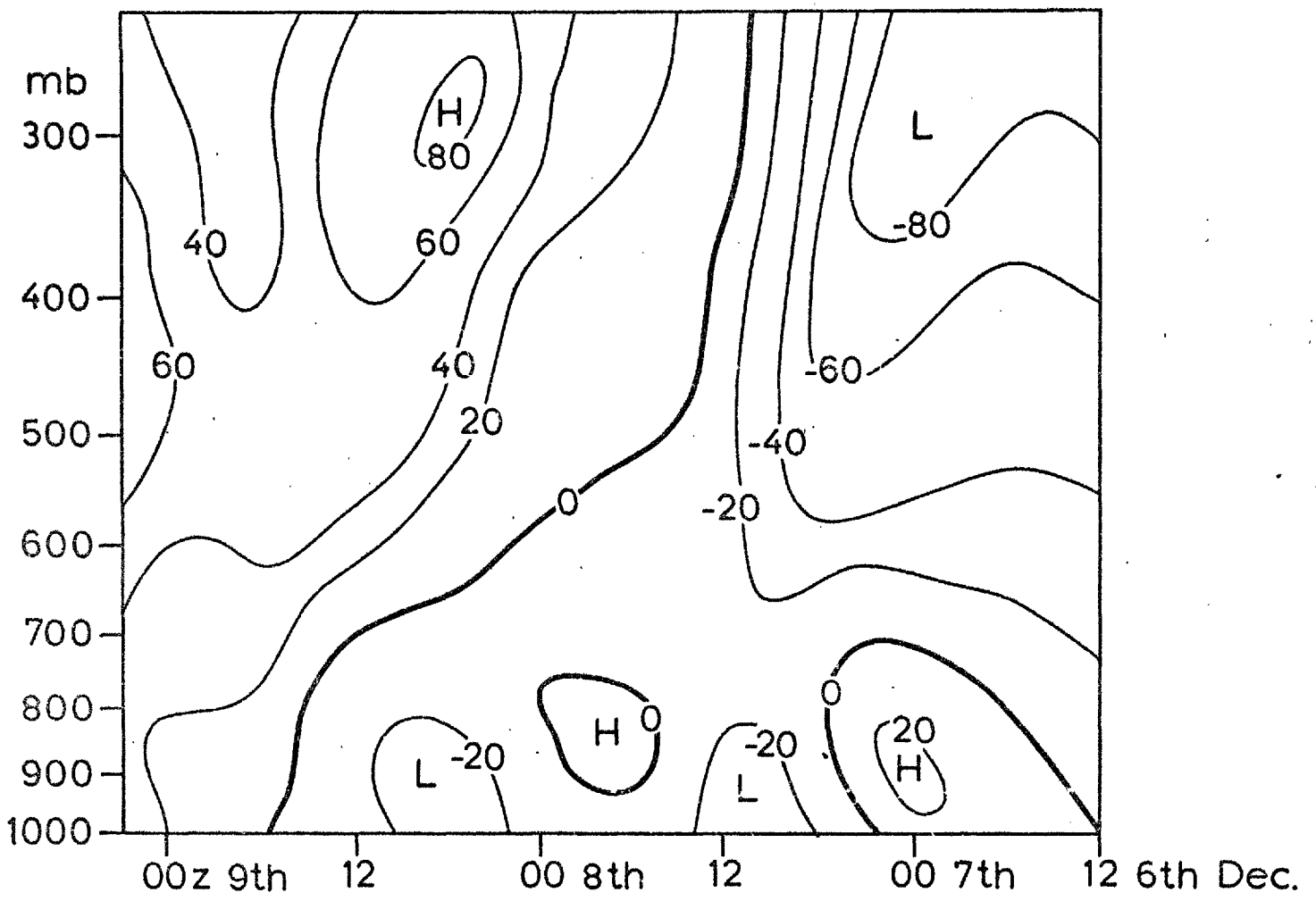

● } Position of } 500 mb trough
▲ } centre of 1st } surface low
○ } Position of } 500 mb trough
△ } centre of 2nd } surface low
Numbers indicate multiples of 12 hours added to 00Z 6th to give time
10°W
0°
10°E
70°N
60°N
50°N
20°W
1st surface low
2nd surface low
2nd 500 mb trough
1st 500 mb trough
TRAJECTORIES OF SURFACE LOWS & 500 mb TROUGHS DEC. 6-9 1967

FIG.1.5

FIG. 1.6
Time-height section at OWS I. Isopleths of height perturbations (metres).



CHAPTER II Mechanisms for the concentration of vorticity

2.1 Introduction

To explain the development of polar lows we must develop a theory for the formation or concentration of vorticity on a scale of several hundred kilometres. We envisage four possible mechanisms:

1. The concentration of vorticity by differential heating
2. Horizontal shearing instability
3. Baroclinic instability
4. Disturbance of the flow by orography.

The wavelength associated with polar lows is about 1000 km, hence the Rossby number (U/fL) is about $0.1 \ll 1$, and the motion therefore quasi-geostrophic. The appropriate vorticity equation is

$$\frac{D}{Dt_h}\zeta + v\frac{\partial f}{\partial y} = \frac{f}{\rho}\frac{\partial(\rho w)}{\partial z} \qquad \text{———(2.1)}$$

where $$\frac{D}{Dt_h} = \frac{\partial}{\partial t} + \underset{\sim}{v}_h \cdot \nabla_h$$

$\underset{\sim}{v}_h$ is the horizontal velocity

∇_h is the horizontal gradient operator

and ζ is the vertical component of relative vorticity.

We are concerned with shallow disturbances, and since the depth is small compared to the density scale height the mass divergence effect can be ignored. Green (1960) shows that in a shallow baroclinic fluid the vorticity changes are mainly due to stretching rather than meridional advection. We therefore assume that however the vertical velocity is produced, the stretching is mainly responsible for the vorticity generation, and the vorticity equation can be written:

$$\frac{D}{Dt_h}\zeta = f\frac{\partial w}{\partial z} \qquad \text{———(2.2a)}$$

In the case of shearing instability $w = 0$ and the appropriate equation is

$$\frac{D\zeta}{Dt_h} = 0 \quad . \qquad \text{———(2.2b)}$$

In this case the vorticity of the eddy motion is redistributed by advection of the vorticity of the basic flow.

Since the motion is nearly horizontally non-divergent, advection by the divergent part of the velocity field can be ignored compared to that by the non-divergent part and the flow represented by a horizontal streamfunction (ψ) defined by

$$\underset{\sim}{v}_h = \underset{\sim}{k} \wedge \nabla_h \psi$$

Substituting for w in (2.2a) using the thermal wind equation

$$\frac{\partial \underset{\sim}{v}_h}{\partial z} = \frac{g}{f} \underset{\sim}{k} \wedge \nabla_h \phi$$

and the thermodynamic equation

$$\frac{D\phi}{Dt_h} + wB = Q$$

we obtain an equation for ψ

$$\frac{D}{Dt_h} \left\{ \nabla_h^2 \psi + \frac{f^2}{gB} \frac{\partial^2 \psi}{\partial z^2} \right\} = \frac{f}{B} \frac{\partial Q}{\partial z} \qquad \text{———(2.3)}$$

where B is the static stability

$\phi = \ln \theta$

and Q is the diabatic heating rate.

In the following sections, solutions will be found and mechanisms compared by linearising Eq.(2.3) and by considering small perturbations of a basic flow.

2.2 Differential heating

The effect of differential heating arising from the surface air flowing off the ice-sheet and over a gradient of sea-surface

temperatures is very complicated. The problem becomes tractable if we consider separately the components of the flow parallel and perpendicular to the sea isotherms.

2.21 Heating of a flow perpendicular to sea isotherms

Air flowing off the ice sheet will find beneath it an increasingly warmer sea, and so will experience an increase in heating rate. Further away from the ice, the gradient of sea temperature decreases and as the air is warmed the heating rate will decrease again. Consideration of the thermal wind balance shows that this will produce anticyclonic vorticity along the ice edge at low levels and cyclonic vorticity where the heating gradient reverses, vorticity of the opposite sense being produced at the top of the layer affected by the heating. This pattern will be produced along the length of the ice edge and its scale perpendicular to the edge will be determined by the scale of the sea temperature variations which is of the order of hundreds of kilometres. Thus narrow strips of vorticity are created, whereas the perturbations due to polar lows are nearly circular (see Chapter V).

2.22 Heating due to sea temperature anomalies

Vorticity patterns of the scale of polar lows can be formed by anomalies of sea-surface temperature. Harwood (1969) considered solutions of Eq.(2.3) for the special case of unsheared flow and heating independent of height, and found the vorticity produced by a 'warm patch' of ocean is proportional to the heating rate and inversely proportional to the speed of the flow. A heating rate of 100°K per day is needed to produce vorticity of the order f, when the wind speed is 10 m/s. Even in light winds large vorticities can not be produced since the heat transfer from the

ocean is proportional to the wind speed.

In Harwood's one-dimensional analysis the vorticity produced is found to be independent of the size of the heating patch in the direction of the flow, however large vorticities can be produced if the transverse scale is small. Such a heating pattern would occur if air flows off the ice sheet, but almost parallel to it, but again the vorticity would be concentrated in narrow bands. Further, disturbances produced in such a way remain stationary relative to the heating pattern and cannot be responsible for the production of transient eddies and we conclude that sea temperature anomalies are unimportant here.

2.23 Heating of a flow parallel to sea isotherms

Consider a basic flow parallel to sea isotherms, but perturbed slightly as in Fig.2.1 to form heating differences.

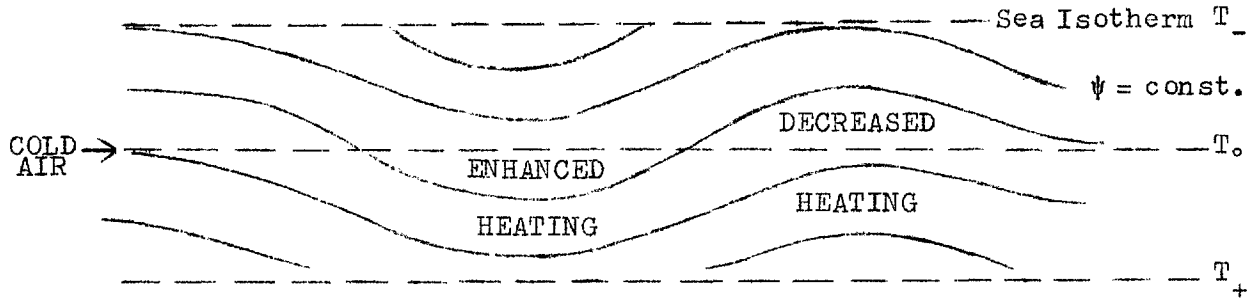


Fig. 2.1

We can dismiss the case of a stationary pattern as it is then essentially the same as §2.22. If the initial flow is barotropic, there will be a differential heating due to the gradient of sea isotherms, but again as shown above the vorticity pattern produced will be weak and stationary. The heating rate due to the perturbation is the same as if the flow were baroclinic and the surface air temperature initially everywhere the same as the sea-surface temperature (see Chapter IV) We shall show that although Harwood finds vorticity generations of the order of f in a day, in this case the pattern will decay rather than grow,

showing that instead of concentrating vorticity this effect is a damping on the generation of polar lows. The essential difference is that Harwood considers a heating pattern determined by the basic flow, whereas here it is produced by the perturbation itself.

For coordinates moving with the barotropic flow and Q independent of height Eq.(2.3) becomes

$$\frac{\partial}{\partial t}\left\{\nabla_h^2\psi + \frac{f^2}{gB}\frac{\partial^2\psi}{\partial z^2}\right\} = 0$$

Seeking solutions of the form

$$\psi = F(t)\,G(z)\,\exp i(\lambda x + \mu y) \qquad \text{———(2.4)}$$

we obtain

$$G(z) = M\sinh(\nu z) + N\cosh(\nu z)$$
$$\nu^2 = (\lambda^2 + \mu^2)\,gB/f \qquad \text{———(2.5)}$$

With 'rigid lid' boundary conditions i.e. w = 0 at the top and bottom of the fluid we obtain

$$\left(\frac{f}{g}\frac{dF}{dt}\frac{dG}{dz}\exp i[\lambda x + \mu y]\right)_{z=\pm H/2} = Q \qquad \text{———(2.6)}$$

Assuming Q of the form

$$Q = Q_o\,S(t)\exp i(\lambda_Q x + \mu_Q y)$$

since the ψ field is produced by the Q field (or vice versa) we must have $\lambda,\mu = \lambda_Q,\mu_Q$ respectively and

$$\frac{dF}{dt} = \text{const} \times S(t) \qquad \text{———(2.7)}$$

which leads to the result

$$\zeta = \zeta_o - \sqrt{(\lambda^2 + \mu^2)\,g/B}\;\frac{\sinh(\nu z)}{\cosh(\nu H/2)}\int_0^t S(t')dt'\,\exp i(\lambda x + \mu y) \qquad \text{———(2.8)}$$

The vorticity produced is proportional to the total amount of heat supplied to the air, positive vorticity at low levels with negative vorticity above being produced by positive S(t).

However, in the particular case when the heating pattern is due to the perturbation in the flow, Q must be proportional to, and opposite in sense to the perturbation of the entropy field. Since from the thermal wind equation and the definition of the streamfunction

$$\phi = \frac{f}{g}\frac{\partial \Psi}{\partial z}$$

Eq.(2.7) becomes

$$\frac{dF}{dt} = aF$$

where a is a constant which is determined by the relation of the heat input to the perturbation of the entropy field

i.e. $$S(t) = F(t) = F_o e^{-at}$$

and Eq.(2.8) becomes

$$\zeta = -(\lambda^2 + \mu^2) M F_o e^{-at} \sinh(\nu z) \exp i(\lambda x + \mu y) .$$

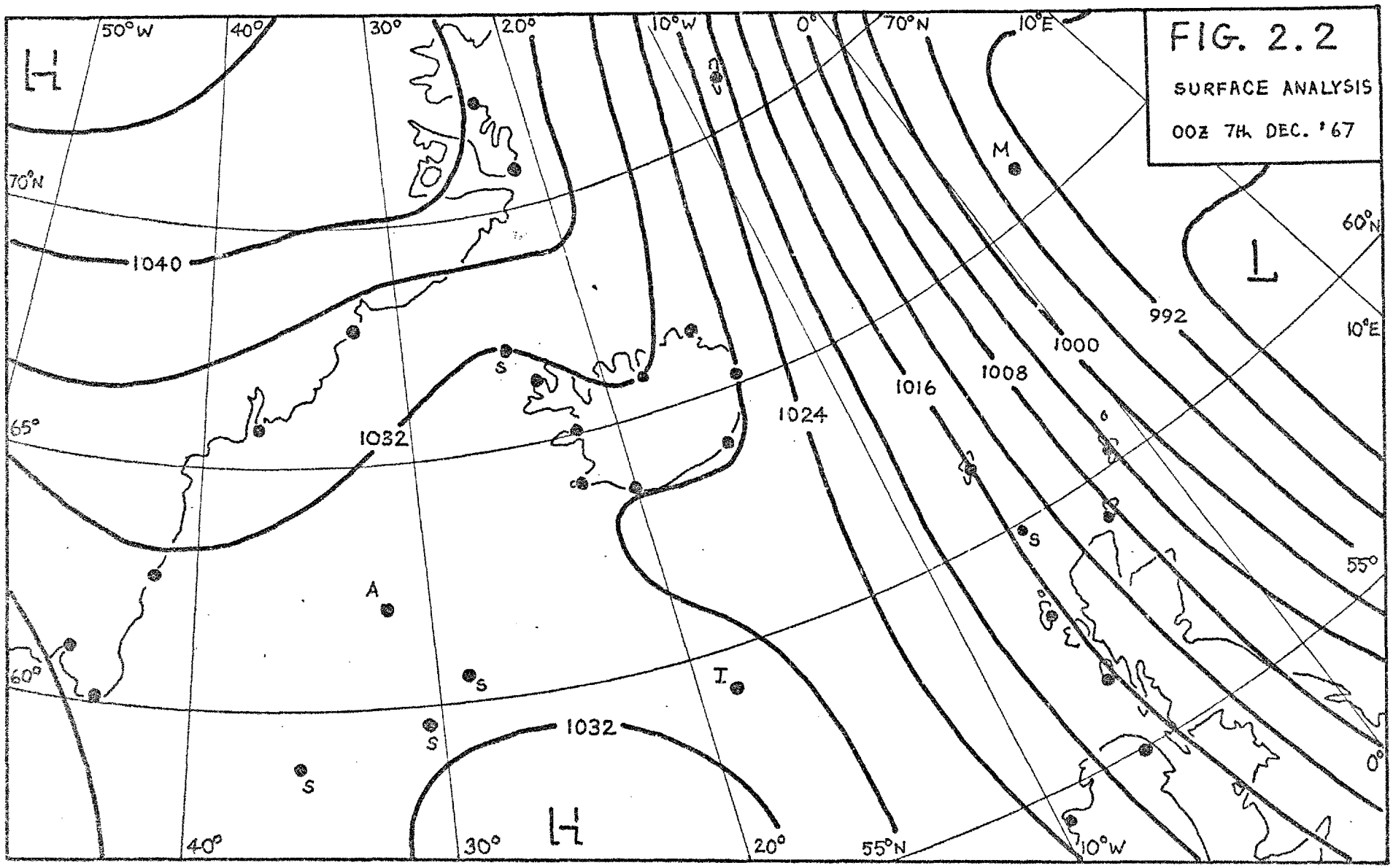
Thus the initial perturbation of undetermined amplitude decays exponentially with time the vorticity produced by the heating being opposite to that of the initial perturbation.

Harwood considers the case when the heating is produced by the basic flow and as its exact form is left undetermined there is no connection between the initial vorticity field and that produced by the heating, the latter growing almost linearly with time to the extent that the effect of the perturbation on the heating field can be ignored as a first approximation.

Returning to the case appropriate to polar lows we can estimate the decay rate by estimating the rate at which the air approaches the sea-surface temperature. The rate of change of temperature for an isothermal column of atmosphere can be written

$$\frac{dT}{dt} = \text{const} \times (T_S - T)$$

where T_S is the sea-surface temperature, and the RHS represents



SURFACE ANALYSIS SHOWING POSITIONS OF OBSERVATIONS ; S INDICATES SHIP REPORT , A, M, I OCEAN WEATHER SHIPS.

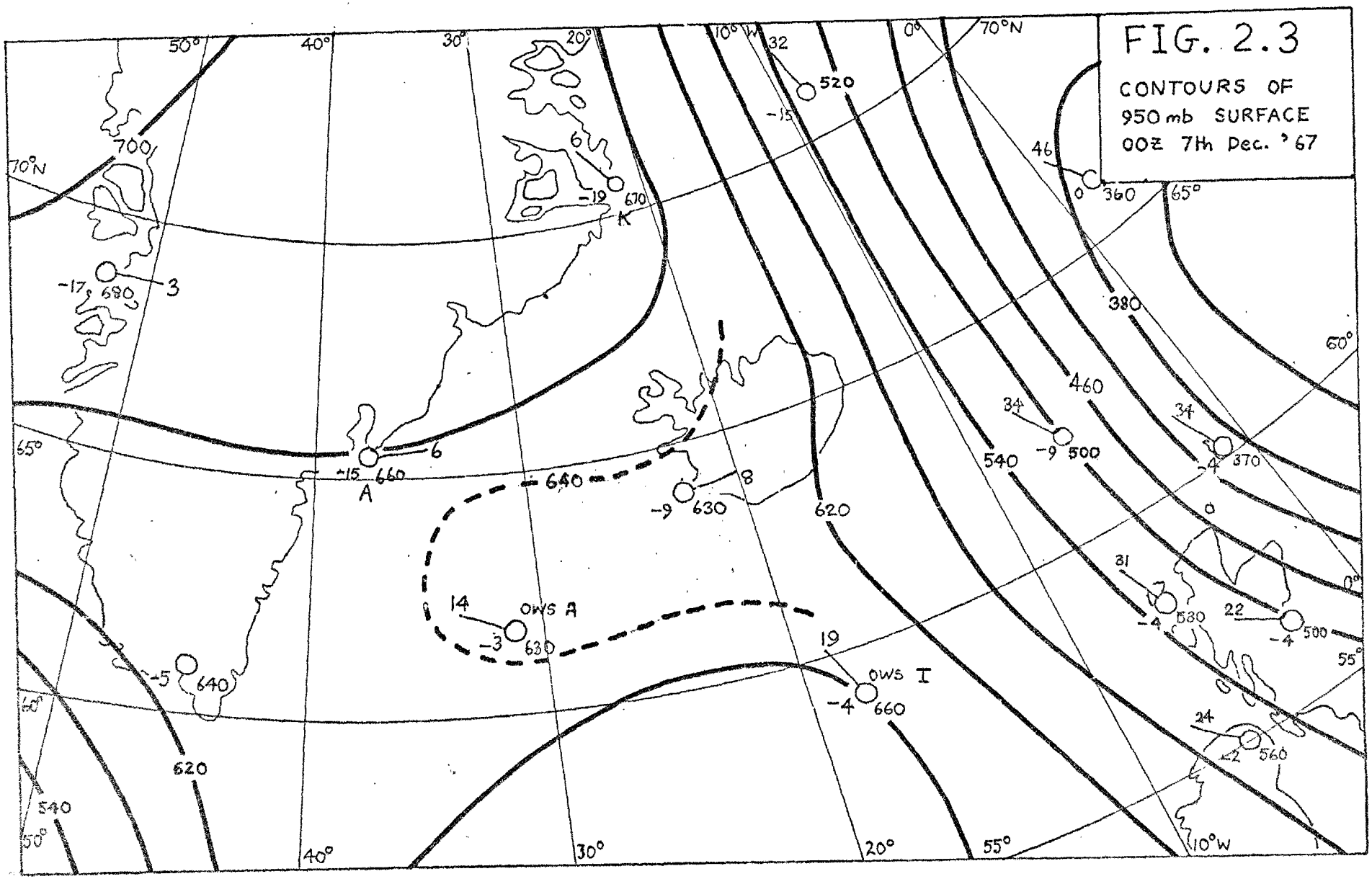
an empirical formula for the heat flux from the sea surface which will be discussed fully in Chapter IV. The constant depends on the drag coefficient, surface wind speed and depth of the column. With a depth of 2 km and a surface wind speed of 10 m/s, the constant = 2×10^{-5} sec^{-1}, thus the perturbation is reduced by a factor of e in half a day. Although this figure may be considerably modified in a more realistic baroclinic flow, this effect will cause damping of any disturbance due to the component of the flow parallel to sea isotherms.

2.3 Horizontal shearing instability

Surface pressure charts for the case study of December 1967 (Fig.2.2) show a moderate pressure gradient to the northwest of Iceland and a very slack gradient south and west of Iceland. This indicates, assuming the winds are approximately geostrophic, a region of cyclonic shear. The pressure field is used here instead of the observed winds because most of the reporting stations are coastal and many are situated in fjords and sheltered positions such that the reported winds are not representative of the wind over the open sea. (This is discussed further in Chapter V.)

Frictional convergence in the eddies produced by the instability of the shear zone and the release of latent heat in the enhanced convection could cause further growth of disturbances. A second and more pronounced shear zone exists to the east and south of Iceland but since this shear is anticyclonic, the associated sinking motion, suppresses the tendency for enhanced convection in this region.

The shear zone can be approximately represented by two regions of uniform velocity U_1 and U_2 separated by a region of constant shear of width b, and assuming this pattern is independent


FIG. 2.3
CONTOURS OF
950 mb SURFACE
00Z 7Th Dec. '67
70°N
65°
60°
55°
50°
40°
30°
20°
10°W
0°
700
680
670
K
660
A
640
630
620
610
600
590
580
570
560
550
540
530
520
500
490
480
460
440
420
400
380
370
360
OWS A
OWS I

of height, perturbation theory can be used to find solutions to Eq.(2.2b) in each of the three regions (Rayleigh, 1945). The growth rate as a function of wavelength (L) can be found by connecting the solutions by applying continuity of pressure and displacement at the boundaries of the regions. The maximum growth rate, given by $0.2(U_1 - U_2)/b$ sec^{-1} occurs when $b/L = 0.13$. Thus a shear of 5 m/s in 100 km would give a wavelength of 800 km and a growth rate of 10^{-5} sec^{-1}, similar to the observed values for polar lows (see Chapter 5). Because of the sparsity of observations, the actual width of the shear zone can not be determined in the case study, but is not inconsistent with the value suggested above. However, the height fields of the 950, 900 and 850 mb surfaces, show that even by 950 mb the pressure gradient northwest of Iceland has almost disappeared (Fig.2.3).

(The relatively strong wind at OWS A at 950 mb is due to the growing disturbance; it is assumed that otherwise the winds in this area would be very light. Unfortunately there is no upper air data for the time 12 hours earlier, just before the lows began to form, from two of the most relevant stations, Angmagssalik (A on Fig.2.3) and Kap Tobin (K) on the Greenland coast, otherwise the charts for this time would have been used.)

It seems unlikely that the disturbances are due to this very shallow shear zone, since although themselves shallow they occupy over twice the depth of the horizontal shear, and whereas waves in this zone would be expected to move with the mean flow i.e. southwestwards in this case, the lows moved away southeastwards out of the sheared zone.

The fact that the low level pressure gradient disappears rapidly with height indicates a strongly baroclinic zone. If Δh is the horizontal change in thickness of the layer in which

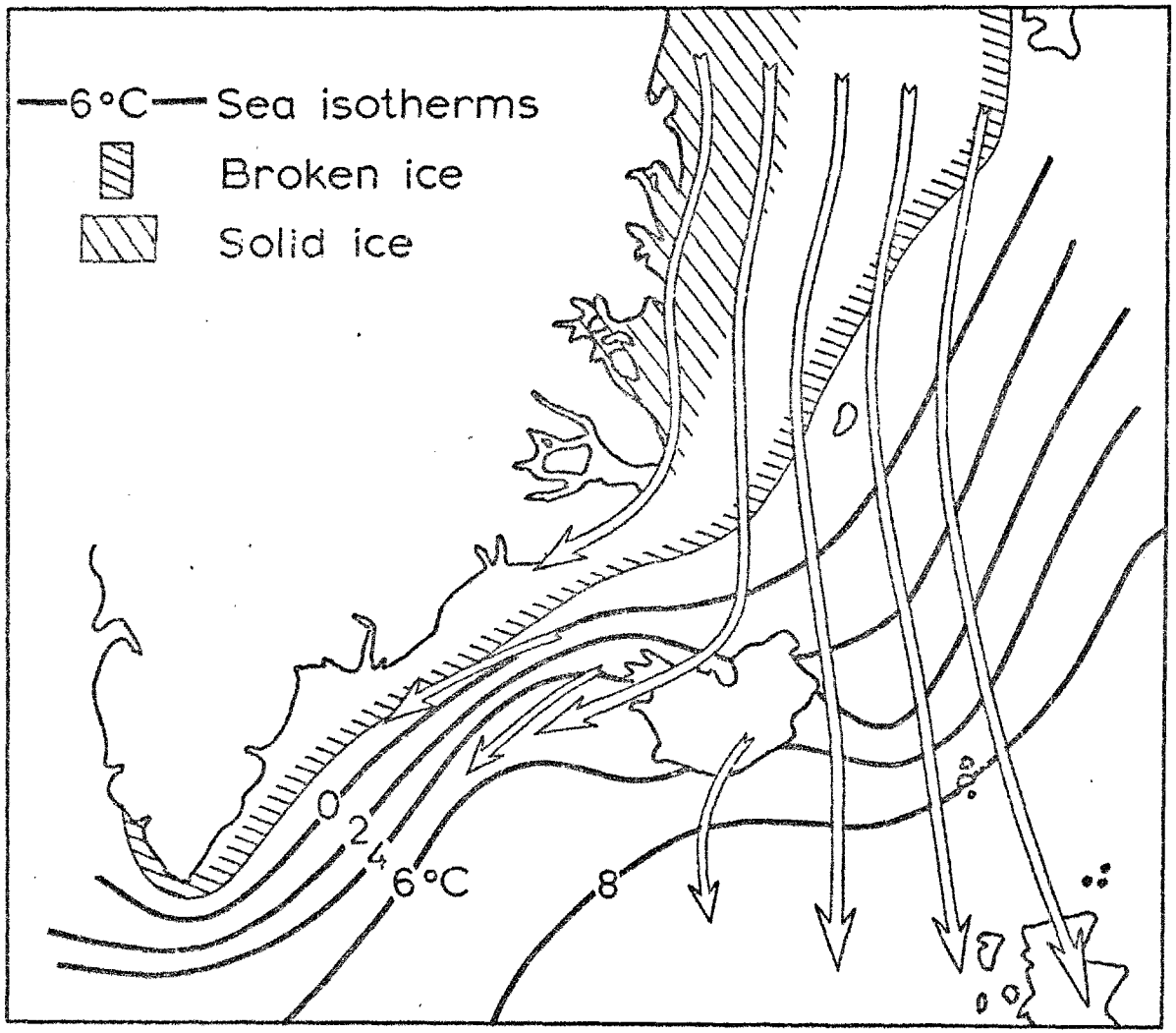


FIG. 2.4 .

Surface geostrophic trajectories and sea isotherms 6 – 8 December 1967

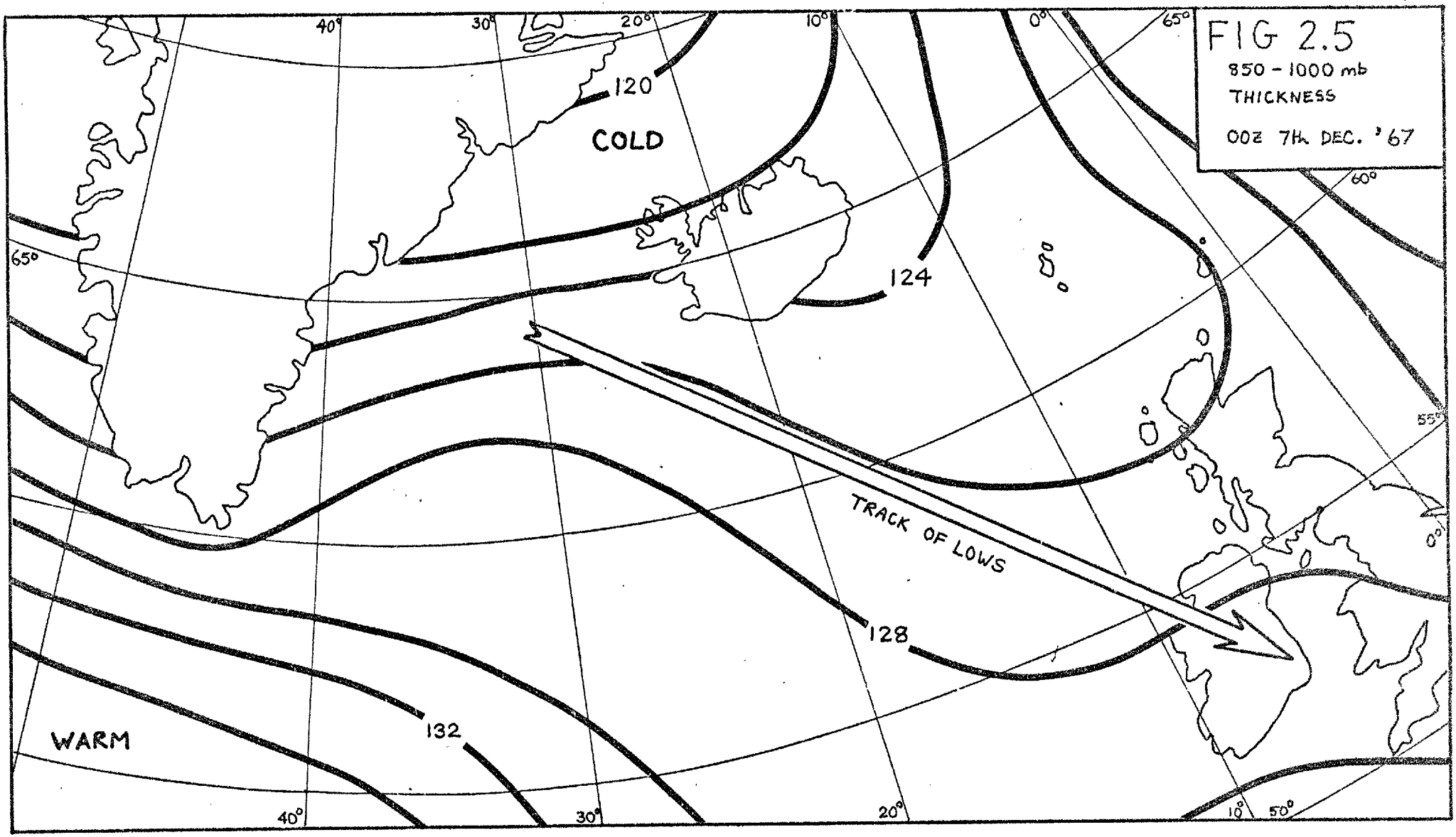
(Positions of ice edges are means for early December)

the pressure gradient disappears, and ΔT the horizontal change in average temperature, $\Delta h/h = \Delta T/T$. For the case study Δh is about 130 m in 100 km and h about 1 km, hence a temperature gradient of 3°C per 100 km is indicated. The stability of this baroclinic region is discussed in the following section.

2.4 Baroclinic instability

85 per cent of the polar lows which occurred in the last 10 years originated to the west or southwest of Iceland. For the case study of December 1967, trajectories deduced from geostrophic surface winds imply heating such that a strongly baroclinic region occurs at low levels between air flowing off the ice-sheet to the north of Iceland and almost stationary air to the southwest which has been warmed by the sea (Fig.2.4). Geostrophic trajectories give a qualitative picture of the low level flow, and since the pressure pattern was similar in all cases, even when the horizontal temperature gradient could not be measured, it could be inferred (i.e. the low level baroclinity would be present). The two lows of December 1967 formed in a region of maximum 1000 - 850 mb thickness gradient (Fig.2.5) and then moved southeastwards almost parallel to the thickness gradient so that baroclinity can explain not only the initial formation of the lows but also the direction of their motion. The second region of large thickness gradient to the south of Greenland is associated with the surface warm front marking the edge of the polar outbreak.

We can estimate the rate of growth of baroclinic waves by considering the available potential energy. By exchanging parcels of potentially warm air near the surface on the warm side of the baroclinic zone with potentially cold air in upper


FIG 2.5
850 - 1000 mb
THICKNESS
00Z 7TH DEC. '67
120
COLD
124
128
132
WARM
TRACK OF LOWS
40°
30°
20°
10°
0°
65°
60°
55°
50°

regions of the cold side, the centre of gravity of the system is lowered and potential energy released. Green (1960), by considering displacements of such parcels, showed that the energy released is a maximum when the slope of the parcel paths is approximately ½ the slope of isentropic surfaces, and the maximum value is given by

$$\Delta E_{pot} = gM(\delta s)^2(\partial\rho/\partial y)^2 / 8B$$

where M is the total mass of the parcels and δs is the displacement.

If this energy is converted into kinetic energy of an exponentially amplifying motion whose horizontal speed V is given by $V = \delta V \exp(ct)$ and displacement $\delta s = \int_{-\infty}^{t} V\,dt$, the increase in kinetic energy is given by

$$\Delta E_{kinetic} = \tfrac{1}{2}Mc^2(\delta s)^2 .$$

By equating the two energies the growth rate of such a system can be estimated. However, since particle paths near the upper and lower lids must be nearly horizontal, they are only close to the optimum slope at middle levels and the energy conversion is at most 50% efficient. An average value of $\partial\theta/\partial y$ for the region is 1.5°C per 100 km (§3.1) which gives a growth rate of about 1.4×10^{-5} sec^{-1}, which is comparable with that of polar lows.

The wavelength of the dominant wave is proportional to the depth of the fluid (Eady, 1949) and since the depth here is about 2 km or a quarter of that of mid-latitude cyclones, the wavelength for polar lows should be about 1000 km, which is consistent with the observed separation of the lows. In the following chapters we therefore extend Eady's theory to discuss shallow baroclinic waves including the effects of friction and the heating discussed in §2.2.

2.5 Orographic effects

Most of Iceland is a plateau about 1 km above sea-level and so it considerably disturbs the low level flow. Eddies are frequently observed downstream of Iceland as whirls of cloud on satellite pictures, and frictional convergence in the cyclonic eddies again could be responsible for further growth of the disturbances. Miller (1968) suggested the comparison with Von-Karman vortex streets.

The extension from the laboratory scale where the molecular viscosity is important to the scale of flow around Iceland is tenuous. Laboratory experiments show that vortex streets form downstream of objects for $50 \lesssim R \lesssim 2000$ (where R is the Reynolds number). For lower R the wake is steady and for higher R it is turbulent, the actual critical values depending on the exact shape of the obstacle. The concept of 'eddy viscosity' could be used to estimate a Reynolds number appropriate here but it is not very useful as the appropriate value of the eddy viscosity is not at all obvious.

An analysis of the surface geostrophic vorticity pattern at 18Z 7th December 1967 when two polar lows were present (Fig.2.6) initially appears to support this comparison. Streets of positive (AB) and negative (CD) vorticity are present, the positive vorticity increasing downstream and corresponding to the two lows while the negative vorticity is greatest near Iceland. The analysis is based on a 100 km grid length using the normal five-point finite difference formula for $\nabla^2 p$. If we consider the initial analysis of the pressure field is only correct to the nearest millibar, this leads to a maximum error of 2f in the calculated vorticities, even if the finite difference formula was exact. The vorticities in the figure have therefore been smoothed by

FIG 2.6 ISOPLETHS OF SURFACE GEOSTROPHIC VORTICITY

UNITS OF 10^{-4} SEC^{-1} 18z 7 DEC. 1967

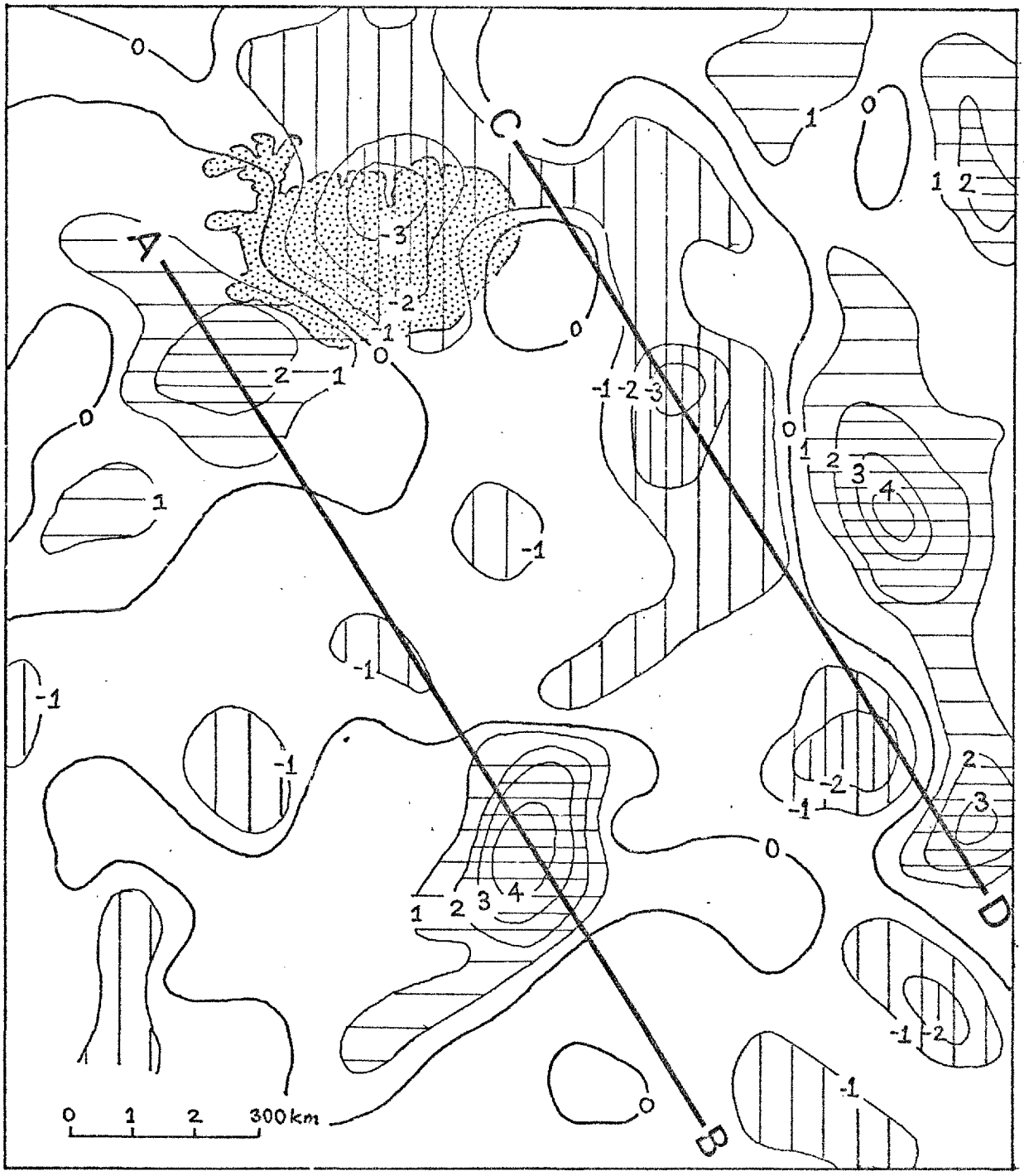
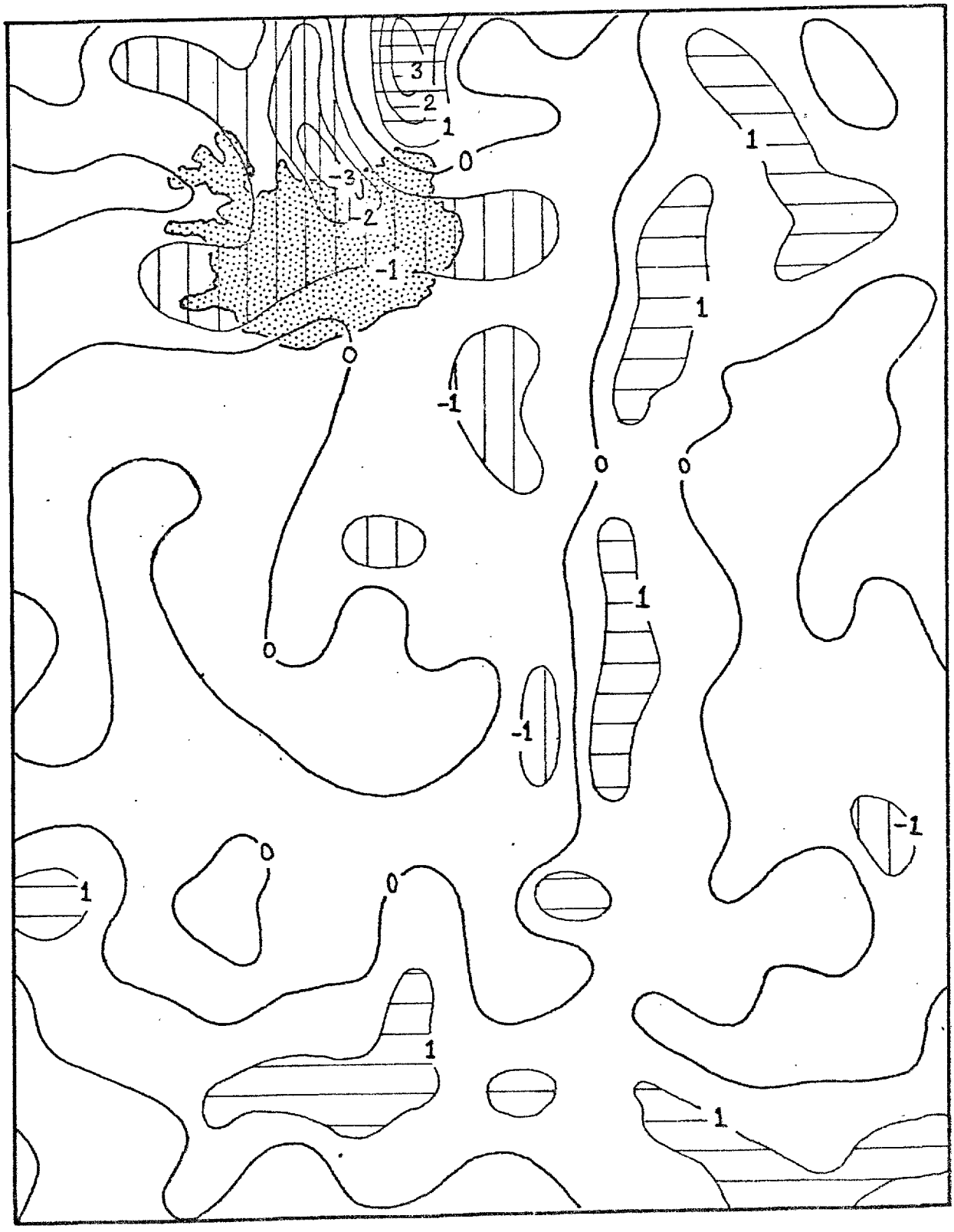


FIG 2.7 ISOPLETHS OF SURFACE GEOSTROPHIC VORTICITY
UNITS OF 10^{-4} SEC^{-1} 06Z 6TH DEC '67



taking a mean of four times the value at a point plus the sum of its four nearest neighbours. (This is in fact equivalent to taking the mean of a similar 5 point formula with twice the grid length and a diagonal 5 point formula.) The maximum error is still high ($\frac{3}{2}$f) but now less likely to occur. A similar analysis for 06Z 6th December when no lows were evident and the flow was relatively smooth is shown in Fig.2.7 for comparison. The surface pressure analyses for these times are shown in Figs. 5.15 - 5.26. Vorticities greater than f appear to be significant. The approximately N-S orientated bands of positive and negative vorticities in Fig.2.7 are associated with cyclonic and anticyclonic shear on either side of a narrow region of maximum velocity, and the E-W band of positive vorticity with a cold front. We therefore consider that the vorticity pattern in Fig.2.6 is significant and not due to errors in the analysis.

Von Karmen's theory for stability of vortex streets (see e.g. Goldstein, 1938), predicts the ratio of the separation of the streets to the separation of the individual vorticies within one street should be 0.28. Since Iceland has an effective width across the flow of 500 km, the separation of the vorticies should be about 1800 km compared to 900 km observed in Fig.2.6. This agreement is considerably less than that of the baroclinic wavelength.

Eddies on satellite pictures are observed much more frequently than polar lows, and since these pictures (at least for the North Atlantic) are available at best for 2 consecutive hours separated by an interval of 12 hours, it is not obvious whether the patterns are stationary or moving. Although the vortex street CD on Fig.2.6 is associated with a region of anticyclonic shear between fast moving air east of Iceland and

slow moving air to the south, we do not consider orography plays a direct part in the growth of polar lows. (The topography of the region on a larger scale is, however, important in that it determines the large scale flow and sea temperature gradient that produce the baroclinity.)

2.6 The effect of the release of latent heat

In the preceding sections we have assumed that frictional convergence in a cyclonic disturbance will lead to enhanced convection and a growth of the disturbance due to the release of latent heat. We now use a linear two layer model of this process, developed by Nitta (1964) to find the importance of this effect. Although only a very crude representation of the process, this model has the advantage that growth rates can be found very simply. The equations of the model are essentially those described in §2.1, the vorticity equation being applied at the centre of each of the two layers and the thermodynamic equation at the centre of the fluid. Combining these equations and using the boundary conditions $\omega = \alpha\zeta$ at the bottom and $\omega = 0$ at the top of the fluid enables a frequency equation to be found. The lower boundary condition represents the effect of frictional convergence in the boundary layer producing a vertical velocity at the top of this layer, proportional to the surface vorticity. In this model this layer is added below the lower of the two layers, as suggested by Charney and Eliassen (1949). (This type of parameterisation of friction is discussed in detail in Chapter III and here we shall simply take the appropriate value for α found there.) Water vapour is transferred from the friction layer and assumed to condense immediately and warm the whole of the air column simultaneously. The latter assumption is justifiable since the time scale of the convection is much smaller than that

of the disturbance but the former causes an overestimation of the heat release in a shallow layer where a considerable portion of the water vapour can not be condensed by lifting.

Nitta's results show that the growth-rate increases with decreasing wavelength and has a maximum for vanishing wavelength unless the shortest waves are damped by the introduction of diffusion. The maximum so produced is indistinct and therefore this process is not considered as defining a dominant wavelength, the space scale being defined by one of the mechanisms discussed in the previous sections.

Nitta finds growth-times of 1 day, but smaller values must be expected in cold air outbreaks since the amount of latent heat available is rather small and because the disturbances are shallow the dissipative effect of friction is increased. If we assume that the stratification of the flow can be represented by air saturated at the surface at a temperature of -3°C and with a lapse rate half way between the wet and dry adiabats to represent the presence of cumulus convection, we obtain a very slight decay-rate rather than growth, the energy gained from the latent heat release not being sufficient to overcome the frictional dissipation. We shall show later that the air where the lows originate is in fact much dryer than this and that the depth occupied by cloud is only a small fraction of the total depth, so that the latent heat release is probably even smaller. Also the effect is exaggerated in the model since for simplicity a corresponding cooling is assumed to occur where the frictional vertical velocity is negative.

However, by the time disturbances pass OWS I, the surface temperature is around 3°C, the available water vapour has nearly doubled, and since the convection now reaches nearly 700 mb the

effect of friction will be diminished. Under these conditions the model gives a growth-rate of about 10^{-5} sec^{-1}, which although probably too large, for the reasons stated above, indicates that here the release of latent heat has overcome the frictional damping and can contribute to the growth of the lows. It must be repeated however that this mechanism can not be responsible for the initial growth of the lows, and it appears that baroclinic instability is the most satisfactory mechanism, latent heat release becoming important only in the later stages of development.

CHAPTER III The effect of surface friction on the baroclinic motion

3.1 The unperturbed flow

To carry out a detailed study of the baroclinic effect in order to compare the results with observation, we must first define the unperturbed flow. A cross-section perpendicular to the flow is needed to determine the strength and distribution of the horizontal and vertical gradients of potential temperature. Because of the large separation of upper air stations in the area, it is unsatisfactory to draw the cross-section through or near to actual stations. The cross-section has therefore been constructed by drawing isopleths of potential temperature at the surface, 950 mb, every 50 mb to 800 mb and then at 700, 600 and 500 mb, and finding the values in the section from these analyses.

The resulting cross-section (Fig.3.1) shows a low level region of large horizontal temperature gradient between OWS A and Keflavik on the southwest coast of Iceland, and a second more extensive region above. Positive values indicate warmer air to the left of the section, that is to the southwest. Separating these two baroclinic layers is a layer of greater static stability. The sharpness of the transition from the relatively low static stability below this layer (except to the northeast of Keflavik) is considerably reduced by the smoothing involved in the method of analysis; there actually being an inversion at 850 mb at OWS A, and to a lesser extent at Keflavik. The large static stability at low levels to the northeast of Keflavik is because the cross-section here passes over or very close to the ice sheet, and there the radiative cooling of the surface and adjacent air is not counteracted by a heat flux from below and a low-level inversion develops. The static stability above 850 mb is four times greater than that below, which is

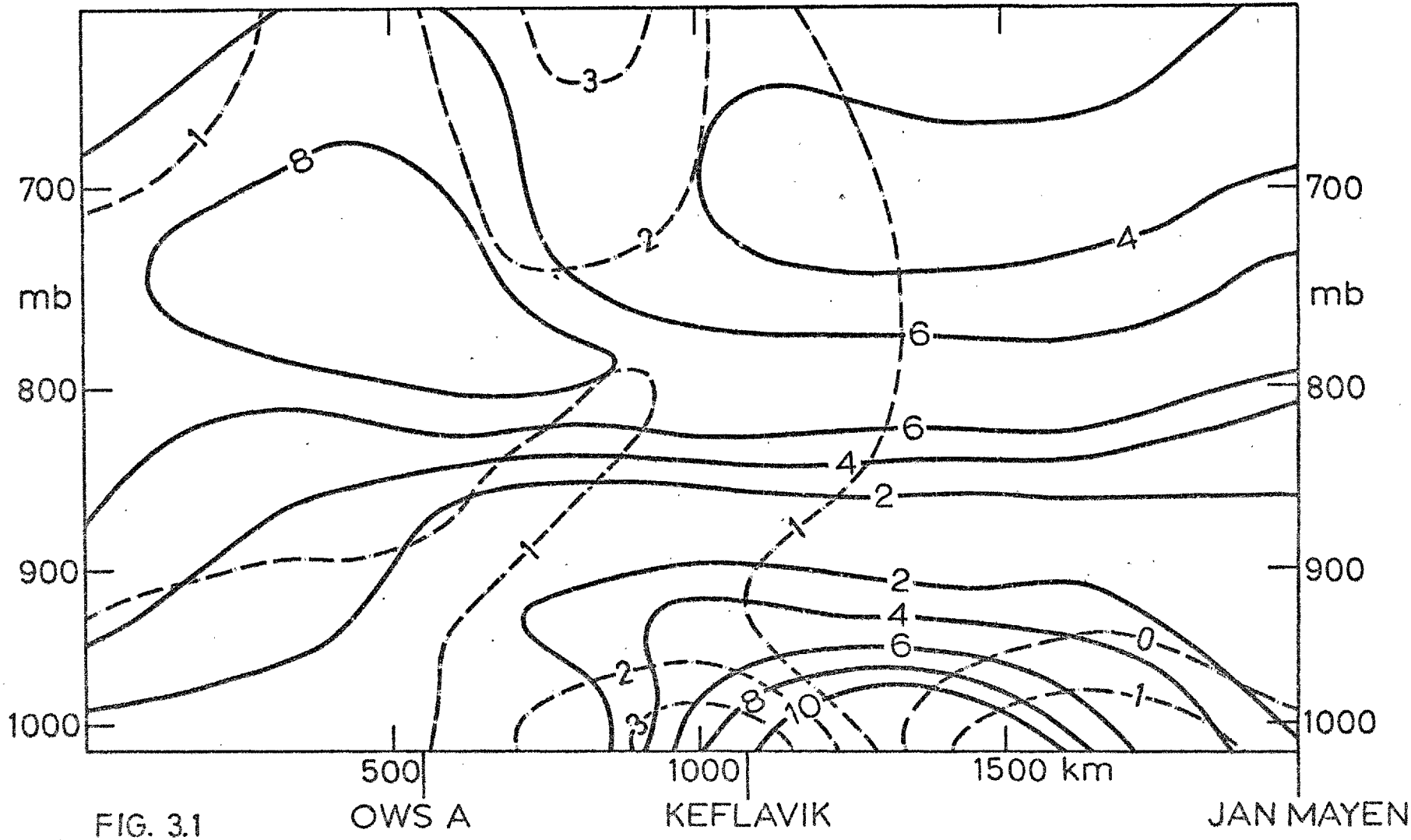


FIG. 3.1

Cross section perpendicular to direction of travel of lows. Static stability ($\partial\theta/\partial z$) in °C/km –(solid lines). Horizontal gradient of θ in °C/km (pecked lines) — positive θ increases to left.

a somewhat larger ratio than that across the tropopause. We therefore suppose that any disturbance growing below the stable layer will not penetrate and therefore not be affected by the upper baroclinic zone, and the assumption that this layer acts as a 'rigid lid' used in Chapter II and again in the following sections is quite reasonable.

Taking averages over a region from 200 km northeast of Keflavik to 600 km to the southwest and from the surface to the stable layer, we obtain the following parameters of the mean flow:

$$H = 1.6 \text{ km}$$

$$B = 1.6 \times 10^{-5} \text{ m}^{-1} \quad \text{(i.e. the lapse rate is 1.5 times the wet adiabatic)}$$

$$\frac{\partial \theta}{\partial y} = 1.4^{\circ}\text{C per } 100 \text{ km}$$

$$\Delta U = 6 \text{ m s}^{-1}$$

where H is depth

B is static stability

$\frac{\partial \theta}{\partial y}$ is horizontal gradient of potential temperature perpendicular to the direction of motion

ΔU is velocity difference between top and bottom of the layer.

The latter is simply the shear corresponding to the above horizontal temperature gradient assuming thermal wind balance. The Richardson number of this flow is 11 compared to an average of about 100 for large scale flow. This suggests that the geostrophic approximation is not very good since the ageostrophic terms are of order $Ri^{-\frac{1}{2}}$. However, Eady (1949) found that the errors do not become serious until Ri becomes fairly close to unity.

3.2 The frictionless wave

A straightforward application of Eady's perturbation theory enables us to find the structure of the growing wave.

Summarising this: substituting a wave-like solution of the form of Eq.(2.4) but with $\mu = 0$ into the linearised vorticity equation with $Q \equiv 0$ we obtain

$$i\lambda(U - c)\left\{-\lambda^2 G + \frac{f^2}{gB}\frac{d^2G}{dz^2}\right\} = 0 \qquad \text{———(3.1)}$$

The solution $U = c$ just advects the perturbation unchanged and is of no interest, we are therefore left with a similar solution for Ψ to that in §2.3 Eqs.(2.4),(2.5). Substituting in the linearised boundary conditions $w = 0$ at $z = \pm H/2$, and eliminating M and N we obtain a frequency equation

$$(c - \overline{U})^2 = (\Delta U)^2\left\{\frac{1}{4} + \frac{1}{X^2} - \frac{\coth X}{X}\right\} \qquad \text{———(3.2)}$$

where $X = \nu H$, ν as defined in Eq.(2.5) but with $\mu = 0$ and $\overline{U}$ is the unperturbed speed at the centre of the fluid. For $0 < X \lesssim 2.4$, c is complex and the solutions correspond to a growing and a decaying wave each moving with the speed of the middle-level fluid. For $X \gtrsim 2.4$ (short waves) the solutions are neutral, and therefore of no interest here. The maximum growth rate is given by

$$\lambda c_1 = 0.31\frac{f}{\sqrt{gB}}\frac{\Delta U}{H}$$

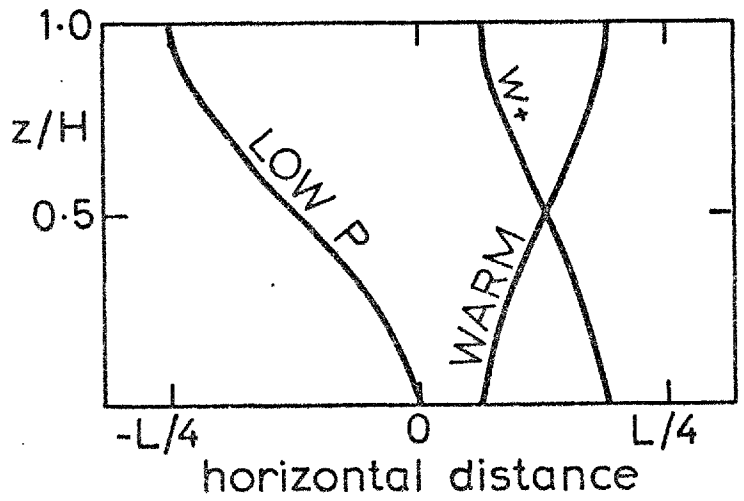
and the dominant wavelength by

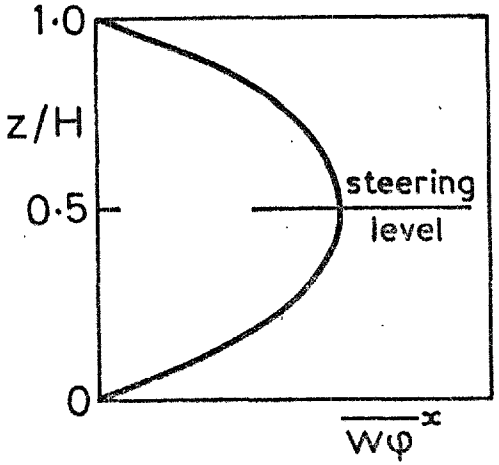
$$L = 3.9(gB)^{1/2} H/f \quad .$$

Substituting the values found in §3.1, and f appropriate for 60°N, we obtain more exact values for the growth time (23 hours) and wavelength (620 km) for baroclinic waves and confirm the results of the cruder energy analysis of §2.4.

The ratio of M and N in Eq.(2.5) can be evaluated in terms of the phase speed and growth rate, and hence the relative phases

FIG. 3.2
Variation of phases and vertical entropy transport with height

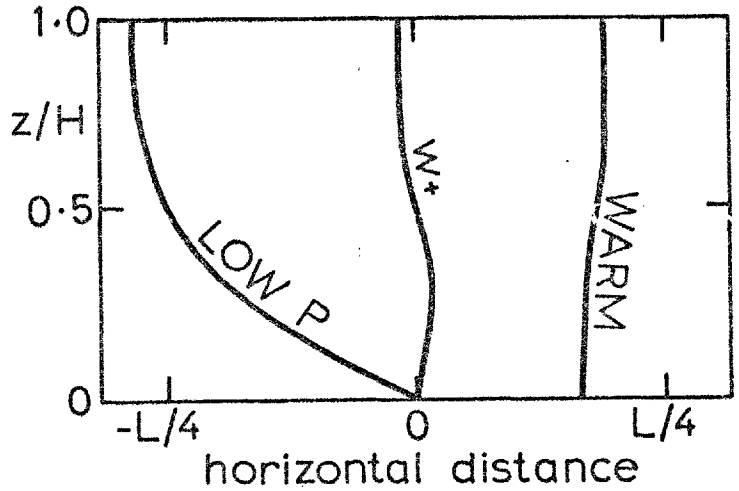


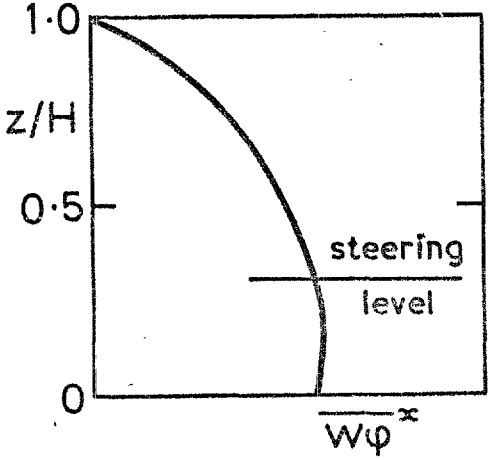


(a) $U_0 = 0$

$vH = 1{\cdot}6$

(max. growth rate)





(b) $U_0 = 10$ m/s

$vH = 1{\cdot}3$

(max. growth rate)

and amplitudes of the pressure, temperature, vertical velocity fields etc. can be found. The fastest growing wave has a high correlation between the warmest air, and the ascending and 'northward' moving air (Fig.3.2a). (Northward moving air here means a positive transverse velocity and is used because of the comparison with the baroclinic westerlies though here the unperturbed flow is northwesterly.) Thus entropy is transported upwards and 'northwards' and kinetic energy is released at the expense of the potential energy of the mean flow. The maximum correlation and entropy transport coincides with the steering level, which, since at this level the air does not move through the wave, means that the greatest transverse displacements coincide with the maximum correlation and the energy conversion is most efficient.

3.3 The parameterisation of friction

Because of their shallow nature the stress divergence is large and we therefore expect surface friction to be important in polar lows. Adding a stress term to the vorticity equation (2.2a) we obtain:

$$\frac{D\zeta}{Dt_h} = f\frac{\partial w}{\partial z} + \frac{1}{\rho}\,\mathrm{curl}_z\,\frac{\partial \underset{\sim}{\tau}}{\partial z} \qquad \text{——(3.3)}$$

Eq.(3.1) for the vertical variation of the stream function then becomes:

$$-\lambda^2 G + \frac{f^2}{gB}\frac{d^2G}{dz^2} = \frac{iF}{\lambda(U-c)}$$

where F is the friction term and is, in general, a function of z depending on the form of $\partial\underset{\sim}{\tau}/\partial z$. A general analytical solution of the above with non-zero F is not known so some other technique must be used to obtain a frequency equation.

Charney and Eliassen (1949) suggested that friction could

be introduced relatively simply by adding a frictional layer below the lower boundary of the frictionless theory, in which the vorticity advection can be ignored, and the frictional dissipation balanced by flow down the pressure gradient. This cross-isobar flow leads to convergence in areas of positive vorticity and divergence in regions of anticyclonic vorticity, and by integrating throughout the boundary layer a vertical velocity (w_F) at the top of the layer can be found. The dissipation takes place in the main body of the fluid, due to a compensating cross-isobar flow up the pressure gradient. This is then included in the model by making the lower boundary condition $w = w_F$ instead of $w = 0$. The magnitude of the cross-isobar flow is determined largely by the speed and static stability of the mean flow, hence the effect of friction is greater the faster the mean flow, and this will be shown to be very important when considering the growth of polar lows.

This approach is not very realistic for shallow waves in which the stress term is important throughout the fluid and some further consideration is necessary to justify its use. Holopainen (1961) and Haltiner and Caverly (1965) have investigated the effect of friction in a two-layer baroclinic model using a Charney and Eliassen type parameterisation, and since in such models the stress term can be incorporated directly in the vorticity equation we shall use a two-layer model to compare different parameterisations of friction.

3.31 The surface drag law

Ekman theory can be used to obtain the vertically integrated mass transport across the isobars in the boundary layer.

$$\underset{\sim}{D} = \rho \sqrt{\frac{K_M}{2f}} \sin 2\alpha \, \underset{\sim}{k} \wedge \underset{\sim}{V}_g \qquad \text{(Brunt, 1941)}$$

where K_M is the momentum transfer coefficient (assumed constant), α the angle of cross-isobar flow and $\underset{\sim}{V}_g$ the surface geostrophic wind. This can then be related to the vertical velocity at the top of the layer (Charney and Eliassen, 1949)

$$w_F = \frac{1}{\rho} \operatorname{div} \underset{\sim}{D}$$

$$\text{or} \qquad w_F = \sqrt{\frac{K_M}{2f}} \sin 2\alpha \, \zeta_g \qquad \text{———(3.5)}$$

where ζ_g is the surface geostrophic vorticity. α and K_M vary considerably with wind speed and static stability and are not well defined. α can be determined from the theory but it is necessary to know the height of the roughness elements and the depth of the constant flux layer (z_a) the latter again being ill-defined.

An alternative approach uses only a surface drag law. The momentum equation in the boundary layer can be written:

$$f \frac{\partial w}{\partial z} = -\frac{1}{\rho} \operatorname{curl}_z \frac{\partial \underset{\sim}{\tau}}{\partial z}$$

Integrating throughout the layer and assuming that the stress vanishes at the top, we obtain:

$$w_F = \frac{1}{\rho f} \operatorname{curl}_z \underset{\sim}{\tau}_s \qquad \text{———(3.6)}$$

The surface stress ($\underset{\sim}{\tau}_s$) can be crudely related to the surface wind by the empirical relation

$$\underset{\sim}{\tau}_s = \rho C_D |\underset{\sim}{V}_s| \underset{\sim}{V}_s \qquad \text{———(3.7)}$$

where C_D is a drag coefficient and $\underset{\sim}{V}_s$ the surface wind. Since we are concerned with small perturbations of a mean flow and are concerned with solutions of the vorticity equation independent of y

the perturbation velocity in the direction of the mean flow is zero and Eq.(3.7) can be written:

$$\underset{\sim}{\tau}_s = \rho C_D U_s (U_s \underset{\sim}{i} + v \underset{\sim}{j}) \qquad \text{——(3.8)}$$

where v is the perturbation and U_s the surface speed of the mean flow. Because of this independence of y on substituting into Eq.(3.6) we obtain the simple result that the vertical velocity is proportional to the perturbation vorticity.

$$w_F = \frac{\kappa \zeta_s}{f} \qquad \text{——(3.9)}$$

where $\kappa = C_D U_s$. This simple relationship does not hold if the perturbation is a function of both x and y and Eq.(3.8) becomes:

$$\underset{\sim}{\tau}_s = \rho C_D U_s [(U_s + 2u)\underset{\sim}{i} + v \underset{\sim}{j}]$$

By considering the simpler case we underestimate the effect of friction because the drag is proportional to V^2 and the addition of a perturbation along the flow has more effect on the modulus of the velocity vector and hence more effect on the drag than one perpendicular to the flow. C_D in Eq.(3.9) varies with wind speed but can be considered a constant determined by the speed of the mean flow if the variations about this value are small. The drag law is then equivalent to $\underset{\sim}{\tau}_s = \rho \kappa \underset{\sim}{v}_s$ where κ is dependent on the mean flow through C_D and $\underset{\sim}{v}_{os}$, thus as anticipated earlier the faster the mean flow the greater the effect of friction on the disturbances. This parameterisation has the advantage that it can be used both for the 'friction layer' approach and to estimate the stress term when included directly in the vorticity equation. The only parameters to be defined are C_D and $\underset{\sim}{V}_s$. Much work has been done in relating C_D to $|\underset{\sim}{V}_s|$ and it can be

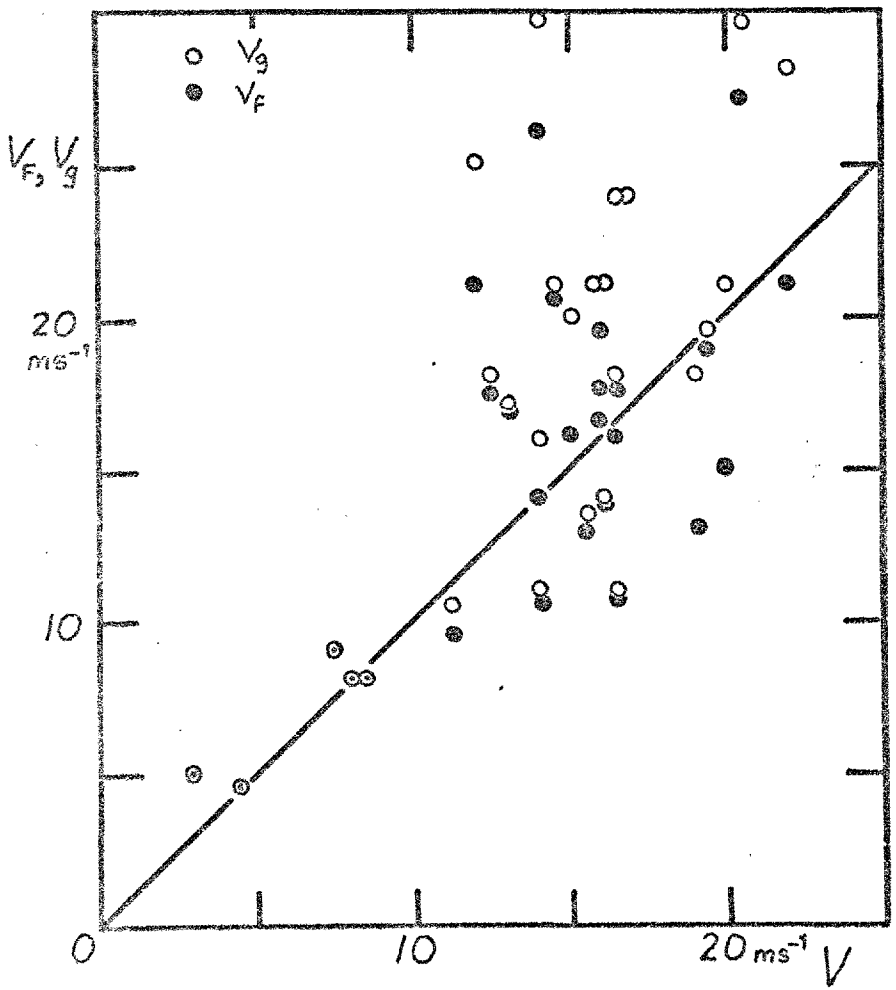


FIG. 3.3a

Comparison of calculated surface wind (V_f) with geostrophic (V_g) and observed (V) winds.

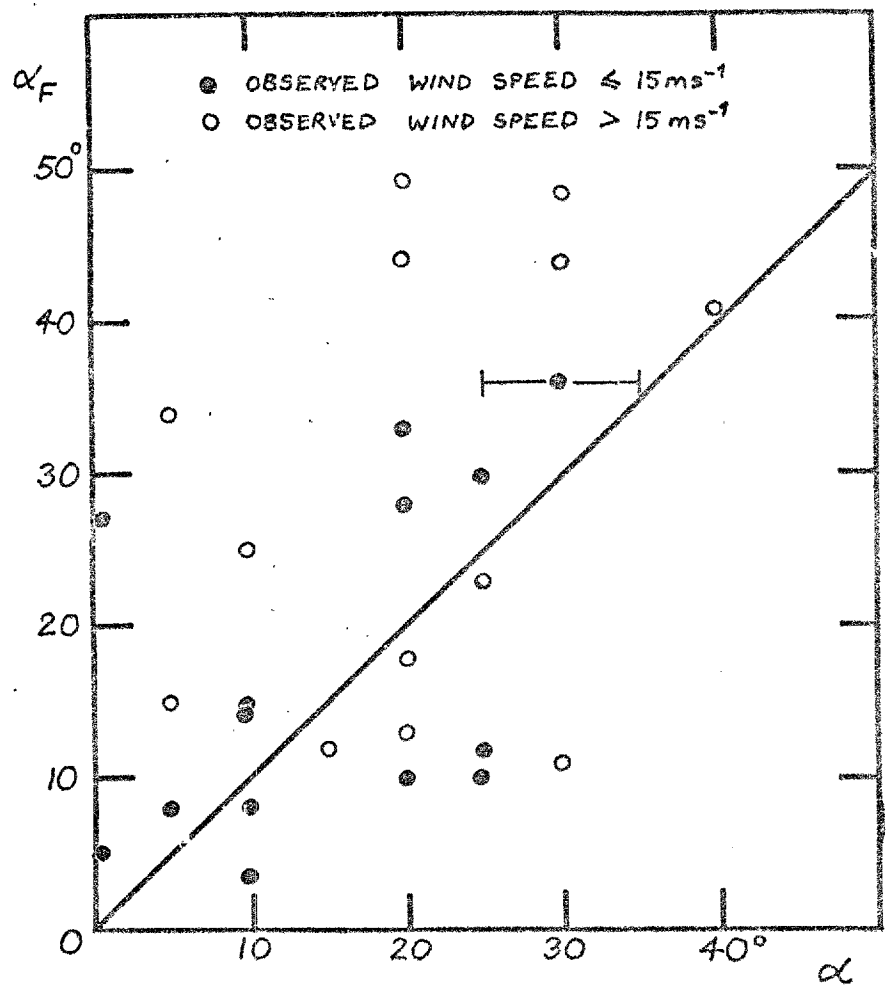


FIG. 3.3b

Comparison of calculated angle (α_f) of cross-isobar flow with observed angle (α).

considered much better defined than K_M or z_a . The surface velocity does not appear explicitly in the equations, only as the surface vorticity and this, it will be shown, is close to the geostrophic value except for very strong winds. This is not true of the Ekman approach; however, given the depth of the mixed layer and the geostrophic wind, the drag law has been used to estimate the surface wind and a comparison with observations shows that below 10 m/s the geostrophic wind speed is very close to the observed speed, suggesting that the constant stress gradient gives a better approximation to the surface wind than the Ekman spiral.

Assuming the stress decreases linearly to zero at some height h, the wind speed in the friction layer (V_F) is given in terms of the geostrophic wind speed (V_g) by

$$V_F = V_g(1+\kappa^2/f^2h^2)^{-\frac{1}{2}} \qquad \text{———(3.10)}$$

and the angle of cross-isobar flow (α_F) by

$$\alpha_F = \tan^{-1}(\kappa/fh) \qquad \text{———(3.11)}$$

Values of V_F and α_F have been compared with the surface winds at ocean weather stations in the North Atlantic (Figs.3.3a, 3.3b). Here h is defined by the convection and κ calculated from the observed wind and the values for C_D suggested by Sheppard (1958). The height, h, was taken as the top of the dry-adiabatic layer or cloud base if there was no dry-adiabatic layer. Since C_D depends on the stability we have used data only from northerly outbreaks for comparison with the case study. We have also ignored cases where the curvature of the trajectories is large and the geostrophic wind is no longer a good approximation to the wind above the friction layer. The calculated wind, depending

on the geostrophic value taken from DWR charts is an average over a space scale of about 100 km, whereas the observed winds are averaged over a few minutes at most and are therefore affected by much smaller scales of motion and considerable scatter must be expected when comparing these quantities. Bearing this in mind Fig.3.3a shows that the model produces reasonable surface velocities. The scatter is much greater when comparing α and α_F. This must be expected since α is given only to 10° and α_F is much more sensitive to errors of κ/fh than V_F for all but the highest values of κ/fh. Note that using this model is, however, much better than assuming geostrophic values in which case all the points would lie along the abscissa in Fig.3.3b. It is also noticable that the scatter is greater for large wind speeds, α_F in this case being consistently higher than α. This is possibly due to C_D being overestimated in high winds. The effect is not so noticable in Fig.3.3a because V_F is less sensitive to errors in κ.

It is more difficult to compare the Ekman spiral approach with observed winds as it is not known how z_a varies with wind speed and stability. However, if we take a typical value for z_a of 50 metres we can estimate the surface wind (V) and the angle of cross-isobar flow (α) as a function of the geostrophic wind (V_g) as follows. z_o is related to the drag coefficient by

$$C_D = k_o^2(\ln z_c/z_o)^{-2}$$

where z_c is the level at which the drag coefficient is appropriate and k_o is Von-Karmen's constant and α and V are given by

$$\frac{(\cos\alpha - \sin\alpha)^3}{\sin^2\alpha} = \frac{2f z_a(\ln z_a/z_o)^3}{k_o^2 V_g}$$

$$V = V_g(\cos\alpha - \sin\alpha).$$

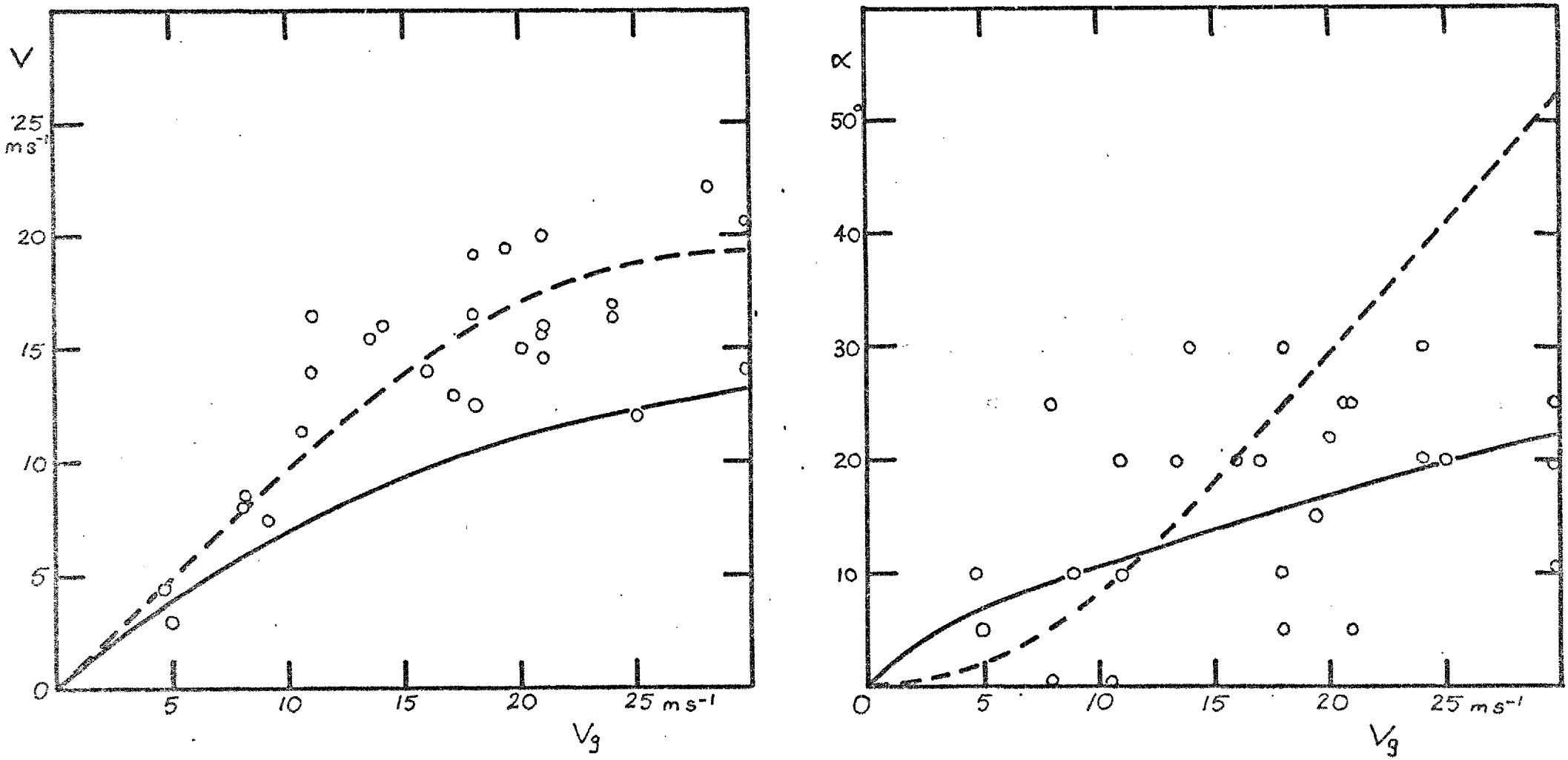


FIG. 3.4 Comparison of observed (circles) and calculated values of wind speed (V) and angle of cross-isobar flow (α) for different geostrophic winds, according to constant stress divergence (pecked lines) and Ekman type (solid lines) theories.

Fig.3.4 compares these functions (solid lines) with the observed wind together with the functions derived from the drag law approach (pecked lines) using the average h (0.8 km) for all the observations. Except for large wind speeds when the drag law gives rather too large values the large scatter makes the comparison of α inconclusive. However the Ekman theory clearly underestimates the velocity while the drag law shows good agreement. We have taken here only cases appropriate for northerly outbreaks when there is a well developed mixed layer and h is well defined. Under such conditions the constant stress gradient is more appropriate than the Ekman spiral, though the latter could be improved by using a larger value for z_a. In stable conditions h is difficult to define and the Ekman approach is more useful.

Especially for light and moderate winds the drag law gives reasonable values for surface winds, and the surface vorticity is close to the geostrophic value (i.e. ζ_o, the value at the top of the friction layer) as long as $(K/fh)^2 \lesssim 0.5$. This value is exceeded in regions of strong winds and high stability, but such regions are of little interest here so when using a friction layer model we can replace ζ_s in Eq.(3.9) with ζ_o.

3.32 The two-layer model

We now use the representation of τ_o discussed above in comparing the 'friction layer' parameterisation of friction with its direct inclusion in the vorticity equation. We consider a two-layer model similar to that used by Holopainen (1961). The model considers two layers of equal thickness (H/2) bounded by the surfaces $z = 0$, $z = H/2$ and $z = H$. Vertical gradients are replaced by finite differences and the vorticity equation (3.3) is applied at the centre of each layer (levels 1 and 3)

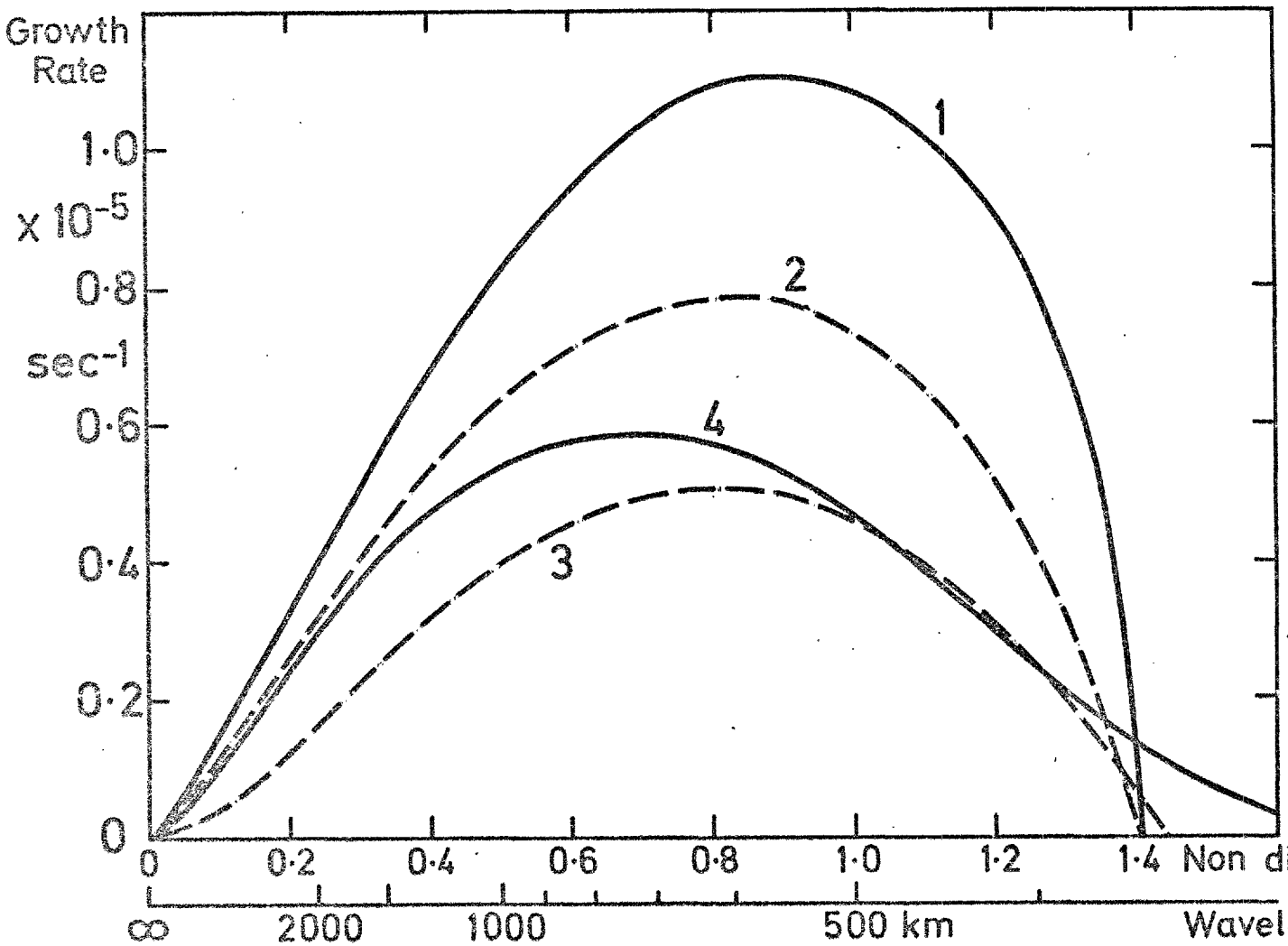


FIG. 3.5
COMPARISON OF DIFFERENT MODELS OF FRICTIONAL EFFECT, USING A TWO LAYER MODEL
Growth rate versus wavelength

Shear = 6 m/s
Depth = 1·6 km
Speed of unperturbed surface flow = 10 m/s

1 No friction

2 Friction evenly distributed

3 Friction in lower layer 4 times that in upper

4 Friction added via lower b.c.

$$\left.\begin{aligned}\left(\frac{\partial}{\partial t}+U_1\frac{\partial}{\partial x}\right)\nabla^2\psi_1-\frac{2f}{H}(w_2-w_0) &= \frac{1}{\rho}\,\mathrm{curl}_z\left(\frac{\partial \underset{\sim}{\tau}}{\partial z}\right)_1\\ \left(\frac{\partial}{\partial t}+U_3\frac{\partial}{\partial x}\right)\nabla^2\psi_3-\frac{2f}{H}(w_4-w_2) &= \frac{1}{\rho}\,\mathrm{curl}_z\left(\frac{\partial \underset{\sim}{\tau}}{\partial z}\right)_3\end{aligned}\right\}\qquad(3.12)$$

The thermodynamic equation, applied at level 2 is used to eliminate w_2 from the above. The boundary conditions give $w_0 = w_4 = 0$ and $\partial\underset{\sim}{\tau}/\partial z$ is simply estimated by assuming $\underset{\sim}{\tau}$ decreases linearly to zero at level 4. However it might be expected that the stress gradient is larger nearer the surface and to allow for this we take $\partial\underset{\sim}{\tau}/\partial z = n\underset{\sim}{\tau}/H$ so that the stress term can still be written in terms of the surface vorticity but the constants of proportionality n_1 and n_3 are different for the two layers. Finally the surface vorticity is expressed in terms of that at levels 1 and 3 by linearly extrapolating the gradient between these levels. Eqs.(3.12) then contain only ψ_1 and ψ_3 and their horizontal derivatives and again substituting wave-like solutions for ψ_1, ψ_3 we obtain a frequency equation. This is then compared with the frequency equation obtained by putting $\partial\underset{\sim}{\tau}/\partial z = 0$ everywhere and using the 'friction layer' lower boundary condition.

Fig.3.5 compares the growth-rate as a function of wavelength for no friction ($n_1 = n_3 = 0$), friction evenly distributed throughout ($n_1 = n_3 = 1$), friction four times more important in the lower layer ($n_1 = 2$, $n_3 = ½$), and with friction added via the lower boundary condition ($n_1 = n_3 = 0$, $w_0 = w_F$). We find that the results for the most realistic case with friction extending throughout the fluid, but concentrated in the lower layer agree closely with those obtained by adding the 'friction layer' below the lowest level whereas spreading the effect of the same surface stress evenly throughout the fluid reduces the effect of friction. We have demonstrated that Charney and Eliassen's method of parameterising

friction is much better than might be suspected and we therefore use the Eady type model with this included, to investigate further its effect because we avoid the very large truncation error implicit in two-layer models.

3.4 The effect on the structure of the wave

The rate of decay of a barotropic vortex due to friction can be estimated using the 'friction layer' approach. Approximating $\partial w/\partial z$ above the friction layer to

$$-\frac{w_0}{H} = -\frac{\kappa\zeta_0}{fH} \qquad \text{hence} \qquad \frac{D\zeta}{Dt} = -\frac{\kappa\zeta_0}{H}$$

corresponding to a decay time of ½ day for a surface wind speed of 15 m/s and a depth of 2 km. This is nearly twice the rate of growth of the frictionless wave and at first sight the addition of friction would appear to completely stop the growth of these waves. However, in the frictionless wave the motion is reduced in efficiency because near the upper and lower boundaries $w \simeq 0$ and the slope of the trajectories is much less than the optimum of half the slope of the isentropic surfaces. When friction is added this is no longer true at the lower boundary. Because of the phase difference in the vertical and horizontal velocity fields the average trajectory slope at the surface is still zero, but this increases rapidly upwards because the phase of the horizontal velocity field changes rapidly with height at low levels. (See Fig.3.2b, the phase of the positive horizontal velocity is the same as that of the pressure minimum, but displaced to the right by 1/4 of a wavelength.) Thus because of the increased vertical velocity at low levels the slope becomes closer to the optimum here and the efficiency is increased so that the damping does not swamp the baroclinic growth.

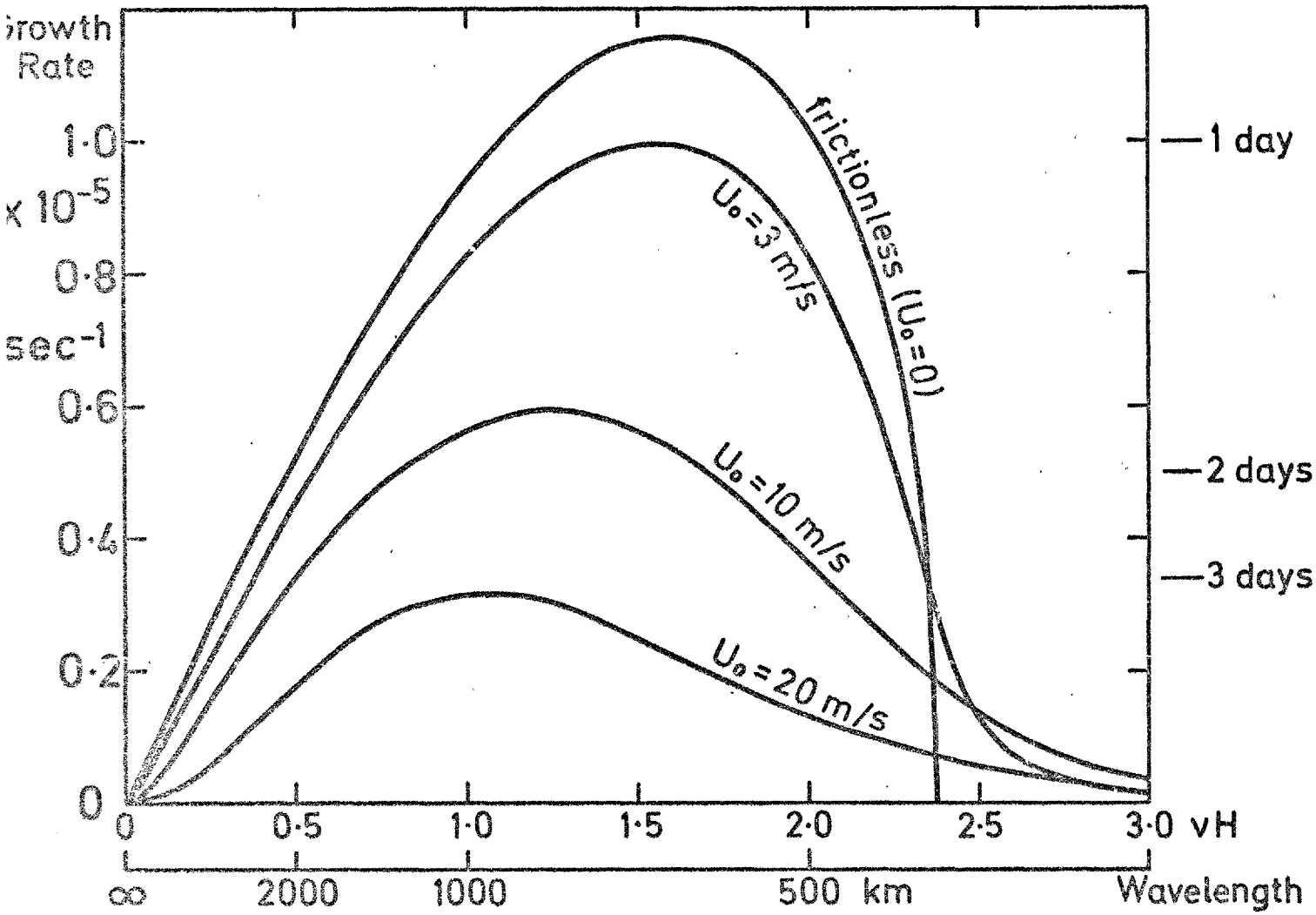


FIG. 3.6

EFFECT OF FRICTION ON EADY'S MODEL
Growth rate versus wavelength for various surface wind speeds

Shear = 6 m/s
Depth = 1·6 km

The solutions of the vorticity equation with friction included via the lower boundary condition have the same form as those of §3.2, but the ratio M/N is altered and the frequency equation becomes

$$(c-\overline{U})^2 + i(c-\overline{U})A\coth X + \Delta U^2\left(\frac{\coth X}{X} - \frac{1}{4} - \frac{1}{X^2}\right) + i\,A\,\Delta U\left(\frac{1}{X} - \frac{\coth X}{2}\right) = 0 \qquad (3.13)$$

where $A = \frac{\lambda}{f}\sqrt{gB}\,\kappa$.

The solutions for c are again complex and there is a growing wave for all values of X. Figs.3.6 and 3.7 show the growth rate and phase speed as functions of wavelength for several values of the surface wind. It is at first sight surprising that short waves which are neutral in the frictionless case grow slowly when friction is added. Both of the pair of neutral waves have zero correlation between the warm and ascending and 'northward' moving air. The warmest air coincides with the pressure minimum near the surface but the sign of the temperature field reverses at higher levels. The two waves are distinguished by the difference in height of the phase reversal and their differing steering levels. The addition of a frictional vertical velocity at the surface at the cyclone centre produces a positive correlation at low levels between the ascending and warm air. This leads to a slight growth of the wave in which the warm air above the cyclone centre extended above the middle levels. The other wave decays as the positive correlation is confined to near the surface and is offset by a negative correlation at upper levels.

Fig.3.2 compares the structures of the dominant waves with and without friction. The upward motion at the cyclone centre and corresponding adiabatic cooling (with the opposite effect at the anticyclone centre) introduced by friction,

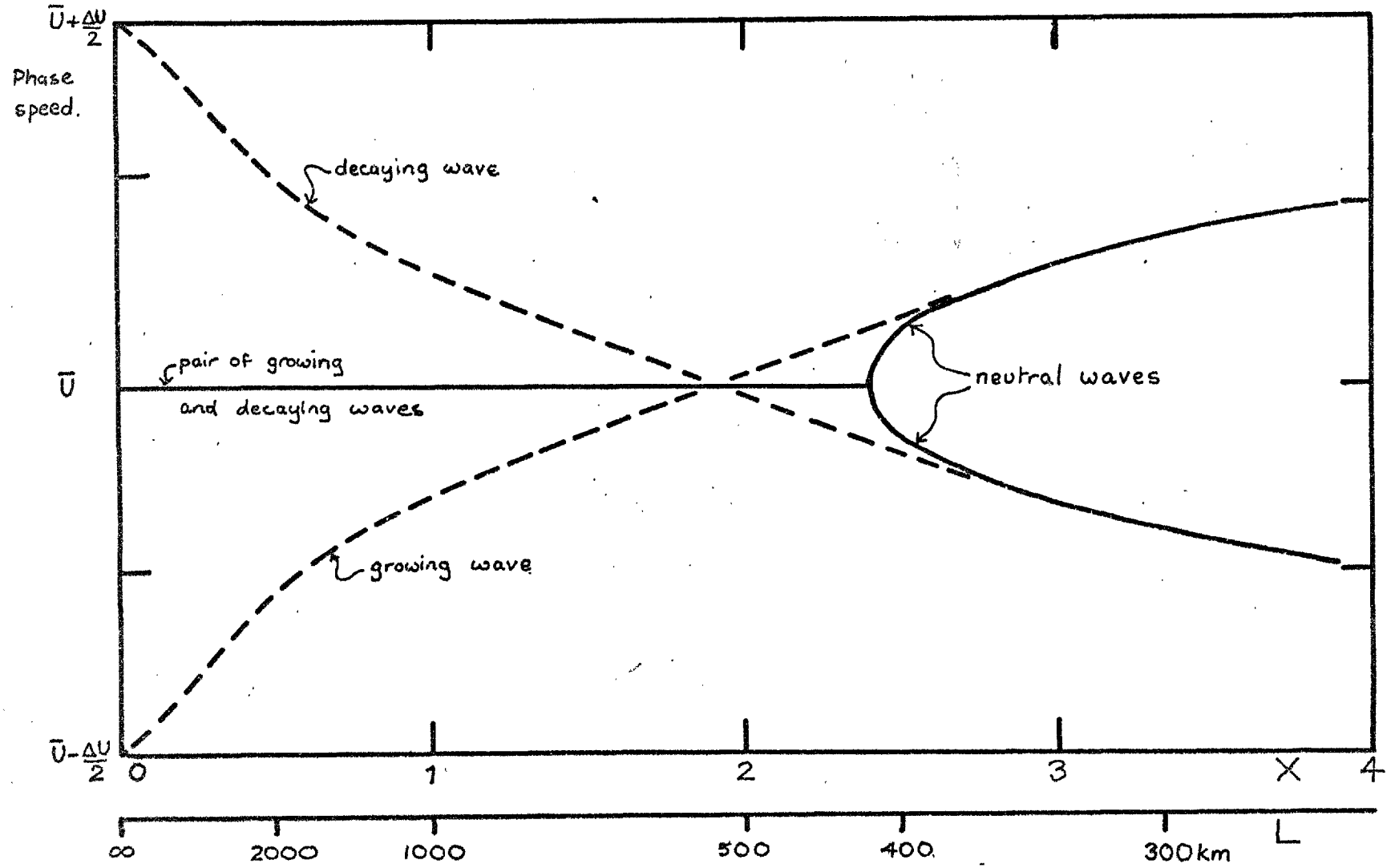


FIG. 3.7 Phase speed versus wavelength (L) with (pecked lines) and without (solid lines) friction

increases the phase difference between the warm and the ascending air. The positive correlation between the two is everywhere reduced, as is that between the warm and the 'northward' moving air except at low levels. For growth rates of about 10^{-5} sec^{-1} or less, the local rate of change of vorticity is small compared to other terms in the vorticity equation, and the advection term is approximately balanced by the stretching term. Since the latter vanishes at the vertical velocity maximum (or minimum), the advection must also be small (i.e. $U \simeq c_o$) such that the level of maximum vertical velocity almost coincides with the steering level. Hence the addition of a frictional vertical velocity at the surface lowers the steering level. We note, however, that it is still close to the level of maximum correlation of the warm and ascending air.

The results in Figs.3.2 and 3.6 show that friction makes the waves grow considerably less rapidly and much less efficiently, which is in general agreement with the results obtained by Holopainen (1961), Haltiner and Caverly (1965) and Winn Nielsen et al (1967) using two layer models. Since the frictional vertical velocity is proportional to the vorticity which can be written as $\nabla_h^2\psi$, the effect varies with the square of the horizontal wavenumber. Hence the shortest waves are most affected and the maximum growth rate is shifted towards longer waves. This is shown in the results both for the two layer model (Fig.3.5) and the continuous, Eady model (Fig.3.6).

Haltiner and Caverly (1965) suggested that the maximum growth rate was shifted towards shorter waves but since their method does not pose a complete problem and they have to assume an arbitrary phase difference between the pressure and thermal fields, which is then varied for each wavelength to produce the

maximum amplification, this result is somewhat misleading.

We note that the growth rate is drastically reduced by strong surface winds; for example the growth time of 23 hours in the frictionless case is cut by a factor of four to about 4 days when the surface wind speed is 20 m/s (Fig.3.6). These results are consistent with those of previous authors though in their studies friction appears to have less effect. Winn Nielsen et al (1967) for example, find the growth rate cut by only 25% at most, depending on the shear, with a frictional effect appropriate for surface winds of 15 m/s. However in their case the friction is distributed over a much greater depth. Also the values of the shear they used, ranging from 4 to 20 m/s per km, are rather large for the whole depth of the troposphere, as is shown by the large growth rates (growth times of less than half a day) that they obtained. Thus if the depth of the layer or the shear is reduced friction has a greater effect and their results are consistent with those presented here.

CHAPTER IV The effect of surface heating

4.1 Introduction

Heating from the surface is important in that it is responsible for the production of the low level baroclinity on which the polar lows grow, and also because as shown in Chapter II, it can cause damping of these disturbances. In this chapter a model of the heating is developed to investigate further these two effects.

4.2 A model of the heating of cold air over the sea

Air moving southwards over the ice sheet to the north of Iceland can be assumed to be statically stable except possibly for a small mixed layer due to mechanical turbulence. As the air moves over the sea a mixed layer develops and its increase in depth and temperature with distance from the ice edge defines the strength and depth of the baroclinic zone. A model of this process will be compared with the observed development of the boundary layer. Because the low level air in the baroclinic zone to the south west of Iceland was almost stationary over the period for which detailed data were available, it was not possible to obtain any trajectories crossing the ice edge northwest of Iceland. Trajectories over the Norwegian Sea are found to pass close to Spitsbergen, Jan Mayen, Thorshaven and Lerwick and comparison of soundings along this track with the model show it produces realistic increases in temperature.

We ignore the effect of the large-scale vertical velocity because calculations suggest it is small and thus it is not possible to obtain a reliable estimate from the widely separated upper air observations in the area. Radiative cooling can also be ignored since it is of the order of $1°C\ day^{-1}$ where the observed

warming is in excess of 10°C day^{-1}. We approximate the thermal structure by a constant potential temperature in the mixed layer above which it increases linearly with decreasing pressure. Thus we do not include any heat flux due to entrainment at the top of the convective layer. This could be expected to lead to a serious underestimation of the heating if, as suggested by Ball (1950), the entrained flux is approximately equal to the surface flux. However overestimating the surface flux to compensate for the lack of entrainment can be shown to give a temperature and depth development of the mixed layer close to that given by including entrainment. We will show that a bulk aerodynamical formula for the sensible heat flux used in the model gives approximately the observed warming, without taking into account any entrainment thus suggesting that the formula overestimates the surface flux.

From the first law of thermodynamics, applied to unit mass of air

$$-\frac{1}{\rho}\frac{\partial q}{\partial z} = c_p\frac{DT}{Dt} - \frac{1}{\rho}\frac{Dp}{Dt}$$

where q is the vertical flux of sensible heat. From the definition of potential temperature (θ)

$$-\frac{1}{\rho}\frac{\partial q}{\partial z} = c_p\left(\frac{p}{p_*}\right)^{R/c_p}\frac{D\theta}{Dt} \qquad \text{——(4.1)}$$

where $p_* = 1000$ mb.

As the effect of the heating will be spread throughout the convective layer, we integrate throughout the depth of the layer to obtain the warming in terms of the surface flux (q_s) assuming the flux vanishes at the top of the layer. Using the hydrostatic approximation we have

$$q_s = -\frac{c_p}{g}\int_{\text{bottom}}^{\text{top}} \left(\frac{p}{p_*}\right)^{R/c_p} \frac{D\theta}{Dt}\, dp \qquad \text{———(4.2)}$$

We assume that the motion is steady and the sea-surface temperature remains constant with time and can then put $\partial/\partial t \equiv 0$. We also take the x-direction along the flow, assumed homogeneous, so $\partial/\partial y = 0$. If there is a vertical wind-shear, for parcels moving horizontally, $D\theta/Dt$ must be a function of height, if θ is to remain independent of height. However as the air is well mixed the parcels will not move horizontally and an average $D\theta/Dt$ for the column should be used. This amounts to using an average wind speed since $D\theta/Dt = U\,\partial\theta/\partial x$ and $\partial\theta/\partial x$ is independent of height.

Hence

$$q_s = \frac{c_p}{g}\,\bar{U}\,\frac{\partial\theta}{\partial x}\,\frac{p_*}{(R/c_p+1)}\left[\left(\frac{p_1}{p_*}\right)^{(R/c_p+1)} - \left(\frac{p_2}{p_*}\right)^{(R/c_p+1)}\right] \qquad \text{———(4.3)}$$

where p_1, p_2 are the pressures at the bottom and top of the convective layer respectively and

$$\bar{U} = \int_{p_1}^{p_2} U(p)\, p^{R/c_p}\, dp \Big/ \int_{p_1}^{p_2} p^{R/c_p}\, dp$$

The surface heat flux can be expressed empirically in terms of the wind speed and air-sea temperature difference as follows (e.g. Burke, 1945).

$$q_s = \rho\, c_p\, C_D\, U_{10}(\theta_s - \theta) \qquad \text{———(4.4)}$$

where U_{10} is the 10-metre wind speed, C_D the appropriate drag coefficient, θ_s the sea-surface temperature, and θ the potential temperature of the dry-adiabatic layer. Combining Eqs.(4.3) and (4.4) we have

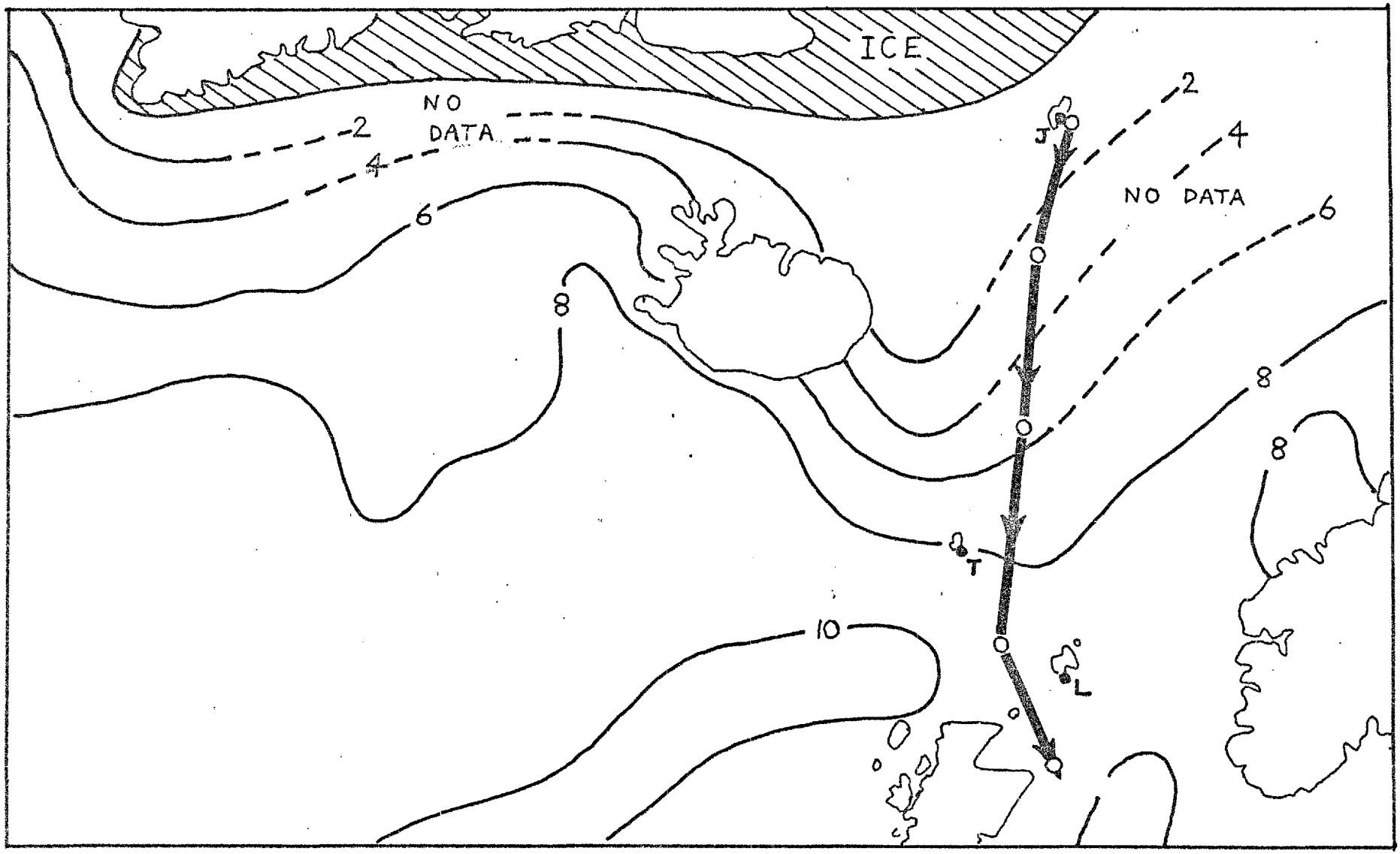


FIG 4.1 Sea isotherms Dec 6-9 1967 and Norwegian sea trajectory using climatological means where there is no data. These have also been used for the ice edge.

$$(\theta_s - \theta)dx = \frac{p_*}{\rho C_D g}\frac{\overline{U}}{U_{10}}\frac{1}{(R/c_p+1)}\left[\left(\frac{p_1}{p_*}\right)^{(R/c_p+1)} - \left(\frac{p_2}{p_*}\right)^{(R/c_p+1)}\right]d\theta \qquad \text{——(4.5)}$$

Since $\overline{U}$, U_{10}, p_1, p_2 and θ_s are in general undefined functions of x, some simplification is needed before Eq.(4.5) can be integrated. If in Eq.(4.2) we ignore the variation of density in the column, i.e. replace p by an average pressure $\overline{p}$, Eq.(4.5) becomes

$$(\theta_s - \theta)dx = a(p_1 - p_2)d\theta \qquad \text{——(4.6)}$$

where $a = \frac{1}{\rho C_D g}\frac{\overline{U}}{U_{10}}\left(\frac{\overline{p}}{p_*}\right)^{R/c_p}$ and $\overline{U}$ becomes $\int_{p_1}^{p_2} U(p)\,dp / (p_2 - p_1)$.

The heating is slightly underestimated by making this approximation, but the error is only 2% for a 500 mb column. p_1 can be considered constant as the air flows approximately parallel to the isobars, and we will assume $\overline{U}$ and U_{10} are constant along the trajectory. (The latter assumption is not important because if $\overline{U}$ and U_{10} vary significantly Eq.(4.6) can be integrated piecewise.) p_2 is determined by the potential temperature of the mixed layer and the lapse rate above the convection. θ_s can be estimated as a function of y and hence Eq.(4.5) can be integrated to obtain θ (and therefore p_2) as a function of x.

4.3 Comparison of the model with the Norwegian sea trajectory

Fig.4.1 shows the trajectory passing close to the radio-sonde stations Barencburg (Spitsbergen), Jan Mayen, Thorshaven (Faeroes) and Lerwick, which is used for comparing the model with observed heating. The part of the trajectory from Spitsbergen to Jan Mayen is close to the ice edge and probably largely over broken ice. The heat flux is difficult to estimate in this case so the initial conditions are taken as those at Jan Mayen and the model results

compared with the soundings at Thorshaven and Lerwick.

The trajectory was drawn by adjusting the surface geostrophic wind to take account of the thermal wind so that the wind was appropriate for 900 mb and thus representative of the convective layer. Since the thermal wind was in the opposite sense to the surface wind it combined with the effect of friction to make the wind almost constant in the lowest 2 km, so we have taken $\overline{U}/U_{10} = 1$ in Eq.(4.6). The sea isotherms shown on Fig.4.1 are averaged over the period 5th - 9th December and where there was no data available the analysis has been extrapolated using climatological means for December for sea-surface temperatures and the position of the ice-edge. The sea-surface temperature increases almost linearly from about 0°C at Jan Mayen by about 8°C per 1000 km to 10°C at Lerwick.

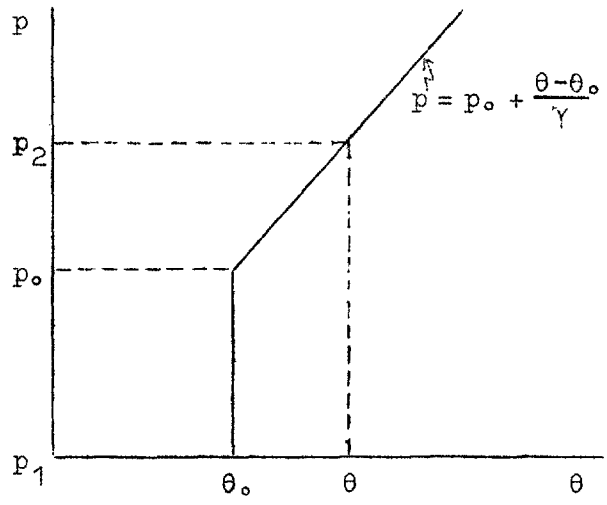


Fig. 4.2

In Fig.4.2; p_o, θ_o define the initial conditions on a p,θ diagram; p_2 and θ represent the state a distance x downstream. If the lapse rate $(\partial\theta/\partial p)$ above the mixed layer is γ, we can substitute for p_2 in Eq.(4.6) and at the same time putting $\theta_s = \theta_{s_o} + ax$ we obtain

$$(\theta_{s_o} + ax - \theta) = a\left\{\frac{(\theta - \theta_o)}{\gamma} + (p_1 - p_o)\right\}\frac{d\theta}{dx} \qquad \text{——(4.7)}$$

FIG. 4.3

Comparison of model with ascents along the trajectory. Potential temperature (θ) of adiabatic layer versus distance (x) from Jan Mayen.

$\theta_0 = -10°C$

$\Delta p = 180\,mb$

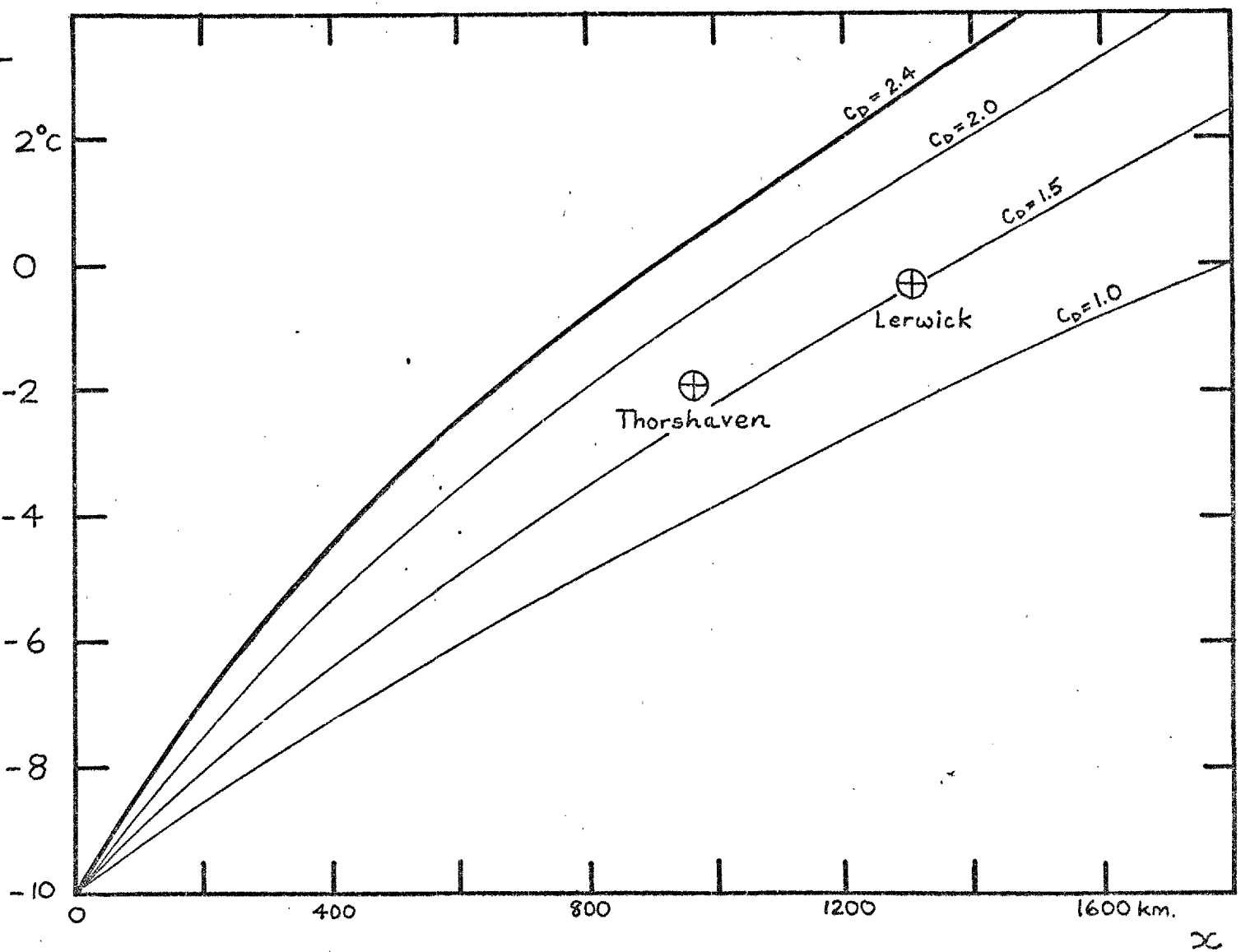
$\frac{\partial \theta}{\partial p} = -6°C/100\,mb$

$\frac{\partial \theta_s}{\partial y} = 8°C/100\,km$

Initial conditions

Thick line: C_D appropriate for observed winds;

thin lines: other values of C_D.



The average speed along the trajectory is 17 m/s so we take C_D as 2.4×10^{-3} using Sheppard's (1958) values as in Chapter III. a is then determined and Eq.(4.7) has been solved graphically by the method of isoclines and the resulting curve of $\theta(x)$ is shown in Fig.4.3. This is compared with the potential temperatures at Thorshaven and Lerwick (shown as crosses on the diagram) adjusted, to allow for the distance between the track and the stations, using gradients of θ from similar charts to that in Fig.4.5 for the appropriate times.

Surprisingly, since we have not included any heat flux due to entrainment the heat flux appears to have been overestimated as the final temperature is some 2.5°C higher than that observed. This is probably because the drag coefficient used in the heat flux formula is too large.

4.31 Errors in estimating the warming

Part of this discrepancy could be due to errors in the trajectory, which would lead to error in the air-sea temperature difference and, since the trajectory is not perpendicular to the gradient of potential temperature of the convective layer, an error in the final temperature. The trajectory was reconstructed after a sufficiently long time for details of the initial analysis to be forgotten. The separation of the trajectories at the ends of the tracks was 80 km. This, with the gradients of sea-temperature shown in Fig.4.1, causes an error of about 1.5°C averaged over the track, leading to a similar error in the final temperature. The error in the final temperature due to the horizontal gradient of θ is also about 1.5°C but opposite in sense to that due to the sea-temperature gradient and thus the errors due to error in the trajectory tend to cancel.

Errors also arise due to the uncertainty of the sea-surface temperature and due to radiative cooling. The probable error in the sea-temperature analysis is about ± 2°C causing a similar error in the final temperature. The radiative cooling rate for the convective layer at Thorshaven has been calculated using an Elsasser radiation chart, and allowing for the reported 3/8 cloud cover is found to be only 0.6°C/day. Since the air is dryer and colder than this for the greater part of the trajectory and the time taken for the track is slightly less than a day, radiative cooling can at most amount to 0.5°C. Thus an estimate of the total error is about 2.5°C, covering the observed discrepancy, but we have not included any heat flux due to entrainment. It is unlikely that this is negligible; Ball (1950) suggests that it is approximately the same as the surface flux for vigorous convection. We must therefore conclude that the empirical formula overestimates the surface heat flux. The sea-surface temperature representative of about the top ½ metre of the sea, may not be appropriate for the heat transfer formula, the actual surface temperature being lower due to evaporative cooling. Further measurements of the drag coefficient have not been carried out for wind speeds as high as 17 m/s, and the extrapolated values in this region may be too large. If a superadiabatic layer greater than 10 m deep exists over the sea, the potential temperature of the mixed layer will be less than that at 10 m, and if the former is used in the heat flux formula, since the drag coefficient is appropriate for 10 m, the heat flux is overestimated. The soundings near our trajectory are from islands and so there is no direct evidence for or against the existence of a deep superadiabatic layer. These effects combined could be responsible for the overestimation of the heat flux.

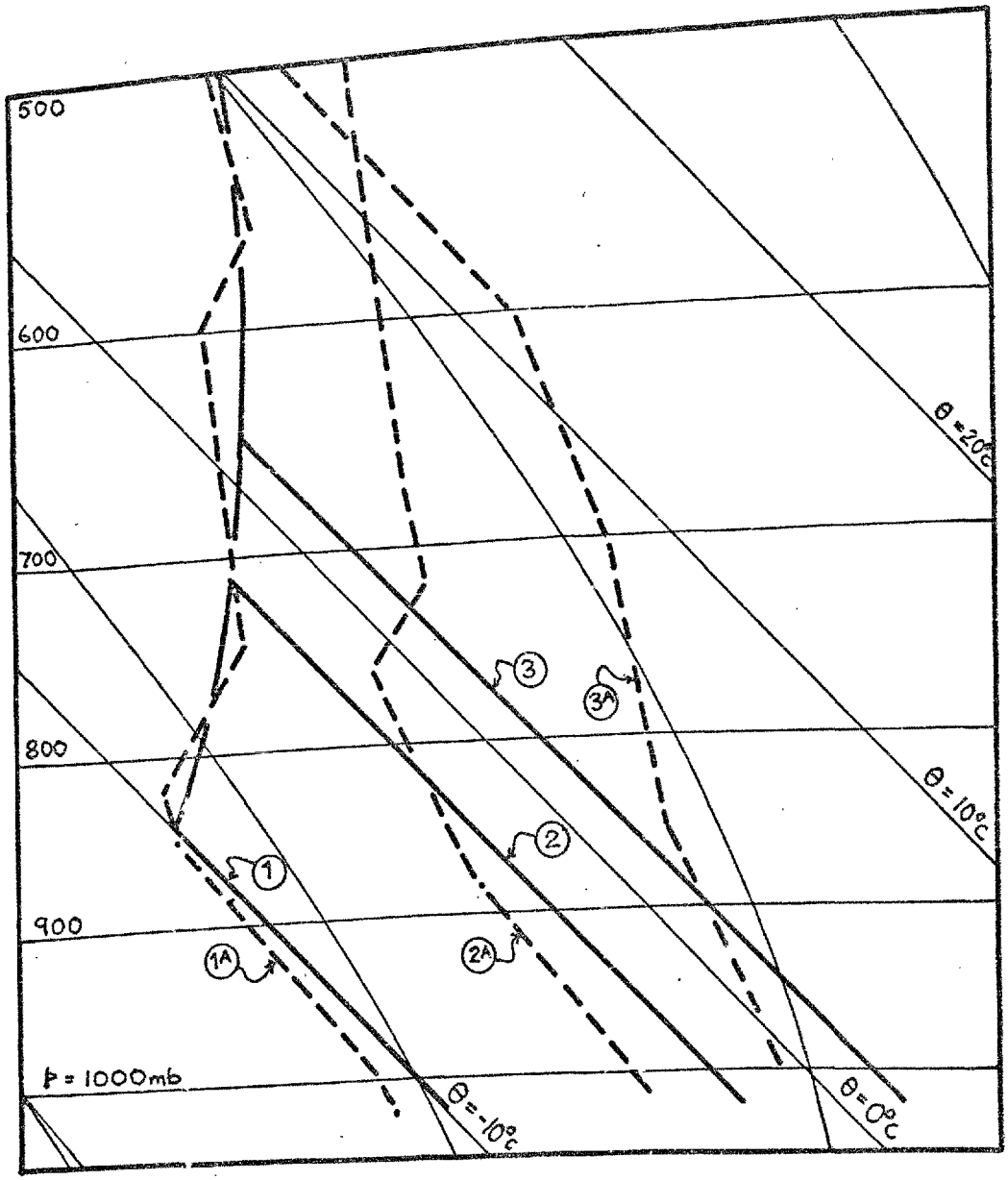


FIG. 4.4

Comparison of soundings along North Sea trajectories at Jan Mayen (1A), Thorshaven (2A) and Lerwick (3A), and predictions of the model after appropriate distances (1), (2) and (3) respectively.

Fig.4.4 compares the ascents at Jan Mayen, Thorshaven and Lerwick with the initial sounding and soundings after appropriate distances from the model, adjusted to allow for the distance between the trajectory and Thorshaven and Lerwick. The flux of water vapour and eventual release of latent heat, ignored in the model, causes large difference between the model and the Lerwick ascent where the air is saturated at the surface. There are also large differences above the convection due to the trajectory not being representative of air at this level. We conclude that the model can be used to predict the temperature and depth of the convective layer for short distances, the neglect of entrainment being compensated for by the over-estimation of the surface flux; but it becomes increasingly inaccurate away from the ice-edge as the depth increases and water vapour becomes important.

4.4 The production of the baroclinic zone

Here we use the model to demonstrate that the baroclinity observed in the case study will be present at about the same intensity, whenever air flows off the ice-sheet to the northwest of Iceland. Air leaving the ice-sheet will be relatively dry and so water vapour will not be important until the air has travelled some distance from the ice-edge.

The soundings for the case study from Angmagssalik and Kap Tobin on the Greenland coast closely resemble the mean December soundings for stations further north. This suggests that the air arriving at Angmagssalik has travelled southwards over the ice-sheet with little modification. As conditions change little over the ice cap in winter the case study soundings can be expected to be representative of northerly outbreaks.

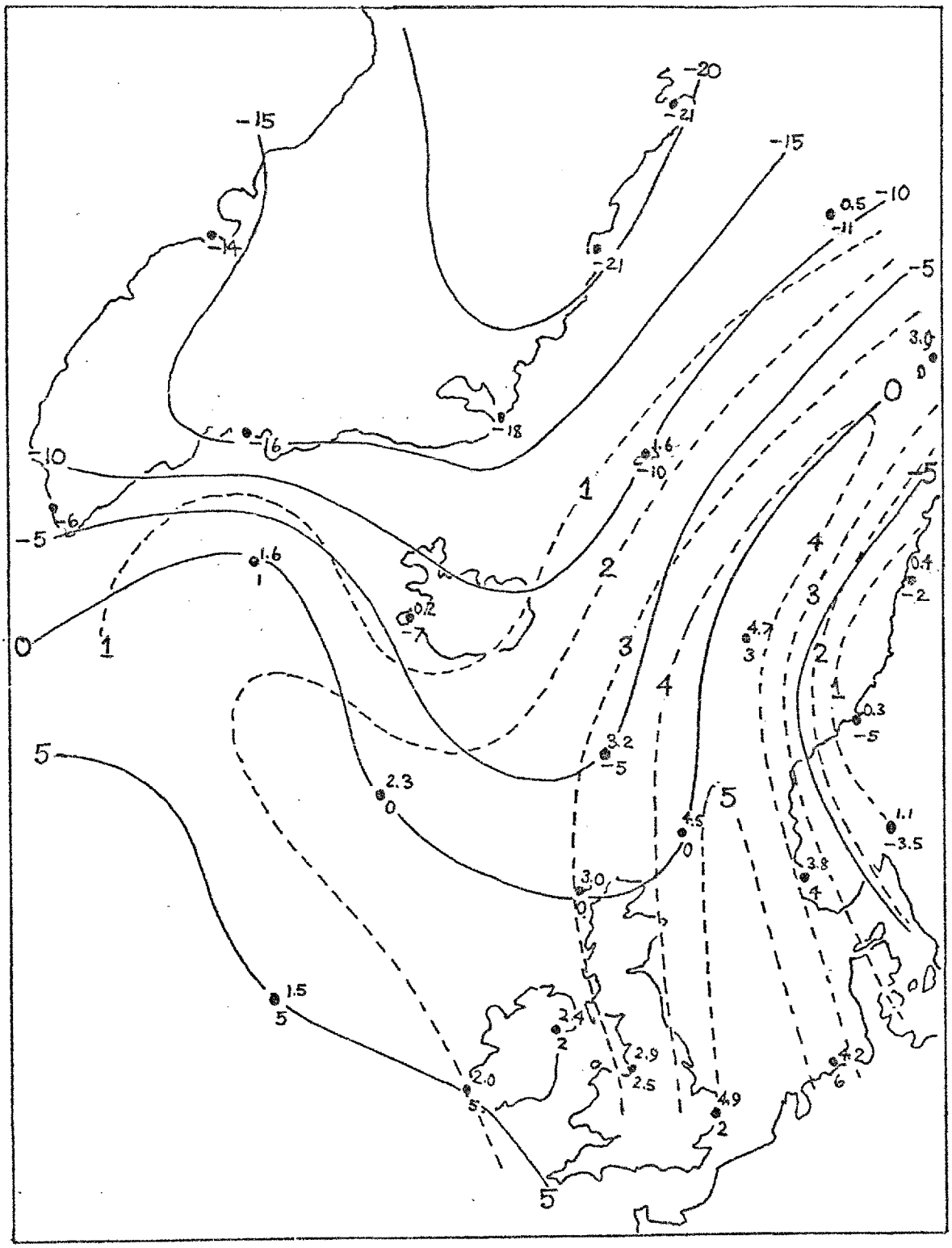


FIG. 4.5

Isopleths of potential temperature of the dry adiabatic layer (or that at 1000 mb if there is no convection) — solid lines. Depth of convection (km) — pecked lines. CCE 7 Dec 1967.

Ignoring the shallow surface inversion, the initial conditions for air leaving the ice-sheet northwest of Iceland, were taken as a surface potential temperature of -16°C increasing upwards by 6°C/100 mb, the mean of the soundings at Angmagssalik and Kap Tobin. The sea surface temperature in the area can be approximated by a linear increase of 1.3°C/100km away from the ice-edge.

If we consider air moving off the ice-sheet at 10 m/s, 500 km from the ice the model predicts a convective layer 2.4 km deep with a potential temperature of -1.5°C, an average gradient within the layer of 2.9°C/100km, compared to an average observed depth of 1.7 km and a gradient of 3.3°C/100km in the case study (Fig.4.5). The observed depth is less and the temperature gradient correspondingly higher probably due to subsidence of about 1.5 cm/sec which is not included in the model. The deflection of the maximum gradient to the south and the cold tongue of air to the southeast of Iceland shown in Fig.4.5 is explained by the effect of Iceland and the cold sea-current (shown by the sea temperatures in Fig.4.1) along the eastern coast, reducing the heating in this area.

It is clear however that temperature gradients of the magnitude observed in the case study will be present west of Iceland whenever the flow is off the ice-sheet. Even larger temperature gradients may be expected if the flow is parallel to the ice-edge but as suggested in §2.2 and confirmed in the next section, heating from the surface inhibits the growth of lows in this situation. Since cold air outbreaks occur much more frequently than polar lows this stresses the point made in Chapter III that it is the surface wind speed that governs their development.

4.5 Heating included in the baroclinic model

In Chapter II we showed that heating due to perturbation of a flow parallel to sea isotherms causes damping of the disturbance. We now examine in detail the effects of such heating on polar lows by extending the theory of Chapter III to include the kind of heating described in §2.23 and as before we consider only the heating due to the perturbation.

We assume that the unperturbed temperature of the surface air is everywhere the same as the sea-surface temperature and that the heating (and cooling) is independent of height. The latter assumption appears unrealistic in the case of the cooling. However, in cold air outbreaks the air will in general be heated everywhere and hence the cooling relative to the perturbation will be only a reduction of the large scale warming and therefore spread throughout the depth of the fluid. The vertical divergence of the heat flux can then be expressed as the surface value divided by the depth of the layer, and substituting the empirical formula for this (Eq.(4.4)) into the thermodynamic equation (4.1) we obtain

$$\alpha(\theta_S - \theta_{surface}) = \frac{D\theta}{Dt}$$

where $\alpha = \frac{C_D U_{10}}{H}\left(\frac{p_*}{p}\right)^{R/c_p}$.

We note that the heating, like friction, depends on the speed of the mean flow and we anticipate that it also will be important in strong winds.

Writing $\theta = \theta_o(y,z) + \delta\theta(x,z,t)$ where $\delta\theta$ is the small perturbation, θ_o the temperature of the mean flow and $\theta_o(y,0) = \theta_S(y)$ we obtain

$$-\alpha\,\delta\theta_{z=0} = \frac{D\theta}{Dt}$$

or in terms of the log potential temperature (ϕ)

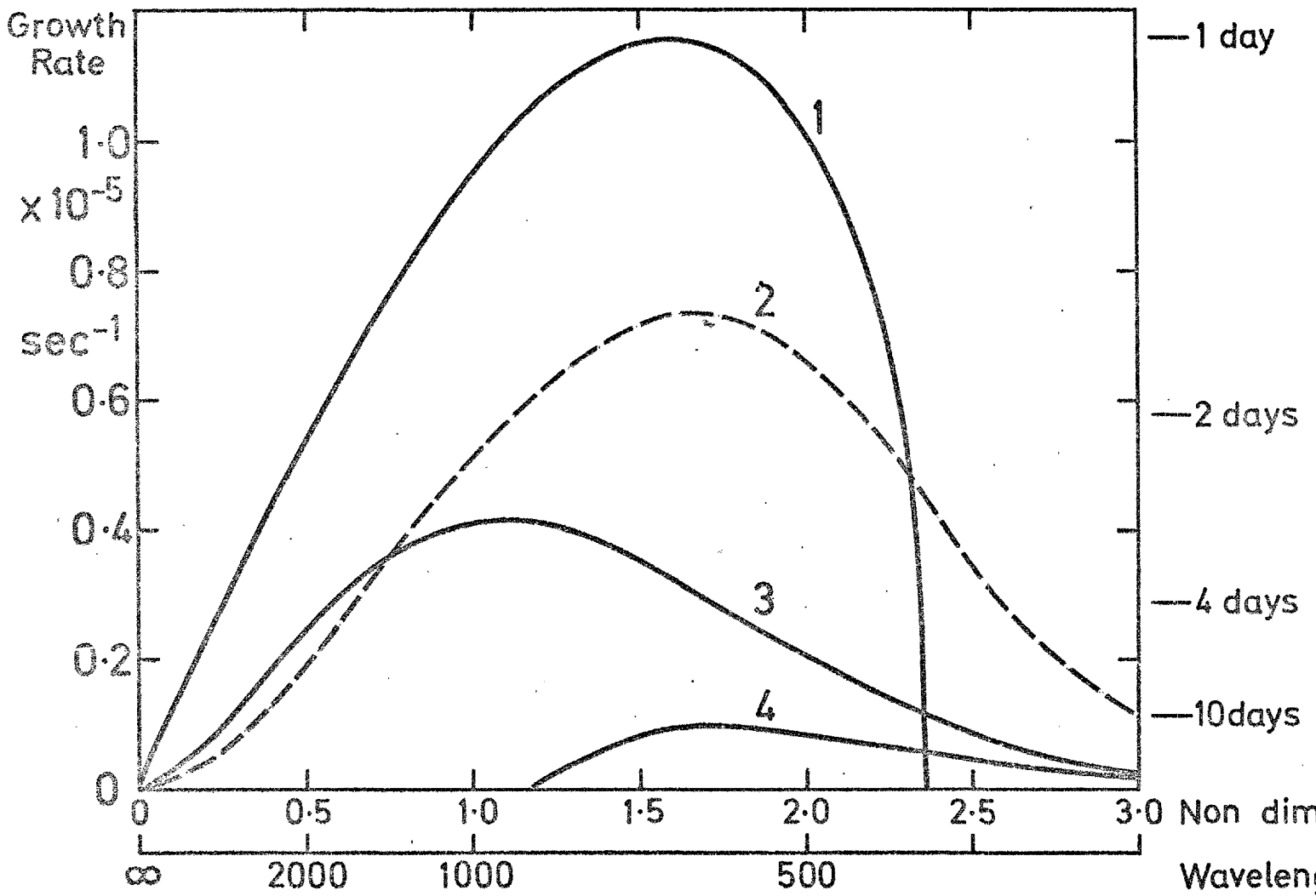


FIG. 4.6

EFFECT OF FRICTION AND SURFACE HEATING ON EADY'S MODEL

Growth rate versus wavelength

Shear = 6 m/s
Depth = 1·6 km

1 Surface wind speed (U_o) zero (no heating or friction)

2 Heating only U_o = 15 m/s

3 Friction only U_o = 15 m/s

4 Friction and heating U_o = 10 m/s

$$-\alpha\,\delta\phi_{z=0} = \frac{D}{Dt_h}\delta\phi + v\frac{\partial\phi}{\partial y} + wB \qquad \text{———(4.7)}$$

As in §2.1 we can express ϕ in terms of the streamfunction ψ via the thermal wind equation and substitute for w in the vorticity equation (2.2a) via Eq.(4.7), giving

$$\frac{D}{Dt_h}\left\{\nabla_h^2\psi + \frac{f^2}{gB}\frac{\partial^2\psi}{\partial z^2}\right\} = -\frac{f^2}{gB}\left(\frac{\partial\psi}{\partial z}\right)_{z=0}\frac{\partial\alpha}{\partial z} \qquad \text{———(4.8)}$$

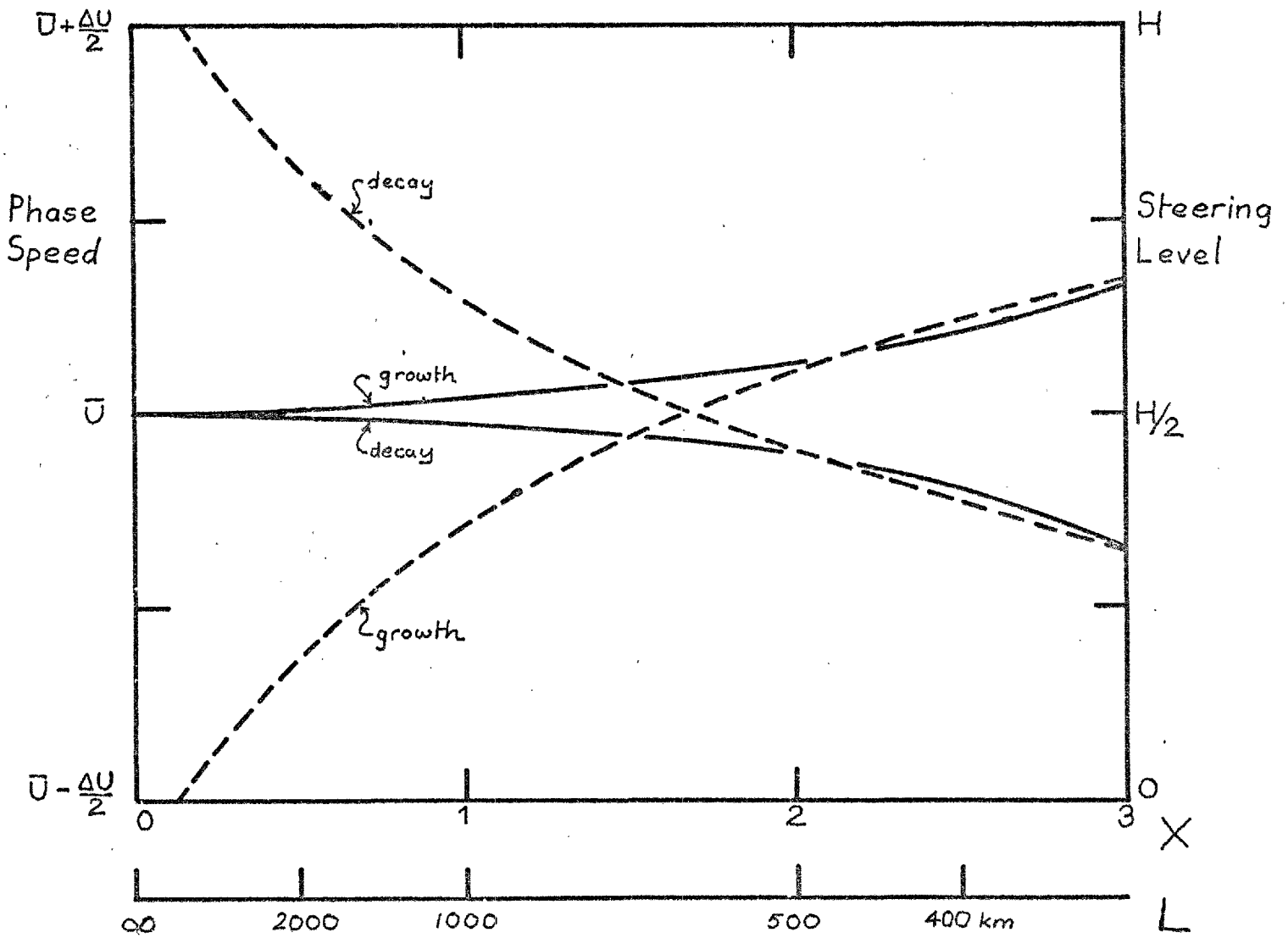
α depends on z only through $(p_*/p)^{R/c_p}$ and as we have shown earlier this is nearly constant, so we can put the RHS of Eq.(4.8) equal to zero. The heating now appears only in the boundary conditions and the solutions are therefore similar to those for the frictional waves discussed in Chapter III, and we do not include the details of the solutions here.

A graph of growth rate against wavelength (Fig.4.6) shows that as anticipated in §2.23 the growth rate is reduced but not so drastically as by the addition of friction. This is in agreement with the results obtained by Winn Nielsen et al (1967) with their two-layer model. The maximum growth rate is shifted towards shorter waves as expected since the longer the wavelength, the longer the air is heated (or cooled) and therefore the greater the damping.

Again we have the surprising result that the addition of heating, like that of friction, causes the neutral short waves to grow. Eq.(4.7) shows that at the boundaries, where w = 0, the addition of heating adds an entropy field in antiphase with that at the surface. In middle levels the heating (or cooling) produces a compensating vertical motion. The effect of this on the short waves depends on the height of the phase change of the entropy field (see §3.4). As this vertical velocity is

FIG. 4.7

Phase speed versus wavelength (L) friction and heating (solid lines) heating only (pecked lines)



in antiphase with the surface entropy, where the phase change is in upper levels the main effect will be a negative correlation of warm and ascending air, and a positive correlation when it is near the surface. Since the heating is proportional to the surface entropy field and this is greatest when the phase change is highest, the negative correlation is more pronounced than the positive correlation. Hence one wave decays rapidly while the other grows only slowly.

Fig.4.7 shows the phase speed of the waves as a function of wavelength. The maximum vertical velocity and hence the steering level is close to middle levels since the heating introduces a vertical velocity at middle levels.

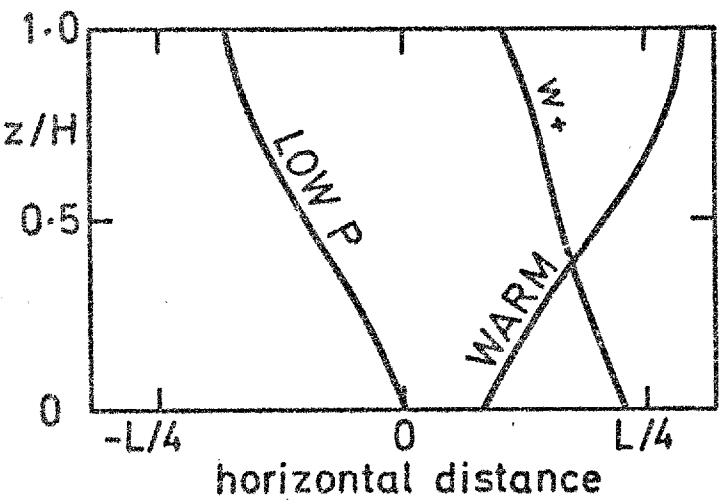
The structure of the fastest growing wave is shown in Fig.4.8. The addition of the heating in antiphase with the surface entropy field shifts the warmest air away from the pressure minimum and the vertical velocity maximum at upper levels. This reduces the correlation between the warm and ascending air and therefore reduces the efficiency of conversion of potential into kinetic energy and the growth rate.

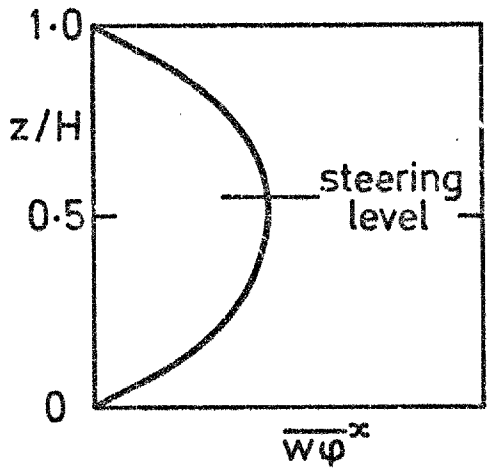
4.6 The effect of friction and heating

Friction can easily be added as in Chapter III by altering the lower boundary conditions. The solutions again have the same form.

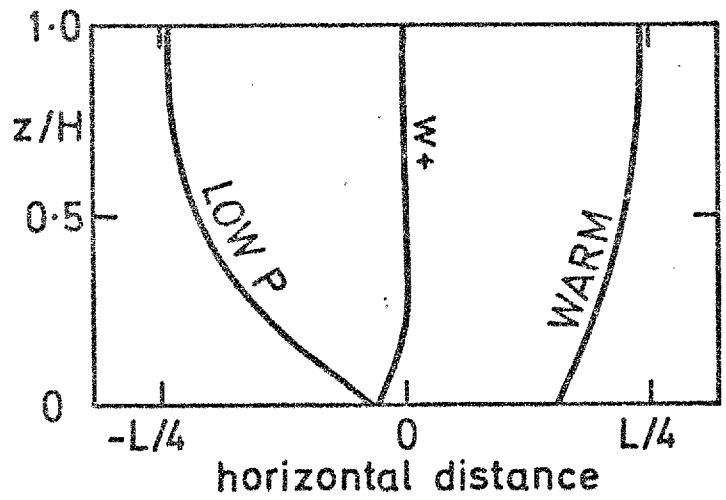
However the damping is considerably increased; indeed the waves do not grow at all for surface wind speeds in excess of 15 m/s. The structure of the wave (Fig.4.8) is similar to that with just friction included (Fig.3.2). Although, as with friction only, the maximum correlation of the warm and ascending air

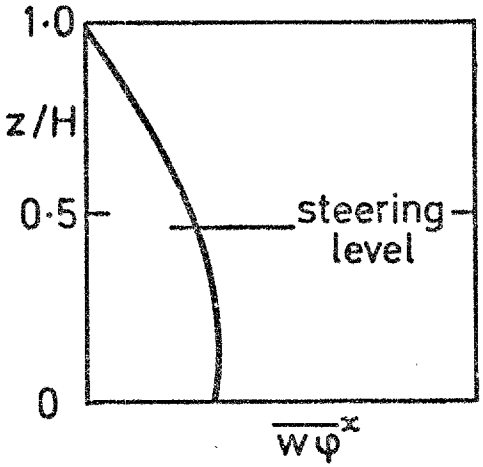
FIG. 4.8
Variation of phases and vertical entropy transport with height





(a) Heating only
U_0 = 10 m/s
(max. growth rate)





(b) Heating and friction
U_0 = 10 m/s

is near the surface, the addition of the vertical velocity at middle levels raises the maximum vertical velocity and hence steering level to near this level. Therefore, unlike the other cases considered the maximum displacements do not coincide with the maximum correlation of ϕ and w and the efficiency is greatly reduced. For strong winds, even though the correlation is everywhere positive the energy released is not sufficient to overcome the damping.

We predict that polar lows will not grow in regions of strong winds or where the flow is nearly parallel to the sea isotherms.

CHAPTER V Comparison of the model with the case study of December 1967

5.1 The data

The data on which these analyses are based is teleprinter data obtained from the Meteorological Office for channels I (U.K.) and II (Europe), supplemented at 00Z at the edge of the area studied with upper-air data from the Northern Hemisphere Data Tabulations. The teleprinter data includes all upper-air reports, all British surface reports and nearly all European surface reports. Analyses have been compared with British and German Daily Weather Report charts to ensure that at the boundaries of the area covered they are consistent with the surrounding areas.

5.11 Upper air data

The average spacing of upper air stations around Iceland is 750 km, approximately the same as the wavelength of polar lows. It is not therefore possible to directly analyse the 3-dimensional flow in the developing system. The situation is somewhat better over the British Isles and with additional ascents at Pershore and use of Doppler radar, Harrold and Browning (1969) were able to obtain a picture of the flow in the mature phase.

Temperature soundings are available only at 12 hourly intervals (except at Keflavik; 6 hourly) and can be used only to determine the structure of the unperturbed flow. However, the 6 hourly wind observations, when combined in a time-section give an equivalent space separation of 300 km since the lows travel at approximately 15 m/s. This just enables the flow due to the lows to be resolved. Such a section at OWS I which is close to the track of lows is discussed in §5.3 and shows flow consistent with the baroclinic model.

5.12 Surface data

The spacing of surface stations is on average considerably less, but most of these stations are coastal and the data coverage over open sea is not much better than for the upper air reports. Ship observations, mainly from fishing fleets are largely clustered between Scotland and the Faeroes and close to the southwest coast of Iceland. Reports are hourly from U.K. stations and ocean weather ships and 3 hourly from other land stations. Ship reports other than from the ocean weather ships are sporadic and often only at 12Z. However, by using the pressure tendency and considerations of continuity between successive maps, the pressure field can be analysed with some confidence. This is not true of the wind field since, as will be shown in the following section, local effects make many of the observations unrepresentative of the large scale flow.

5.13 Surface winds

Many of the stations in the Iceland area are situated in fjords or on the edge of high ground and winds are likely to be considerably modified by local conditions. To demonstrate this the observed surface winds have been compared with a predicted surface wind, calculated by adjusting the geostrophic wind to include the effects of friction as in Chapter III. Over the sea the stress divergence has been taken as constant up to a height of 800 m, the average height of cloud base. Over land, since here the air is stable, as suggested in Chapter III the Ekman spiral type approach has been used with $z_o = 3$ cm and $z_a = 50$ m.

Fig.5.1 shows the vector mean vector difference of the observed minus the calculated surface wind for every 6 hours

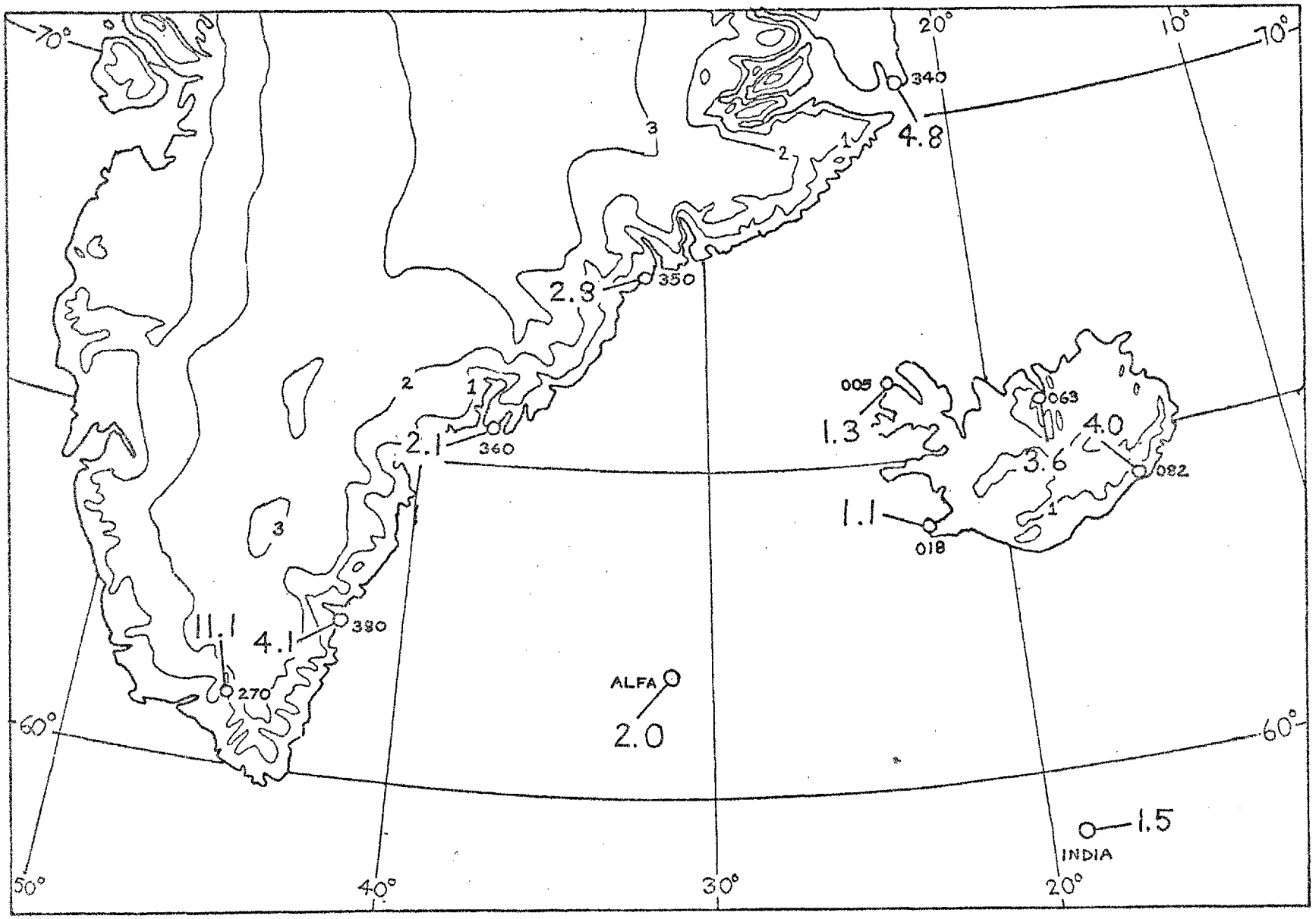


FIG. 5.1 Average vector difference, observed minus estimated surface wind Dec 6-8 1967 and positions of stations. (Thin lines are contours of land surface at 1000m intervals.)

for the period 06Z 6 December to 00Z 9 December 1967 from various stations. The thin lines show the contours at 1000 m intervals of land surface. The largest differences occur at stations close to high ground. (The values at Aputiteq (04 350) and Angmagssalik (04 360) on the Greenland coast, although small in absolute terms are large when compared to the mean wind there.) Akureyi (04 063) and Hornafirdi (04 084) in Iceland show a tendency for the air to flow off the high ground, whereas the Greenland stations show differences in the opposite direction to the predicted wind suggesting the main effect is sheltering. The two ocean weather ships, Alpha and India, and the two stations on Iceland (04 018, Keflavik and 04 005, Galtarviti) in open situations show much smaller differences from the predicted wind. This difference between the 'open' stations and the sheltered ones is emphasised when the components of the calculated and observed winds are plotted separately for both sets of stations. The four 'open' stations show good agreement between observed and calculated winds (Figs.5.2 b, 5.3 b) whereas for the other stations there is little connection between the observed and calculated (and hence geostrophic) winds (Figs.5.2 a, 5.3 a). We must conclude that local effects dominate the surface winds at these stations and therefore they cannot be used to obtain wind fields for large scale motion.

5.14 The surface pressure field

The pressure field will also be affected by katabatic winds and other local effects. The following shows, however, that these effects are small enough to be ignored. We consider pressure deviations due to the hydrostatic effect of local cold air and due to the dynamical effect of local winds. If the average

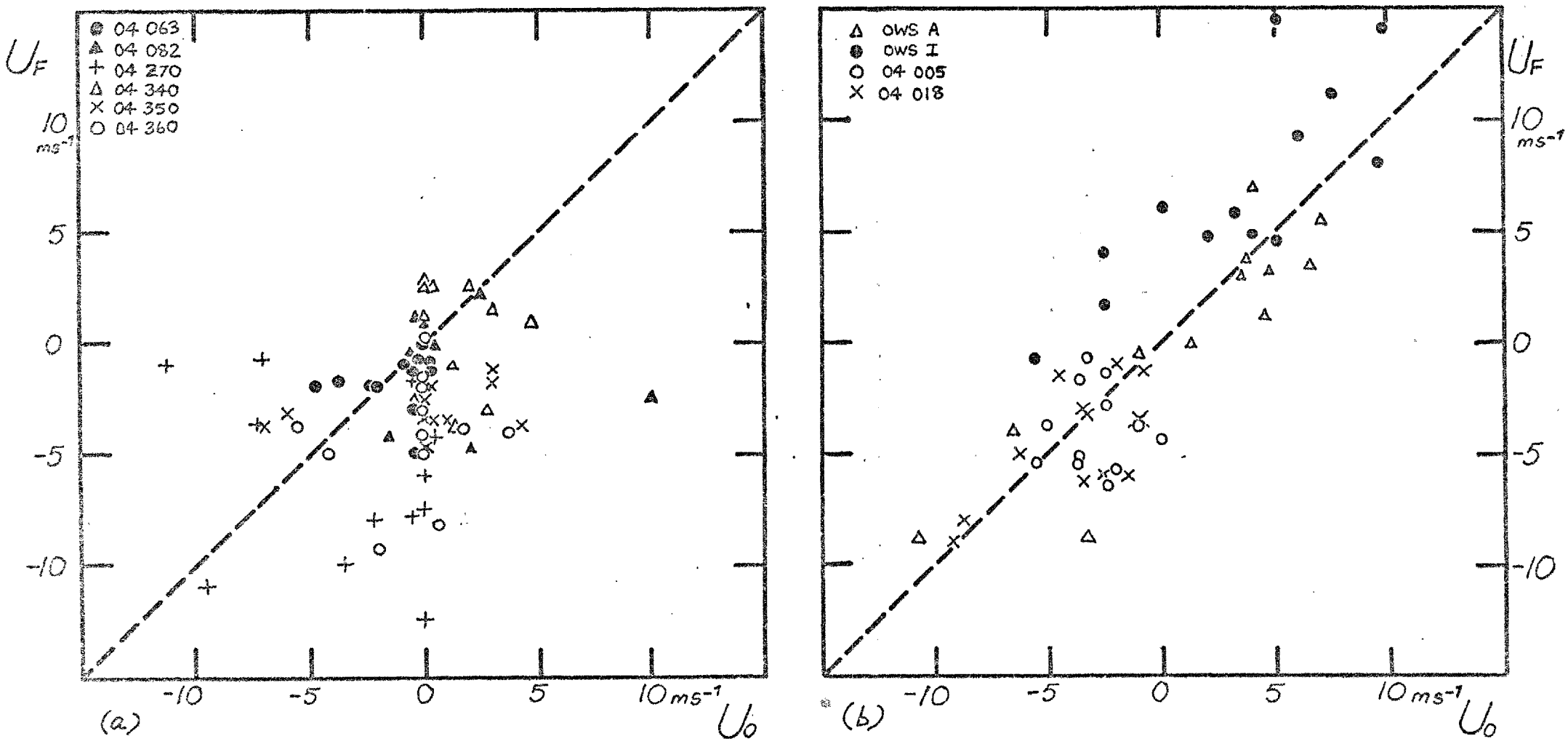


FIG. 5.2 Comparison of westerly components of observed surface wind (U_0) and calculated surface wind (U_F), (a) for 'sheltered' stations (b) for 'open' stations.

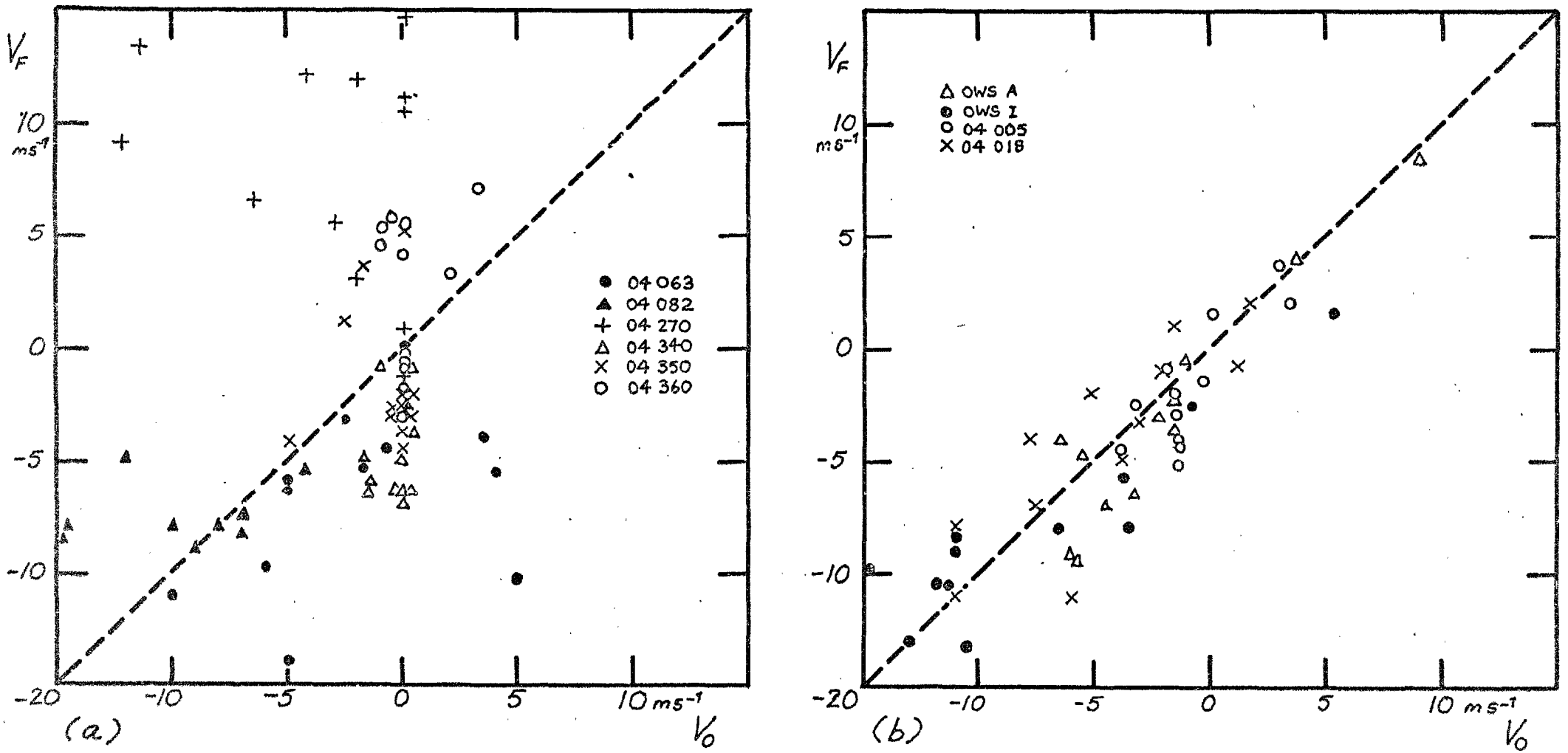


FIG. 5.3 Ditto but northerly instead of westerly, V_0, V_F instead of U_0, U_F.

temperature of a column of air of height h is changed by ΔT, then if the pressure at the top of the column (p_o) is unchanged, as long as gh/RT_o is small (i.e. $h \lesssim 1$ km), and $\Delta T/T_o$ is small, the change in the pressure at the bottom is given by

$$\Delta p \simeq p_o gh\Delta T/RT_o^2 \qquad \text{——(5.1)}$$

where T_o is the average temperature of the column. Some Greenland stations report strong surface inversions and if these are only local they will cause unrepresentative surface pressures. In this case ΔT in Eq.(5.1) is the average temperature difference between the observed sounding, and the sounding produced by extrapolating the lapse rate above the surface inversion. Δp is then the amount by which the surface pressure is unrepresentative. Taking two extreme cases

(a) Kap Tobin $\Delta T = 7.5°C$

12Z 7 December $h = 150$ m

giving $\Delta p = 0.6$ mb

(b) Angmagssalik $\Delta T = 2\ °C$

00Z 7 December $h = 400$ m

giving $\Delta p = 0.4$ mb

The maximum dynamic pressure ($=\frac{1}{2}\rho v^2$) is that obtained if the air is brought to rest from speed v. This is only 0.7 mb for a wind of 10 m/s but increases rapidly with higher wind speeds. Winds of up to 20 m/s occur on the large scale which could give dynamic pressures as high as 2 mb. However, if the wind is this strong then this implies a large pressure gradient and the error is therefore less significant. Local winds of 10 m/s can be associated with local pressure deviations of 0.7 mb, but on the large scale,

because the wind is in approximate geostrophic balance, a pressure difference between two stations, typically 500 km apart, of 8 mb is needed to produce a 10 m/s wind. Thus whereas the errors in the wind field are as large as 100% those in the pressure field are less than 20%. We conclude that the pressure analyses discussed in the following section are reliable.

5.2 The pressure perturbation

As shown in the preceding sections the pressure field is more satisfactory than the velocity field for defining the disturbances. Since the synoptic scale pressure pattern changes much slower than that due to polar lows we can estimate the unperturbed pattern and by subtracting this from the total field obtain the pressure perturbation due only to the developing low. This has been done every 6 hours for the case study of December 1967, enabling the growth and movement of the lows to be resolved. Figs.5.9 - 5.14 showing the perturbation and the unperturbed fields at 12 hourly invervals from when the first low was first detectable, and Figs.5.15 - 5.26 showing the total pressure field are included at the end of this chapter.

Consistent with their being waves with a well defined wavelength, the disturbances did not grow greatly in extent but grew rapidly more intense until they reached the British Isles when they began to decay. The perturbation to the north of Scotland in Fig.5.14 appears to be a third disturbance. It again appeared as a shallow feature moving with the low level wind. It first became evident as it passed close to Jan Mayen, but could have originated south of Spitzbergen where surface winds were lighter, as it can not be resolved by the very sparse data in the area. It is significant that, in accordance with the model,

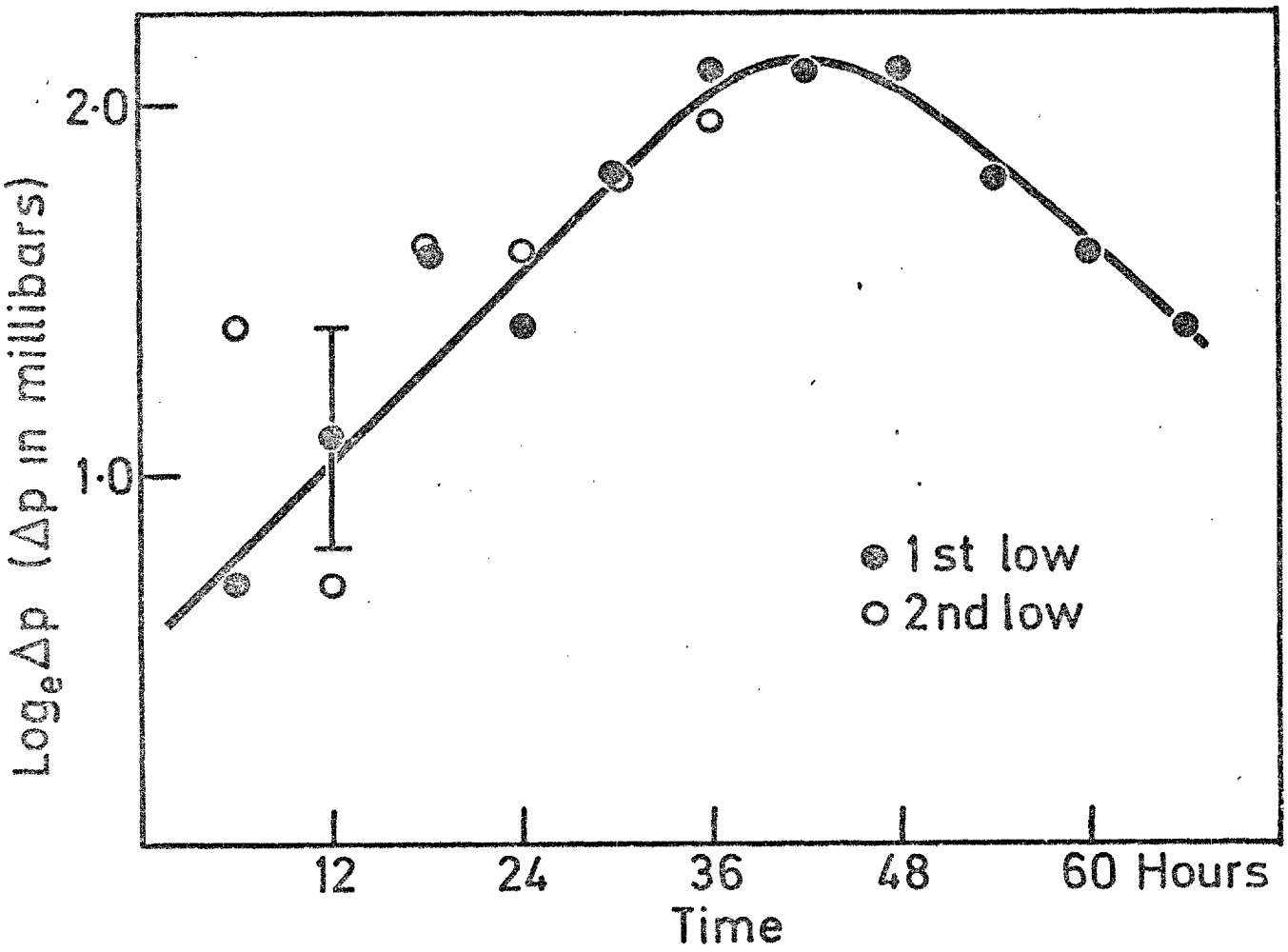


FIG. 5.4

Observed growth in depth of pressure perturbation of the lows of Dec. 1967

as the surface wind was strong and the flow almost parallel to the sea isotherms, it did not grow significantly and had already begun to decay before reaching the British Isles. A plot of $\log_e$ of the maximum pressure perturbation (Δp) against time is shown in Fig.5.4 . The error in Δp is large while the disturbance is over the sea but decreases as the lows cross the network of British stations. An estimate of the error due to analysis (shown in Fig.5.4) has been obtained by reanalysing one surface chart some months after the initial analysis, without reference to it, and comparing the results. A growth time of about 24 hours is indicated for both lows, which is very close to the predicted value for light winds and distinctly less than the 4 days predicted for moderate wind speeds. The phase speed and wavelength were determined by comparing successive positions of low centres and the separation between them. The error in the wavelength is estimated as ± 100 km and in the phase speed as ± 4 m/s. As the first low moved southeastwards and grew in vertical extent, it moved faster because of the stronger winds in this region, and the apparent wavelength increased from about 650 km to 1100 km. Clearly the wavelength is not related to one appropriate to the whole of the troposphere, nor to the upper baroclinic zone and indeed the initial value of about 650 km is strikingly close to that predicted by the theory. The extension to 1100 km is consistent with the increase in speed of travel from about 6 m/s initially to 20 m/s as the lows pass OWS I. As the surface wind increases friction becomes more important but the increase in vertical extent counteracts this effect somewhat and allows the latent heat release to become important so that the waves continue to grow. The change from growth to decay can be predicted to occur as the lows reach Britain both because here the low level

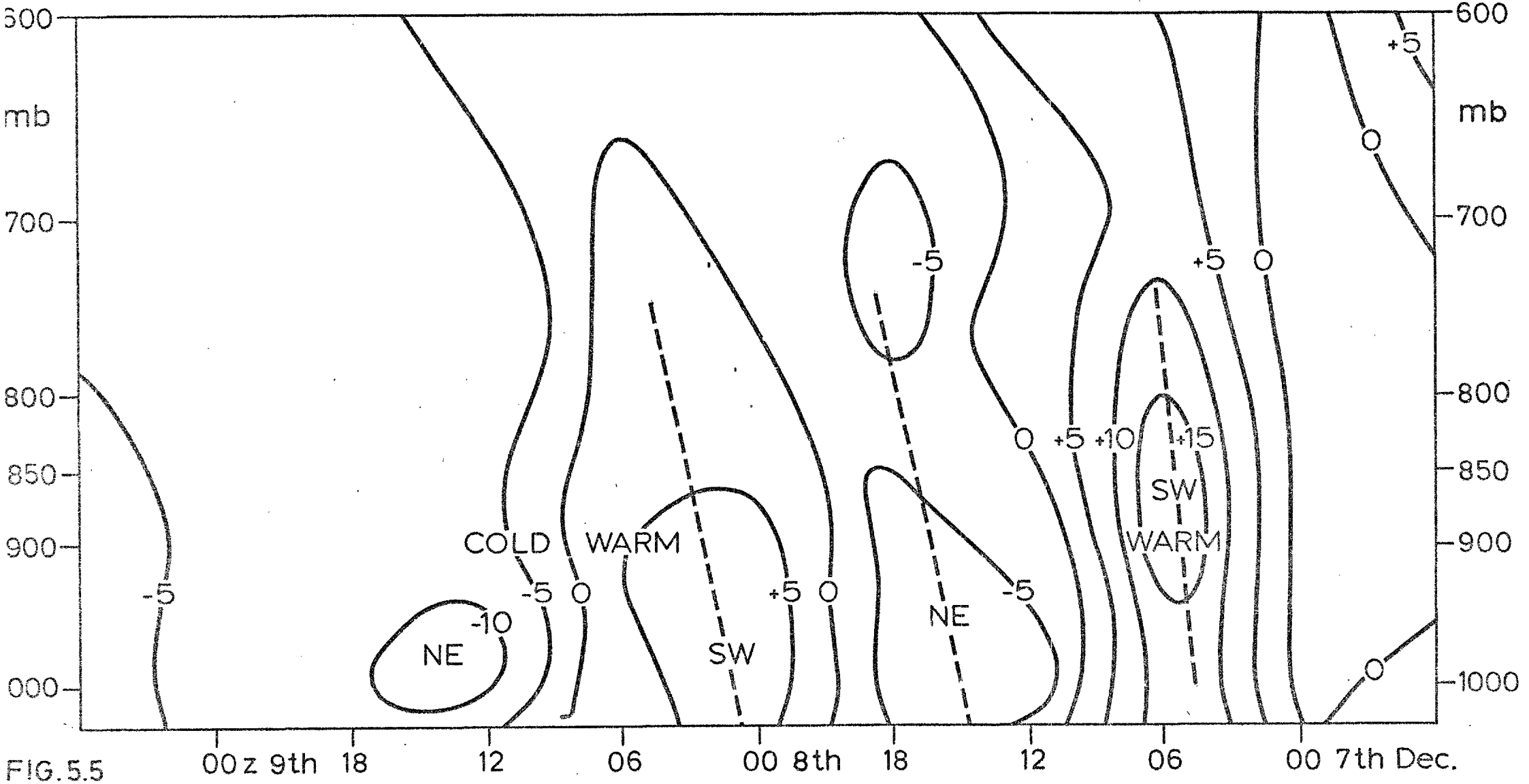


FIG. 5.5 Time-height section at OWS I. Isopleths of wind speed (m/s) perpendicular to track of lows.

baroclinity becomes small and the vertical convection is stopped. The initially low phase speed indicates a low steering level and with the short wavelength explains the importance of low level baroclinity. Since the observed winds are unrepresentative and also affected by the growing disturbance the surface wind to be used in the model is estimated from the unperturbed pressure field. The value of 3 m/s ± 1 m/s obtained by this method implies a phase speed of 6 m/s ± 1 m/s and again the model is in excellent agreement with the observations.

5.3 The time-section at OWS I

The structure and vertical extent of the lows of the case study has been investigated by constructing a time-height section from pilot balloon and radio-sonde ascents as the lows passed OWS India. Fig.5.5 shows the section with isopleths of the wind component perpendicular to the direction of travel of the lows, and shows very clearly that the disturbances are confined to below 700 mb. There is also some evidence for the trough line sloping backwards with height. The model predicts that the upper trough should lag the surface low by a quarter of a wavelength or 6 hours (Fig.3.2) and it is marginal whether 6 hourly ascents can resolve this. Between 12Z and 18Z on the 7th and 00Z and 06Z on the 8th the maximum transverse wind component shifts from the earlier to the later ascent with increasing height, suggesting a backward sloping trough line. This is not shown at 06Z on the 7th because here the maximum occurs at middle levels during the ascent at 06Z and is too far away to be detected at either the top or bottom of the layer at the times of the preceding and following ascents.

The temperature structure can not be resolved by the 12-hourly radio-sonde ascents; however, an estimate of a smaller

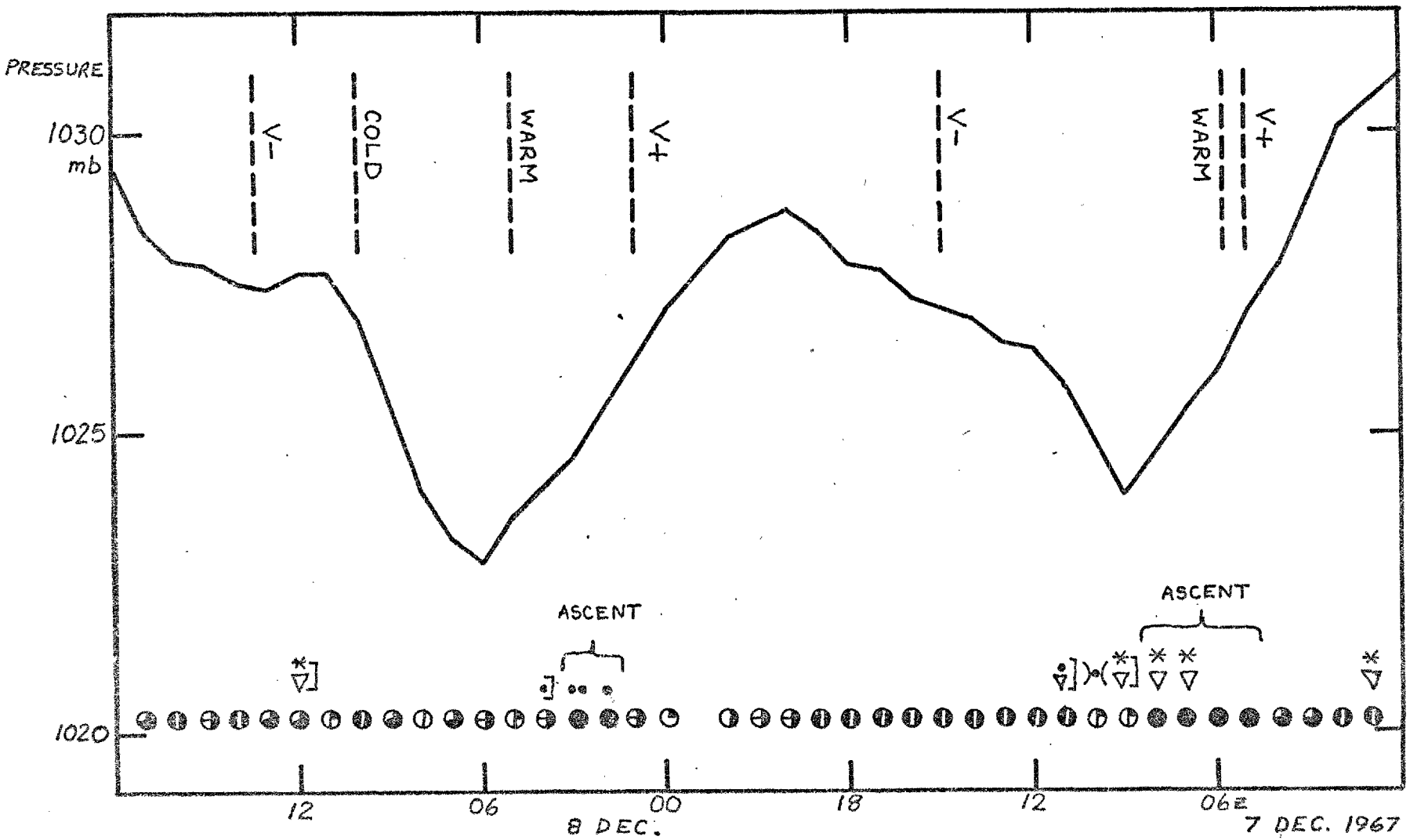


FIG. 5.6 Surface pressure at OWS I against time, showing observed cloud amount and significant present weather. Pecked vertical lines show phases of the perturbation wind and temperature fields.

scale pattern can be obtained using the 6-hourly pilot-wind data and assuming the thermal wind equation is obeyed. From this we find that warmest air coincides with the 'northward' moving air and the cooler air with 'southward' moving air, consistent with the baroclinic model. (The more obvious temperature maxima and minima are shown in the figure.)

An indication of the sign of the vertical velocity is given by the cloud amount and presence of precipitation. Fig.5.6 shows hourly observations of surface pressure, cloud amount and significant weather at OWS I for the period of the time-section. The continuous complete cloud cover between 05 and 08Z on the 7th and the consecutive showers reported at 07 and 08Z suggest general ascent as does the complete cloud cover and rain at 02 and 03Z on the 8th. Adding the maxima and minima of the wind components from Fig.5.5 we find a high correlation between the warm and ascending and northward moving air which is again consistent with the model.

5.4 The mature stage

Harrold and Browning (1969) have described the flow relative to the second of the two polar lows of this case study. They found ascending air ahead of the low and descent behind, consistent with a baroclinic disturbance. Surface analyses suggest that both these lows had warm air ahead and cold air behind the surface low. Since we have not been able to properly define the temperature structure of the growing wave, due to lack of data, an analysis of the temperature structure of the mature phase has been constructed from the large number of surface observations over the British Isles. Although the perturbation theory is strictly only applicable for small amplitudes, the structure of more or less mature

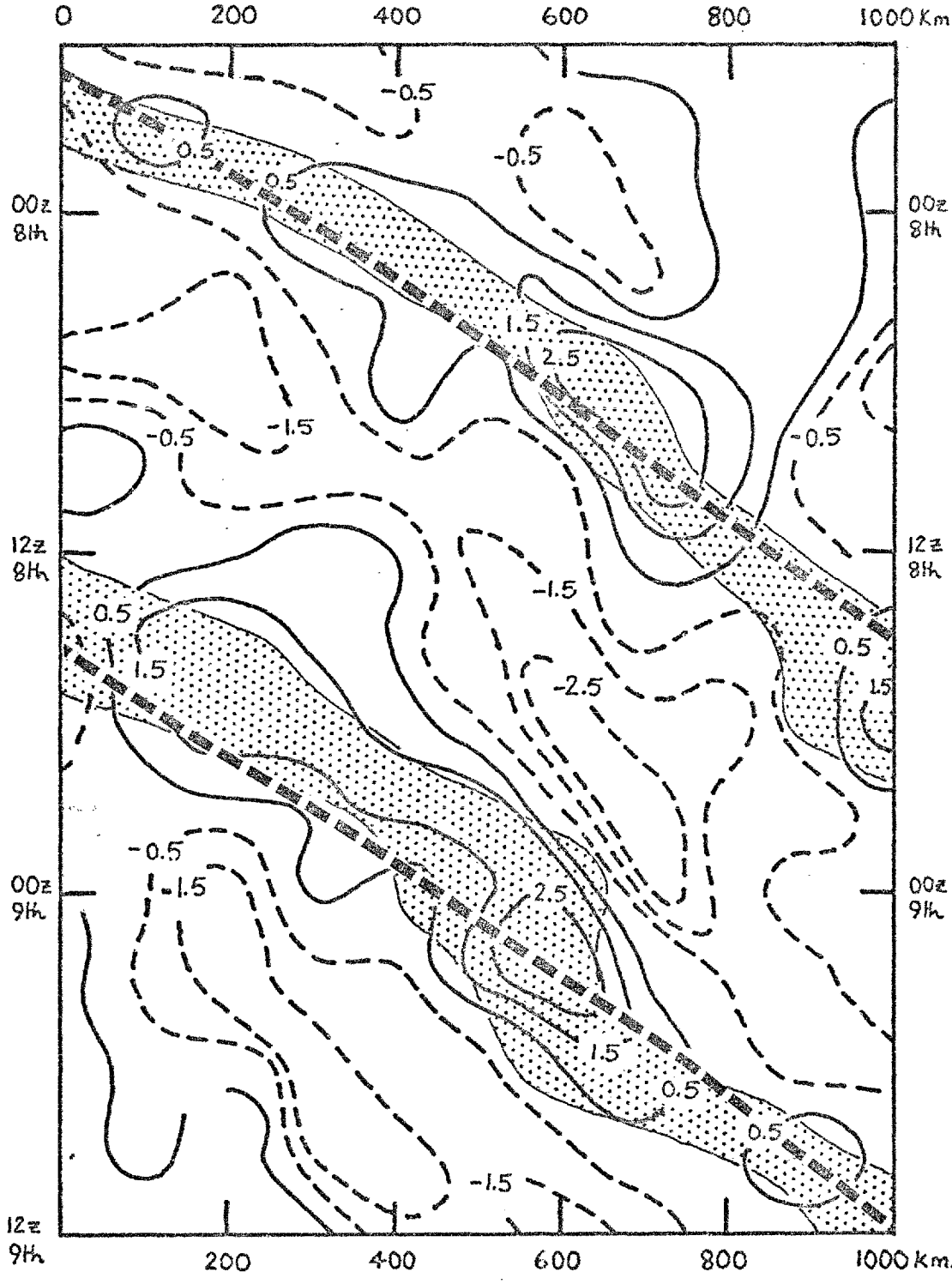


FIG. 5.7

Isopleths of temperature perturbation on a time-distance section across southern Britain. Stippled areas indicate non-showery precipitation and the thick pecked line the passage of the pressure minimum.

cyclone waves is observed to be similar to that according to the perturbation theory, and we can therefore make a useful comparison between the observed structure of the mature lows and the predictions of the model.

The surface temperature field around the British Isles is complicated by the alternation of sea and land along the track of the lows adding an alternating pattern of warm and cold independent of the travelling disturbances. There also appears to be a general cooling over the period, possibly due to radiation. To find the temperature structure due to the polar lows these other fields must be eliminated. The temperature field can be approximately represented by

$$T(x,t) = T_o(x,t) + T_1(x) + T_2(t)$$

T_o is the perturbation (to be found) and is approximately of the form $T_o \cos\omega(x - ct)$, T_1 is periodic in x and is due to alternating land and sea (i.e. Atlantic, Ireland, Irish sea, southwest England, English channel and France) and T_2 is the general cooling. The horizontal structure along the flow and the motion of the temperature field is displayed by plotting the temperature at different times along a fixed line parallel to the direction of travel of the lows. If we choose a line one wavelength long and a time period of two cycles, the averages in space and time of T_o vanish. By forming the time and space averages separately of the total field and subtracting them from it we obtain

$$T_o(x,t) = T(x,t) - \overline{T}^x(t) - \overline{T}^t(x) - \overline{T}_1^x + \overline{T}_2^t$$

but $$\overline{T}^{x,t} = \overline{T}_1^x + \overline{T}_2^t$$

hence $$T_o(x,t) = T(x,t) - \overline{T}^x(t) - \overline{T}^t(x) + \overline{T}^{x,t} \quad .$$

The R.H.S. can be found by taking the appropriate averages of the initial field and so $T_o(x,t)$ can be calculated.

The resulting temperature perturbation along a line through northern Ireland, south Wales and the Cherbourg peninsular is shown in Fig.5.7. The thin pecked and solid lines are isopleths of negative and positive temperature anomalies respectively. The stippled areas indicate non-showery precipitation and are taken to be indicative of large scale ascent. The thick pecked lines show the passage of the pressure minimum. Where moderate or heavy snow is falling surface temperatures average about 2°C lower than in surrounding dry areas. It is assumed this drop in temperature is due to a combination of melting and evaporation of falling snow, and therefore where moderate or heavy snow is reported the temperature has been increased by 2°C. The figure clearly shows an alternating pattern of warm and cold air moving southeastwards. The wavelength is 1000 km and the speed of travel is 13 m/s, consistent with the values obtained from the pressure analysis. The warm and ascending air are highly correlated, the ascent being close to the pressure minimum and the warmest air slightly in advance of it, except at the southeast edge of the section. This compares well with the predicted structure of a baroclinic wave in which friction is important (Fig.3.2b). The comparison can be expected to break down at the southeastern edge, as by this time the lows have begun to decay rapidly. Fig.5.4 shows rapid decay after about 48 hours, which corresponds to about the last 300 km in Fig.5.7.

5.5 Some statistics of polar low formation

The theory predicts that polar lows develop in cold air outbreaks only when the surface winds are light. To see if

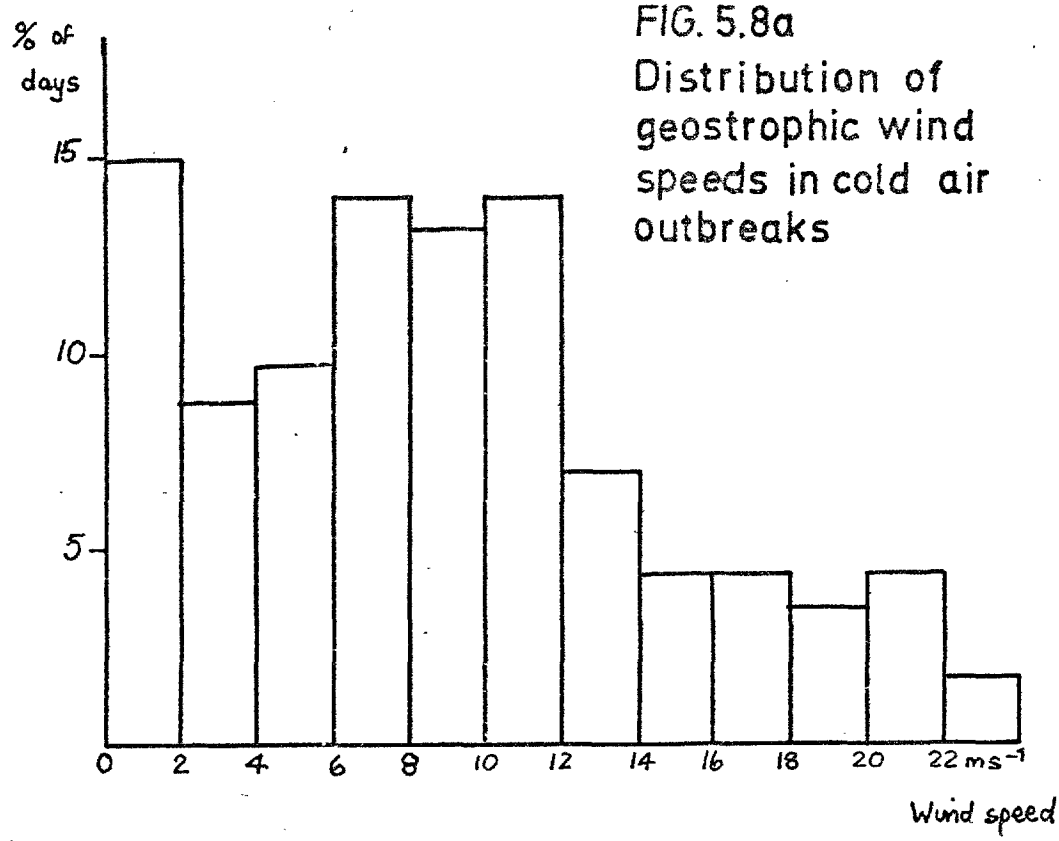


FIG. 5.8a
Distribution of geostrophic wind speeds in cold air outbreaks

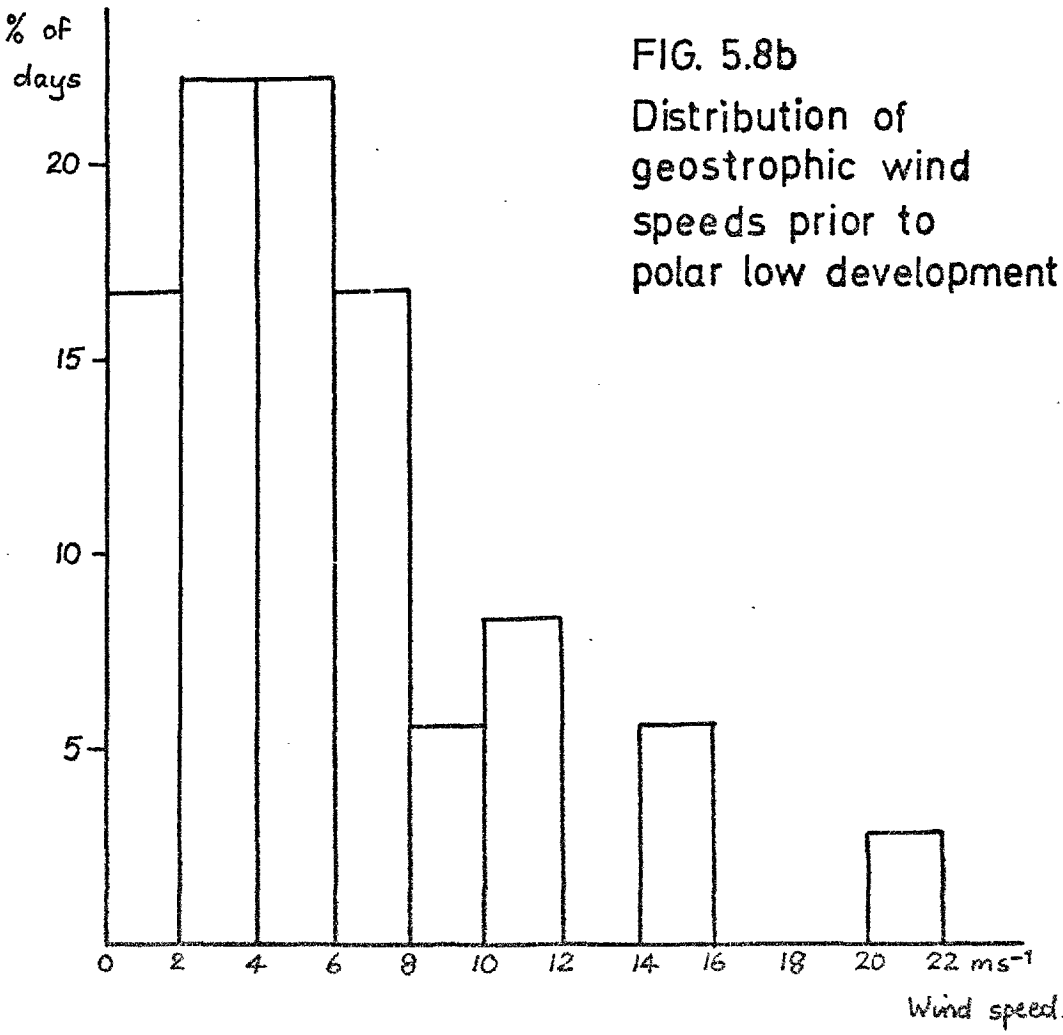


FIG. 5.8b
Distribution of geostrophic wind speeds prior to polar low development

there is any statistical evidence for this the occurrence of small travelling disturbances in the pressure pattern near Iceland, as analysed in British Daily Weather Reports for the years 1960-69 inclusive, have been investigated. 43 outbreaks of cold air have been studied totalling 114 days. The necessary conditions for an outbreak to be included are that the air flow is off the ice-sheet for a period of 48 hours or more so that a low-level baroclinic region may be expected to be present. During this time 36 disturbances were observed in 25 of the outbreaks, however, only 13 of these were sufficiently well developed to be traced as far as the British Isles. British Daily Aerological Report 500 mb charts were checked and any occasions when upper air troughs were present were ignored. This does not completely exclude the possibility of some of the disturbances being deep, as small disturbances are likely to be unresolved by the sparse upper air data.

The geostrophic wind was measured at 06Z and 12Z, averaged over about 200 km centred at 65°N, 30°W (approximately where most of the lows formed) for each day. When disturbances were observed the geostrophic wind was measured where they formed on the chart prior to their formation, except when this was more than 12 hours earlier, in which case the low was smoothed out and the smoothed geostrophic wind at that time measured. Fig.5.8 a shows the distribution of geostrophic wind speeds in all outbreaks (measured at 65°N, 30°W) and Fig.5.8 b the distribution prior to the formation of disturbances. The average wind speed for all occasions is 8 m/s, whereas 78% of the lows formed when the wind speed was below this. The large number of occasions when the wind speed was below 2 m/s is attributed to the passage of cols between depressions moving away east of Iceland and further depressions

approaching from the southwest. There is not a correspondingly large number of polar low occurrences since any development is soon swamped by the approaching depression. If we consider only the well developed lows which reached the British Isles; in all cases the winds prior to formation were less than 8 m/s and the average was only 4.2 m/s. Whereas this survey is based on routinely analysed charts and with very poor resolution in the vertical, it clearly supports the theory that significant polar lows develop only when the surface winds are light.

5.6 Summary

We have shown that the disturbances of 6-9 December 1967 were probably shallow baroclinic waves, the wavelength, phase speed and growth-rate being consistent with the predictions of perturbation theory for waves of this type. The shallow baroclinic region is formed by the heating of cold air flowing over a large sea-surface temperature gradient and disturbances growing in this region are confined to low levels by the sharp change in static stability at the top of the layer affected by the heating. Surface friction is extremely important because in general it causes damping that severely curtails the growth on those occasions when surface winds are strong. When the air is flowing parallel to the sea isotherms, heating from the surface causes serious damping which, when combined with strong surface winds can result in the damping out of all waves. This suggests that polar lows can be expected only when a shallow baroclinic zone coincides with light surface winds and the air flow is approximately perpendicular to the sea isotherms; such coincidence explains why polar lows are observed much less frequently than the cold air outbreaks in which they occur.

Polar lows are rarely observed on the eastern flank of cold air outbreaks, although there is in general a strong temperature gradient between air flowing off the ice-sheet north of Jan Mayen and air warmed rapidly over the warm waters along the coast of Norway. Maximum wind speeds (often in excess of 20 m/s) are observed in this region and the air flow is nearly parallel to the sea isotherms. The theory predicts no growth at all in this region and significantly, although a disturbance was detected there in the case study it did not develop even though the horizontal temperature gradient was at least as large as that southwest of Iceland. The initial development probably occurred undetected further north where lighter winds would allow a slight growth. Further support to the theory is given by the subsequent occurrence of a well developed polar low, again originating west of Iceland, in March 1970. This disturbance has been described by George (1972) and although he suggests it formed on the polar front, its development is so similar to those in our case study that it seems to us likely that it also originated within the polar air. The low steering level and shallow nature support this suggestion. Like the lows of December 1967 it originated in an area of light surface winds, moved slowly at first and then more rapidly as it moved into a region of stronger winds. When over southern England its growth was probably enhanced by an upper trough.

We conclude that only when light surface winds occur near Iceland during cold air outbreaks are polar lows likely to develop. Recognition of these results together with a careful analysis of the critical region and the use of infra-red satellite pictures might well lead to earlier detection and more accurate forecasting of the speed and direction of travel of this rare but troublesome phenomenon.

Figs. 5.9 - 5.14 show the division of the pressure field into the mean (thin lines) and perturbation (thick lines) components. The motion of the perturbation in the preceding 6 hours is shown by pecked arrows.

Figs. 5.15 - 5.26 show the total surface pressure field.

FIG. 5.9

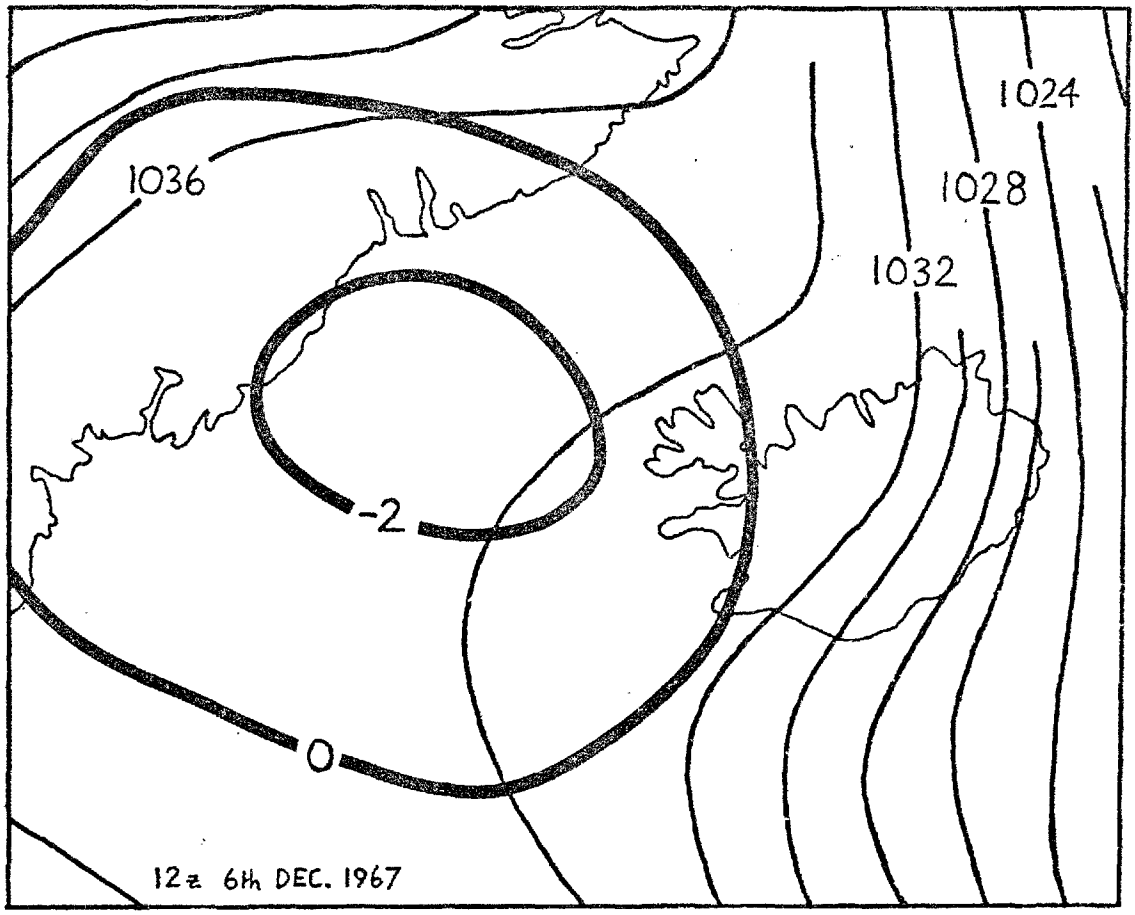


FIG. 5.10

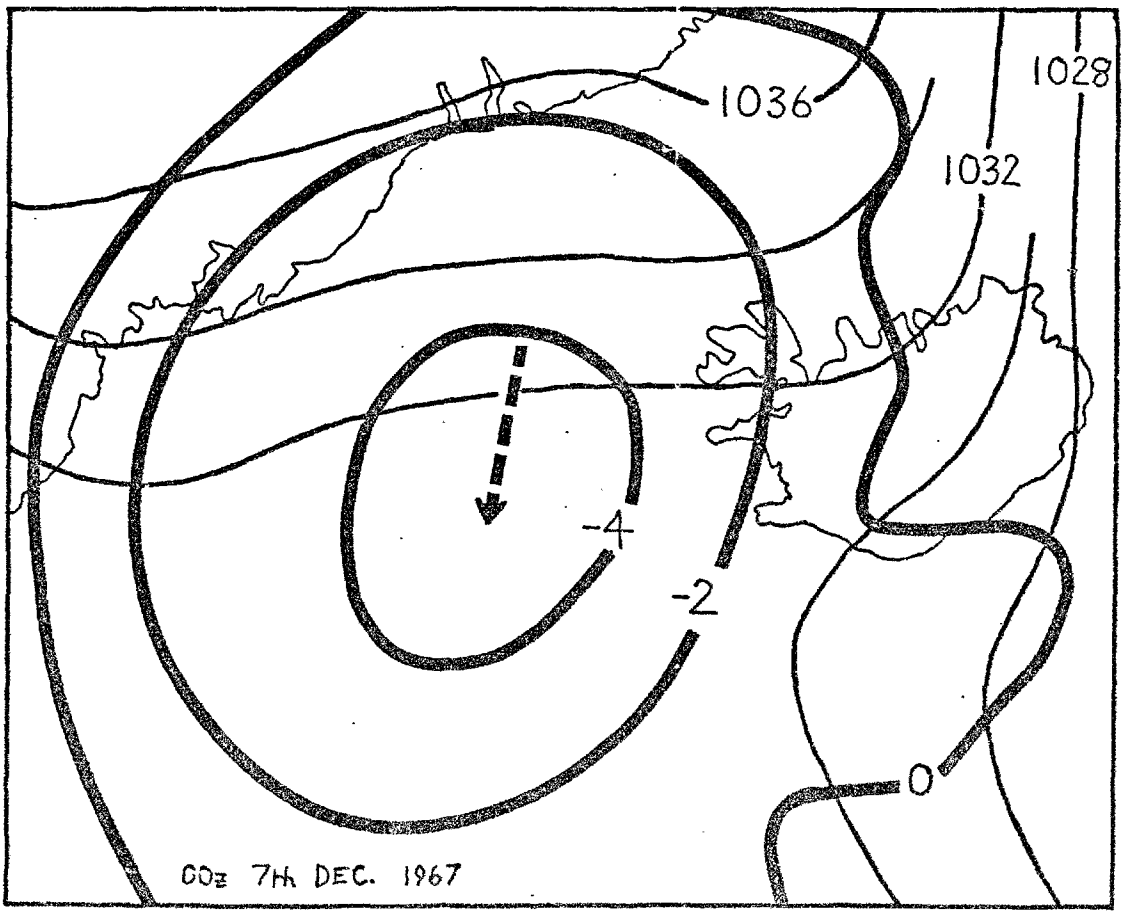


FIG. 5.11

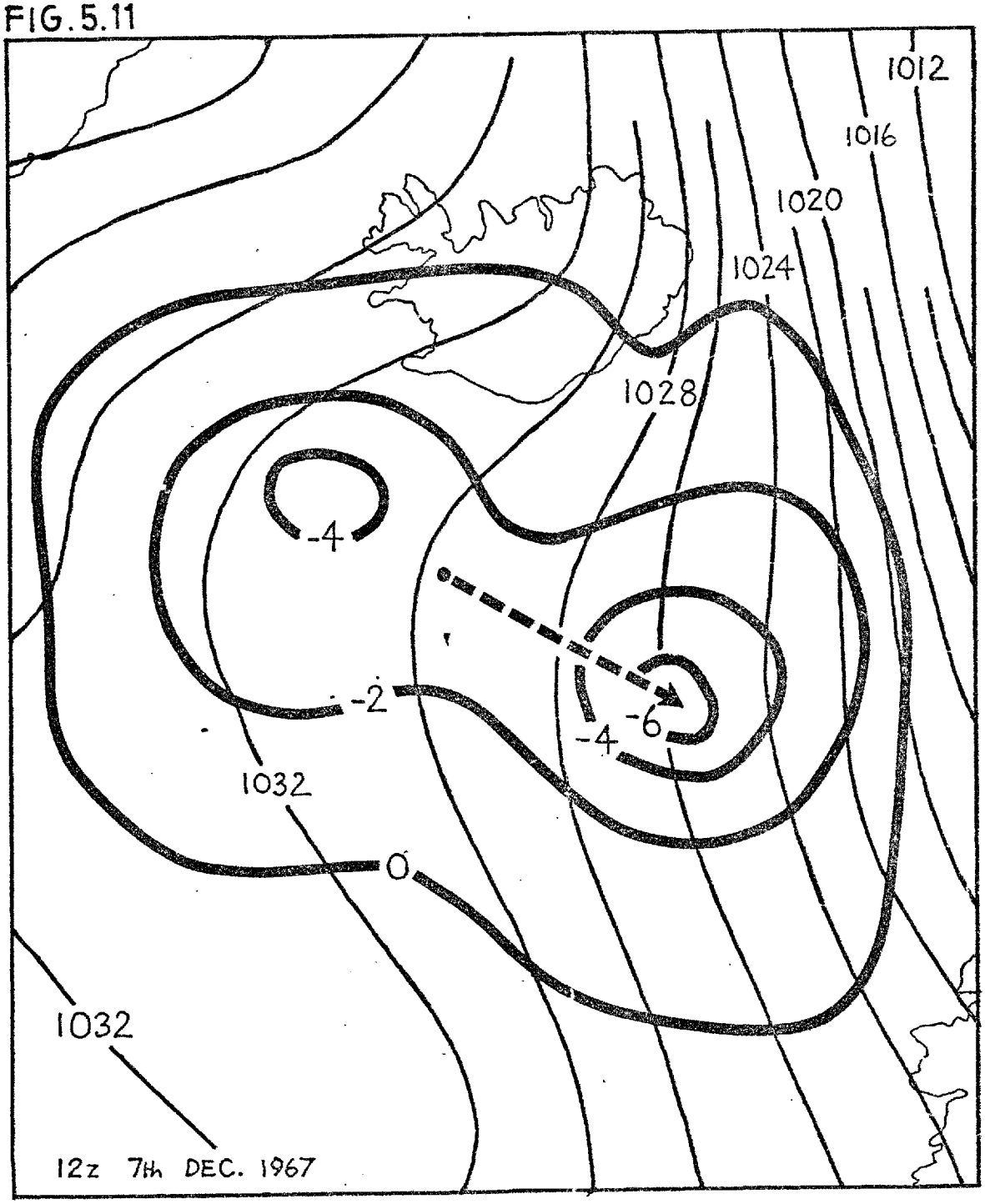


FIG. 5.12

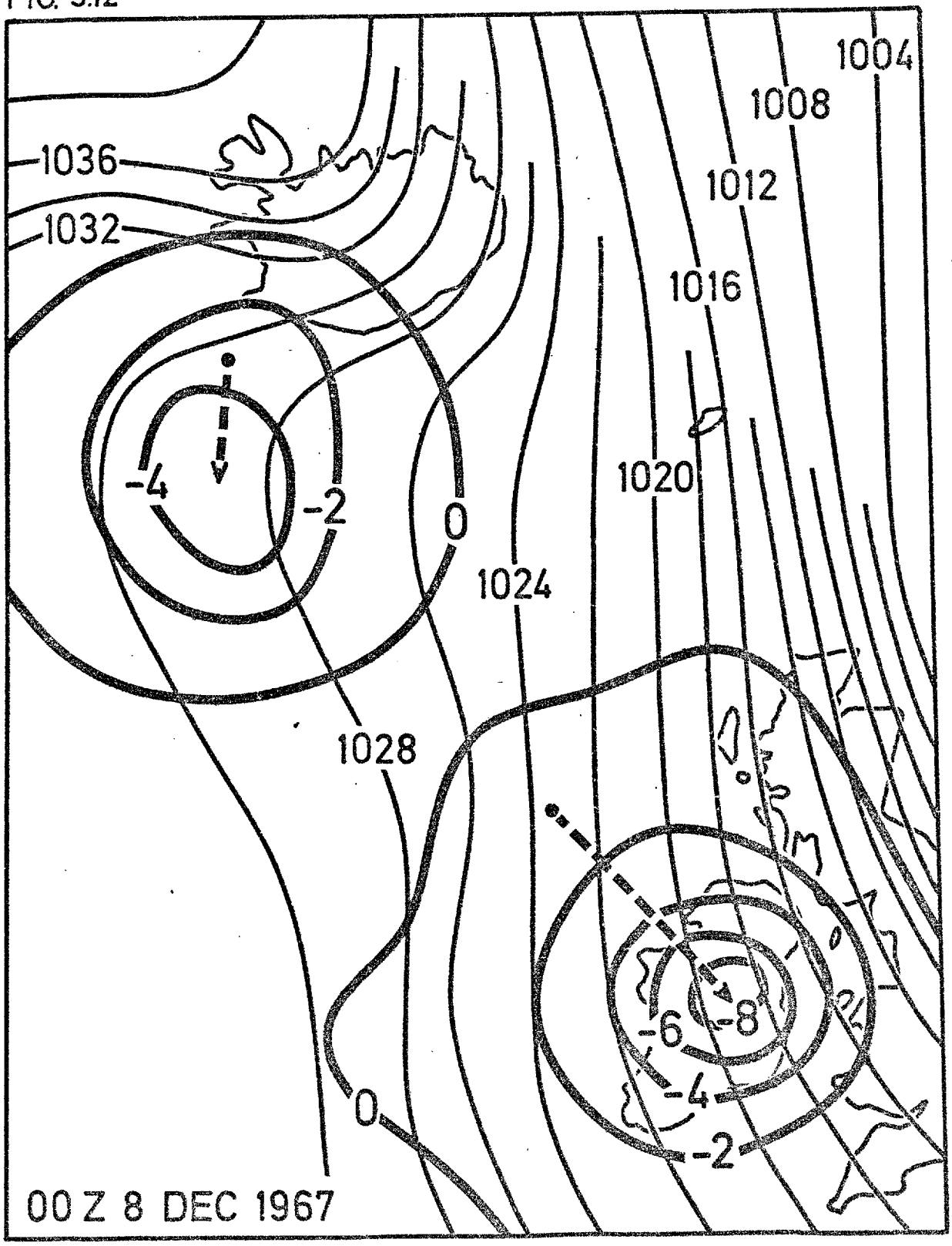

1004
1008
1012
1016
1020
1024
1028
1032
1036
-4
-2
0
0
-2
-4
-6
-8
00 Z 8 DEC 1967

FIG.5.13

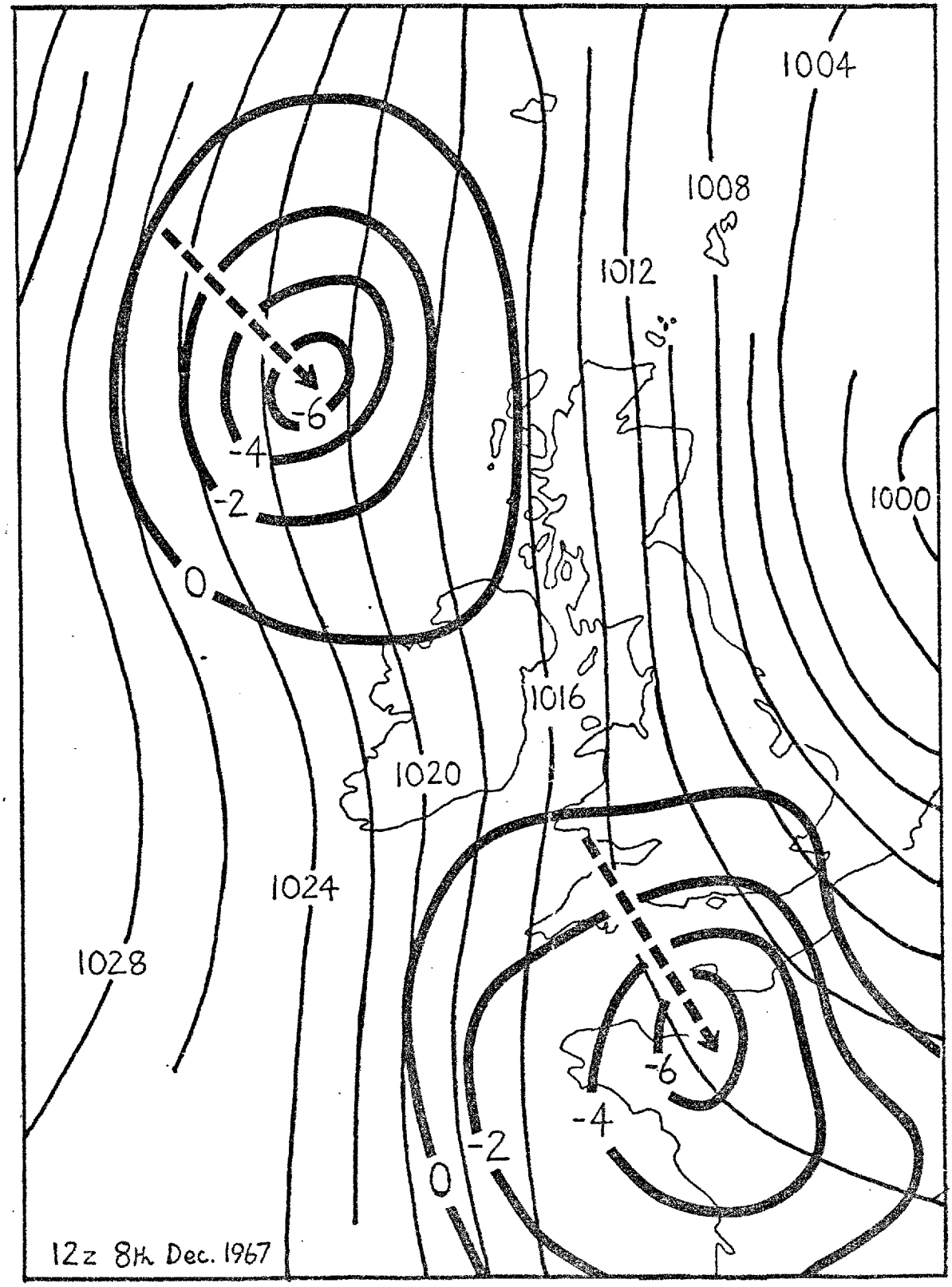
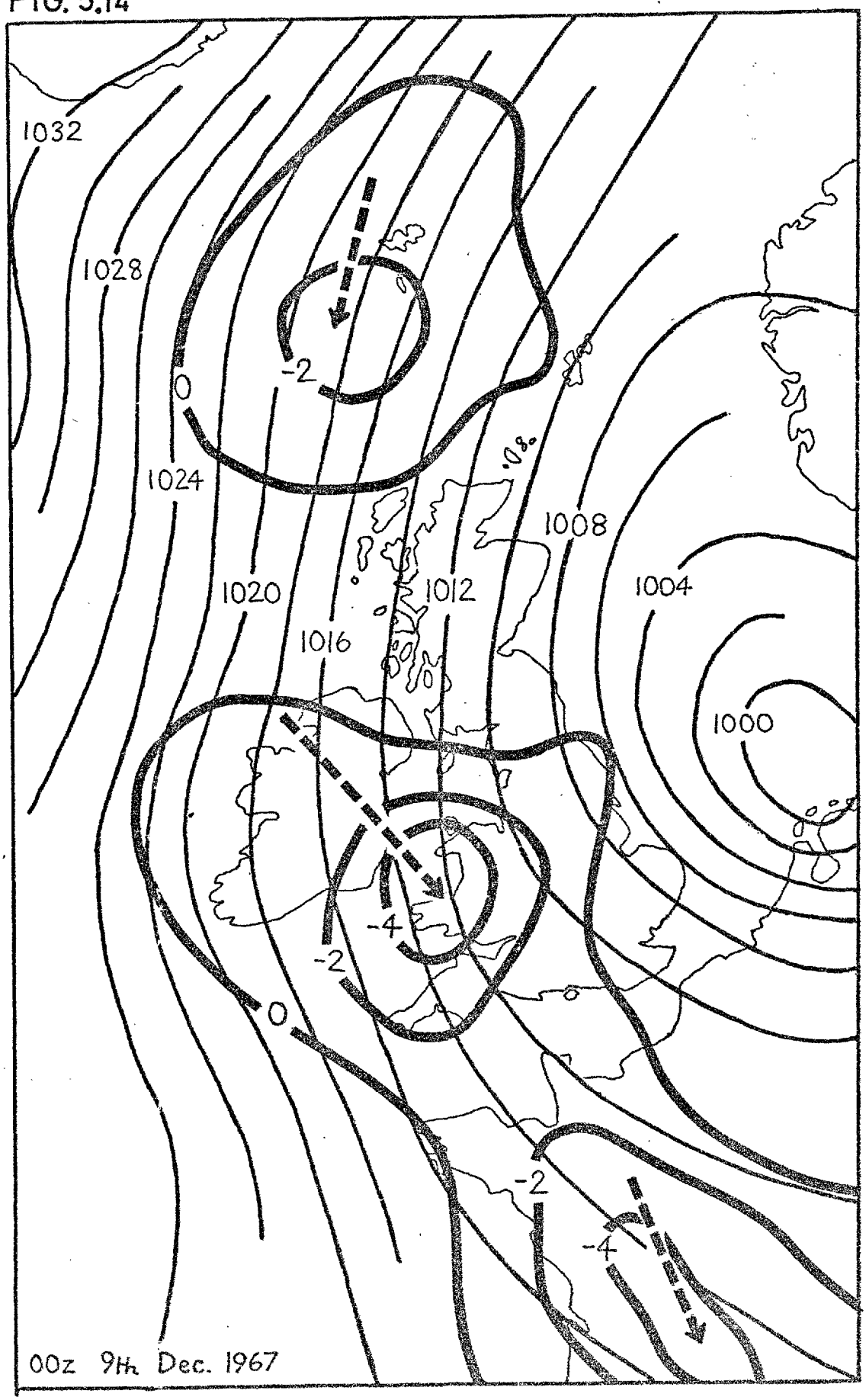

1004
1008
1012
1000
1016
1020
1024
1028
-6
-4
-2
0
-6
-4
-2
0
12z 8th Dec. 1967

FIG. 5.14


1032
1028
1024
1020
1016
1012
1008
1004
1000
0
-2
-4
00z 9th Dec. 1967

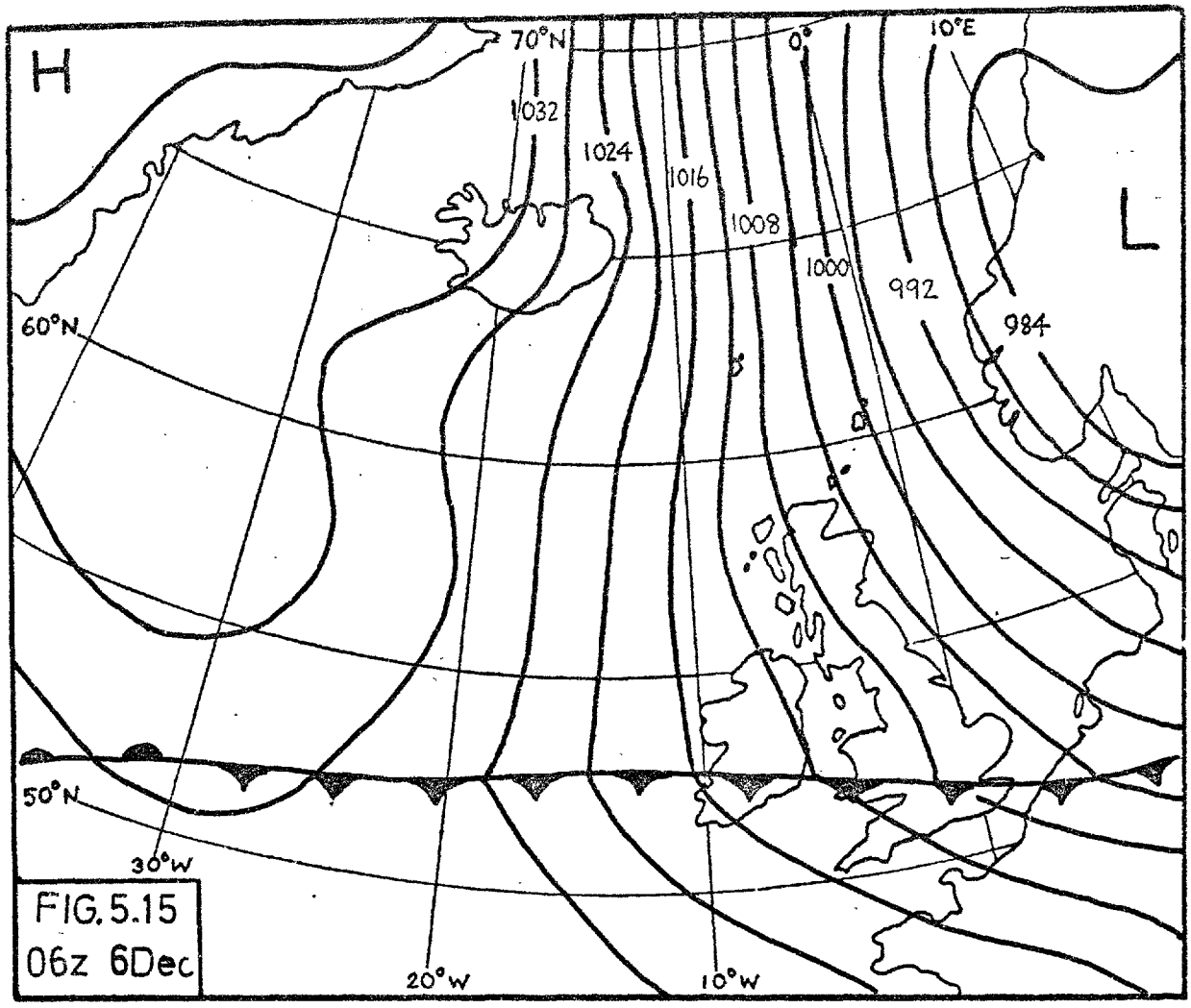


FIG. 5.15
06z 6Dec

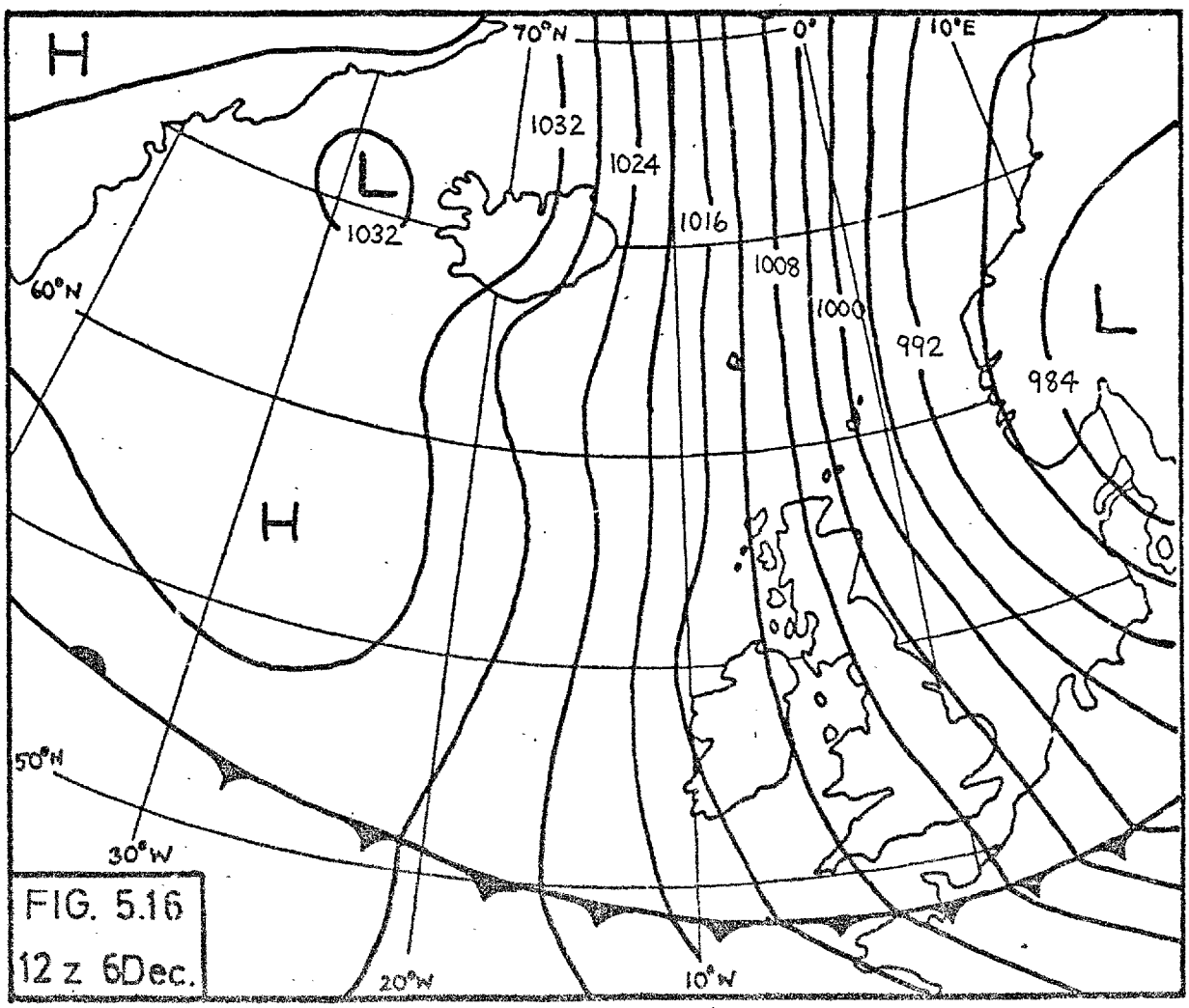


FIG. 5.16
12 z 6Dec.

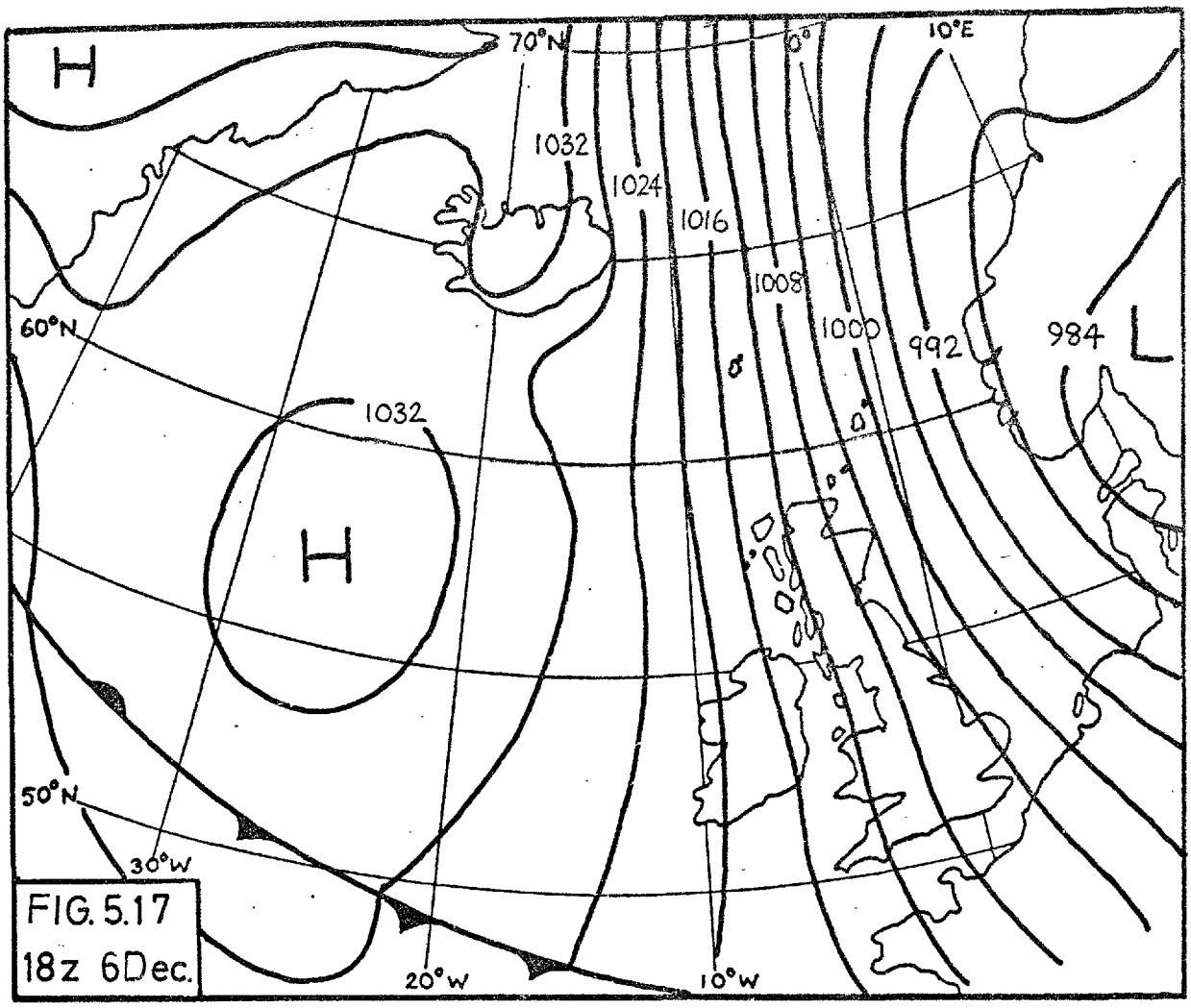


FIG. 5.17
18z 6Dec.

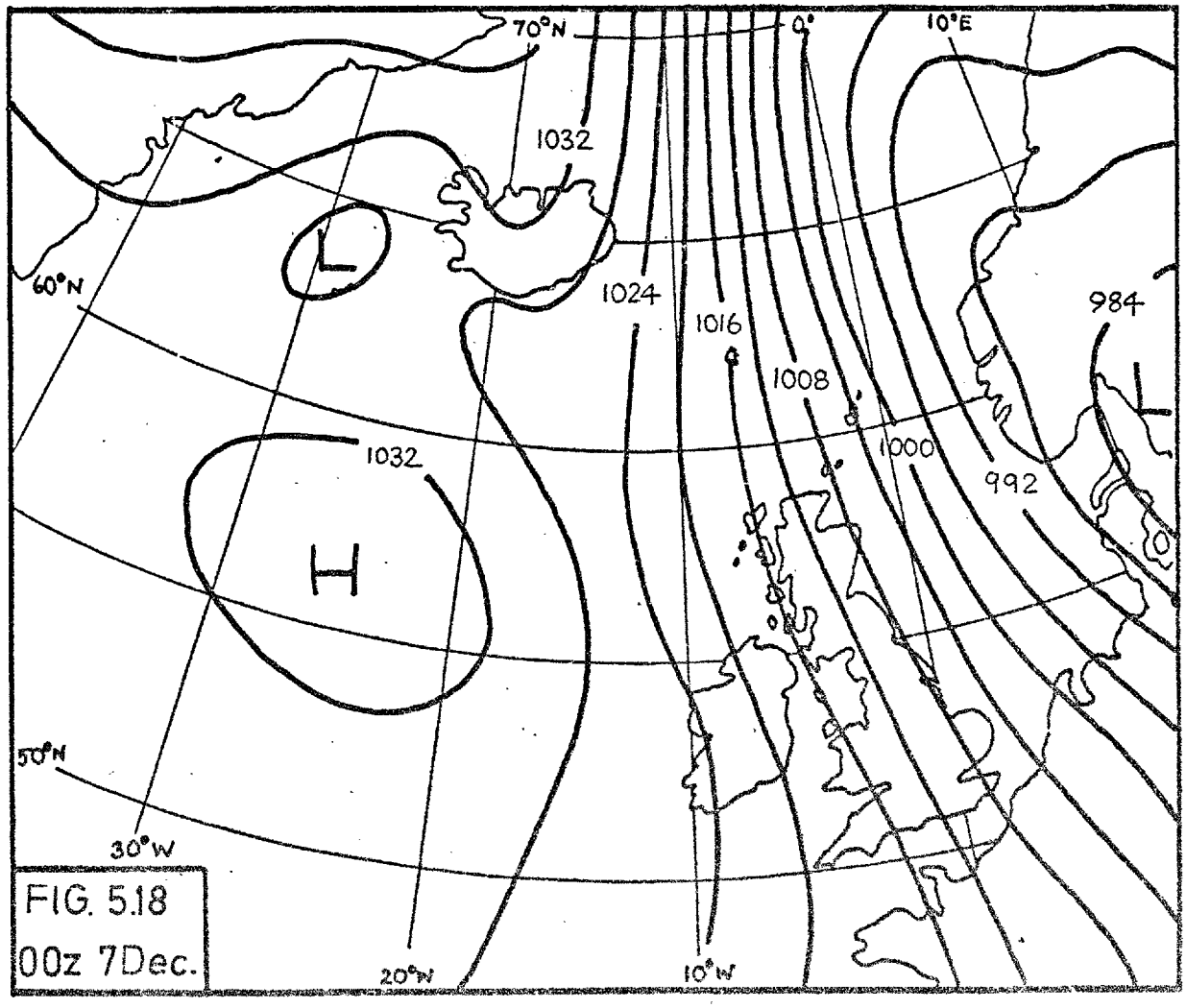


FIG. 5.18
00z 7Dec.

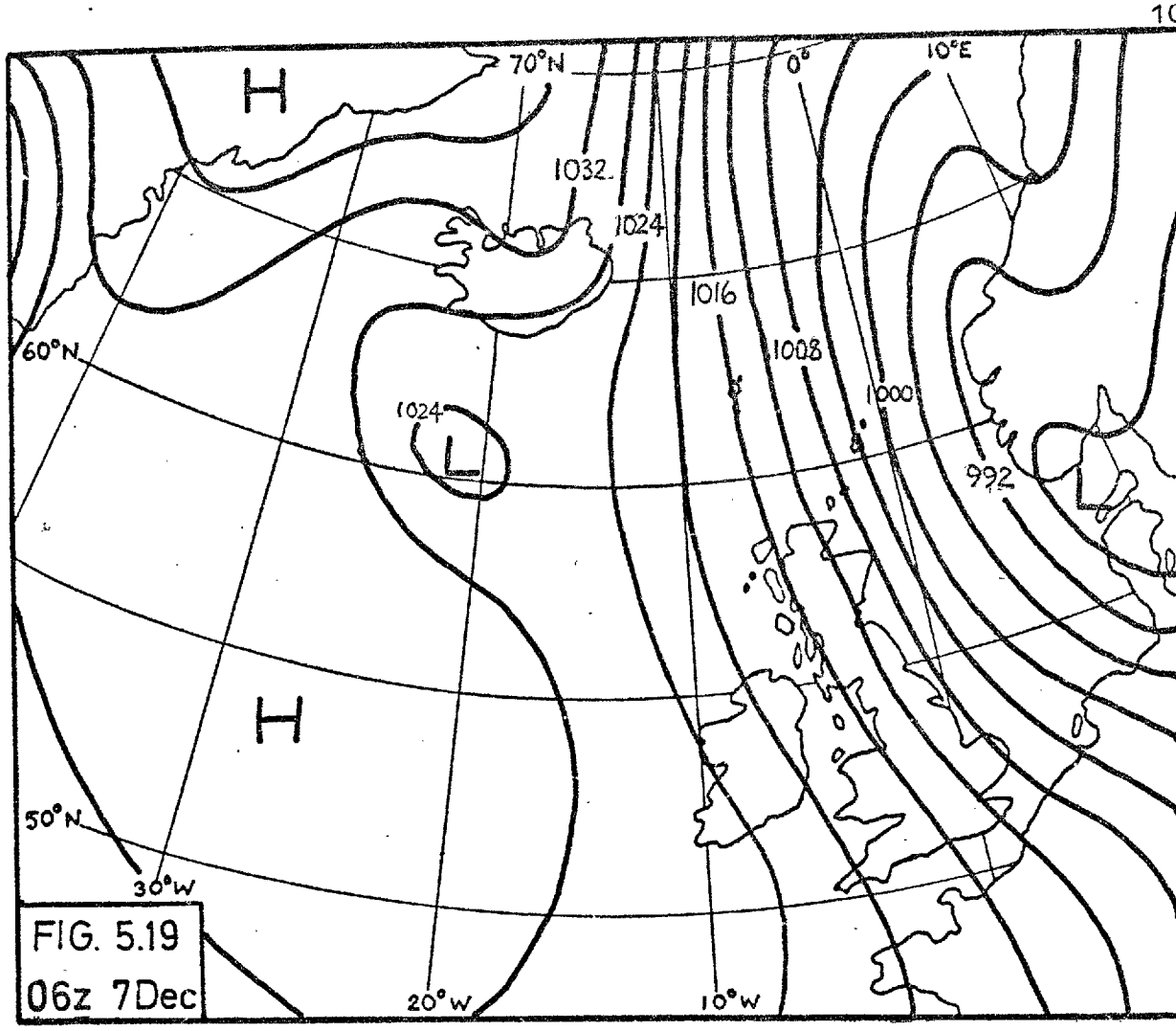


FIG. 5.19
06z 7Dec

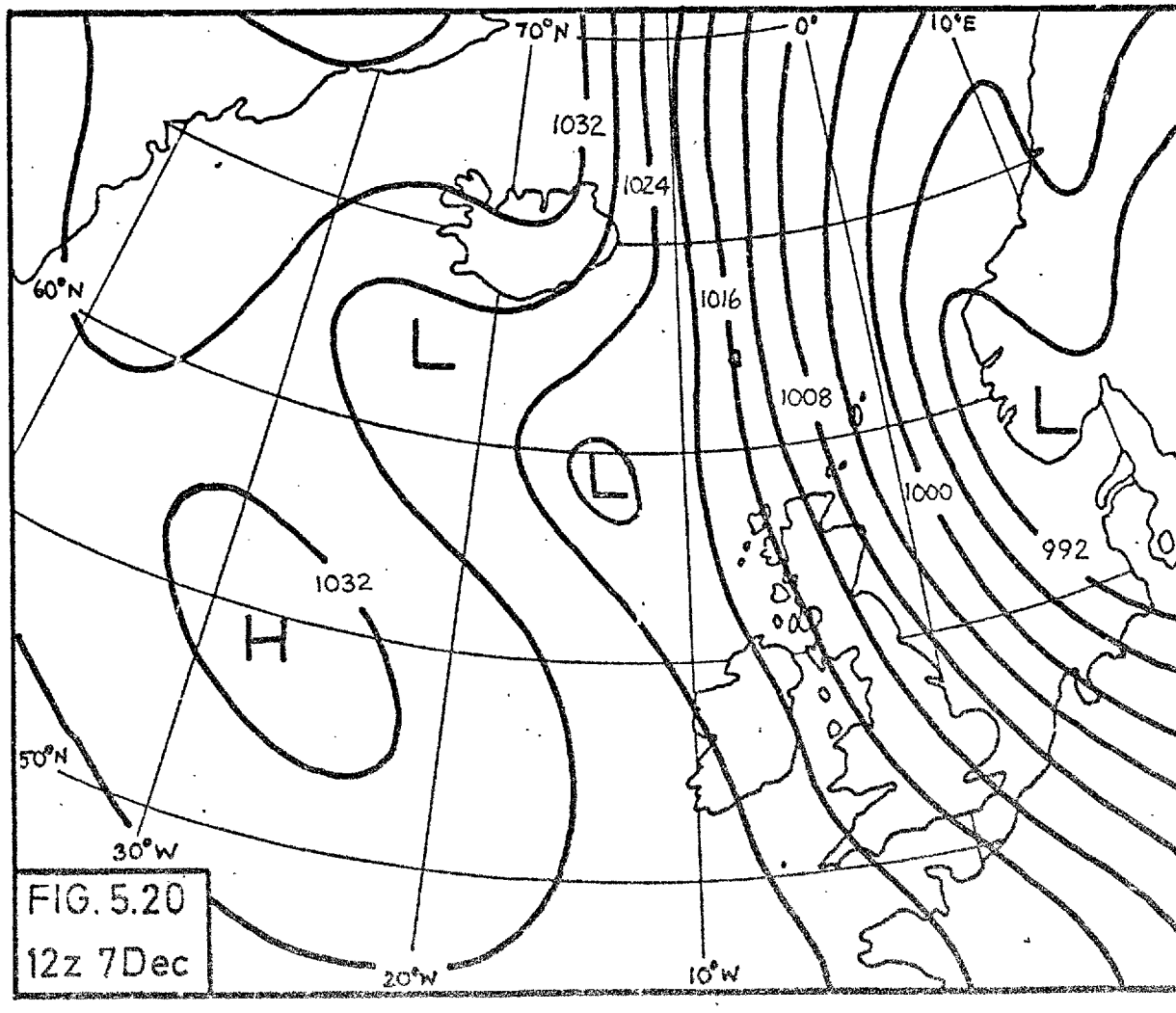


FIG. 5.20
12z 7Dec

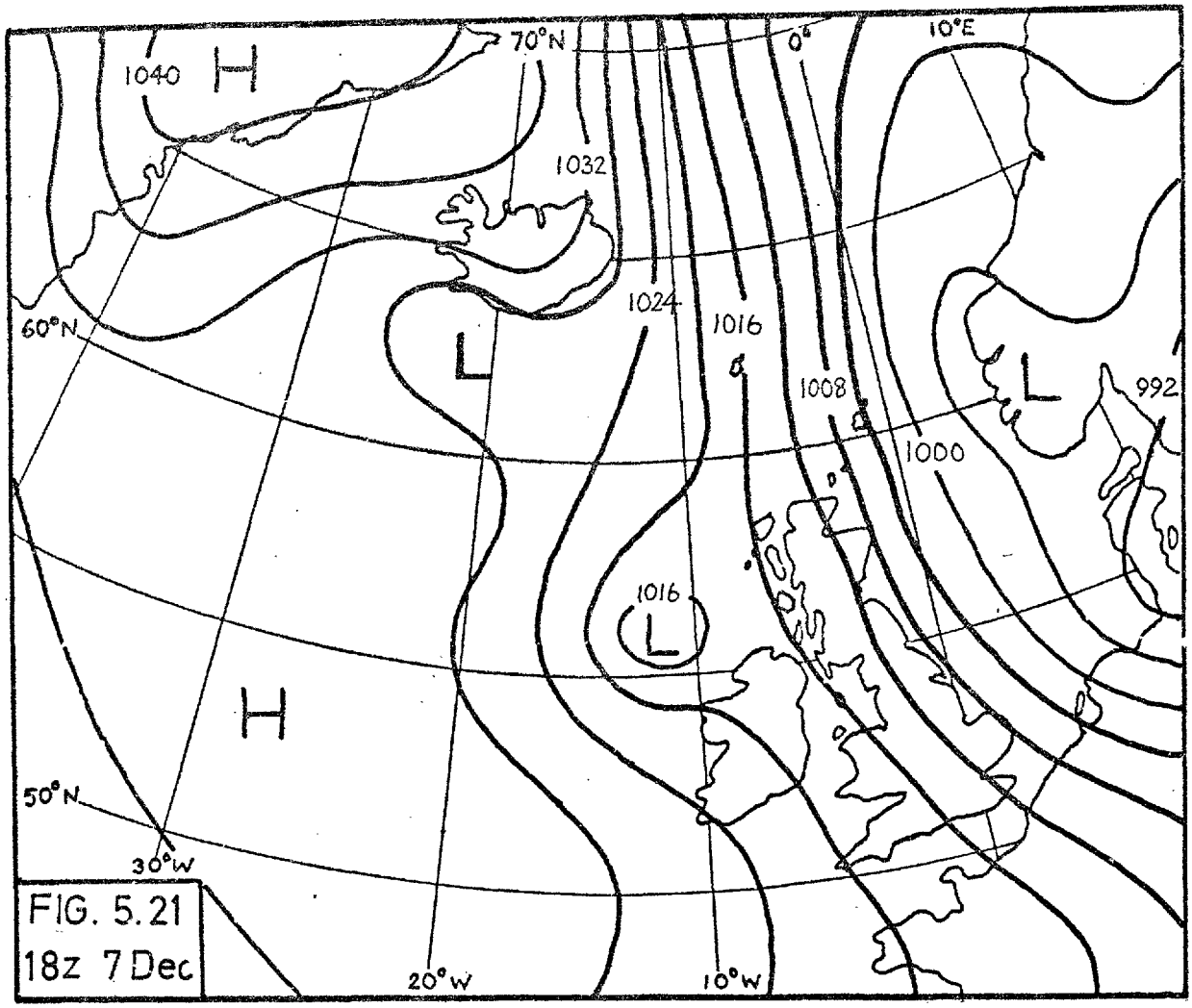


FIG. 5.21
18z 7 Dec

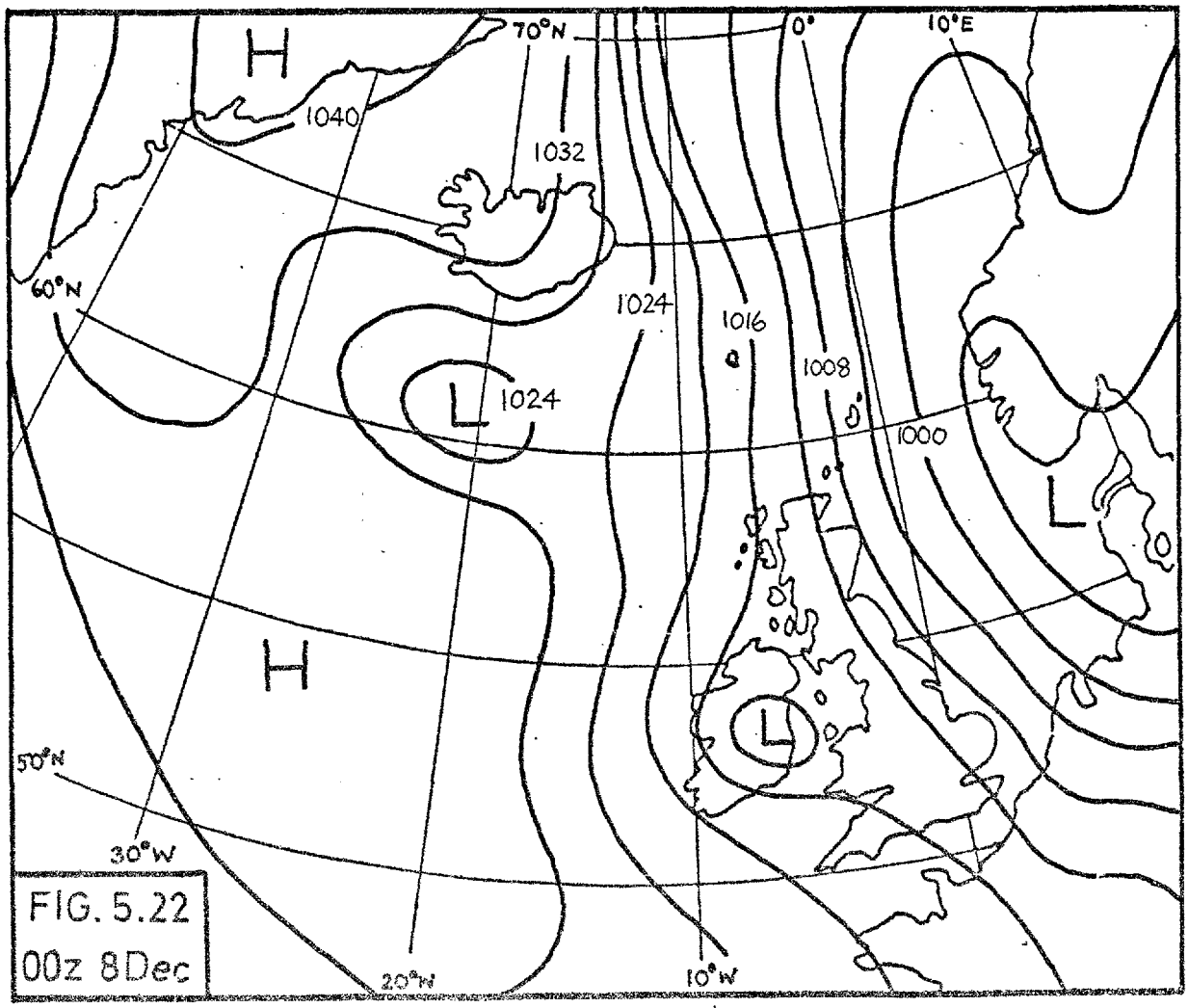


FIG. 5.22
00z 8 Dec

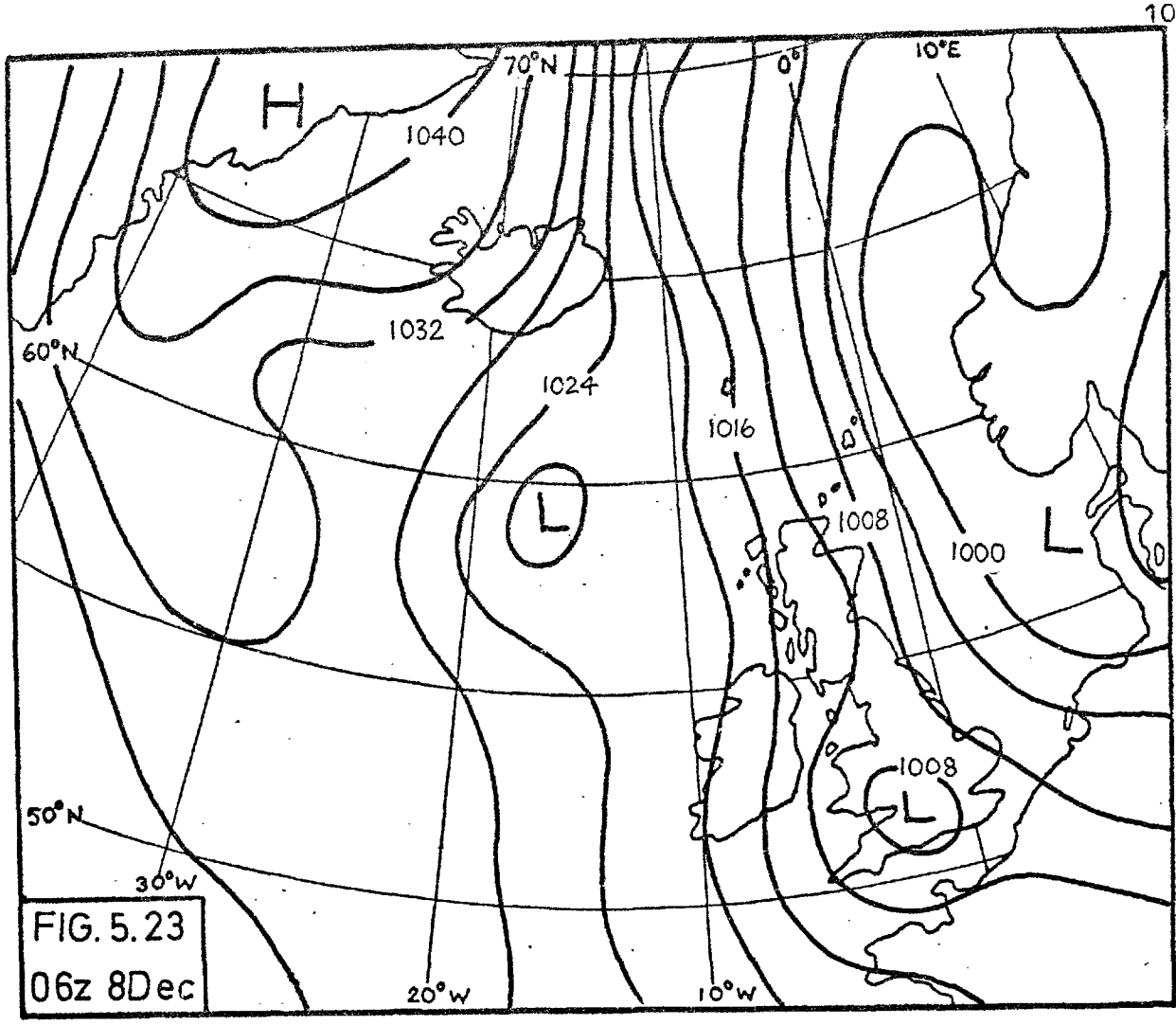


FIG. 5.23
06z 8Dec

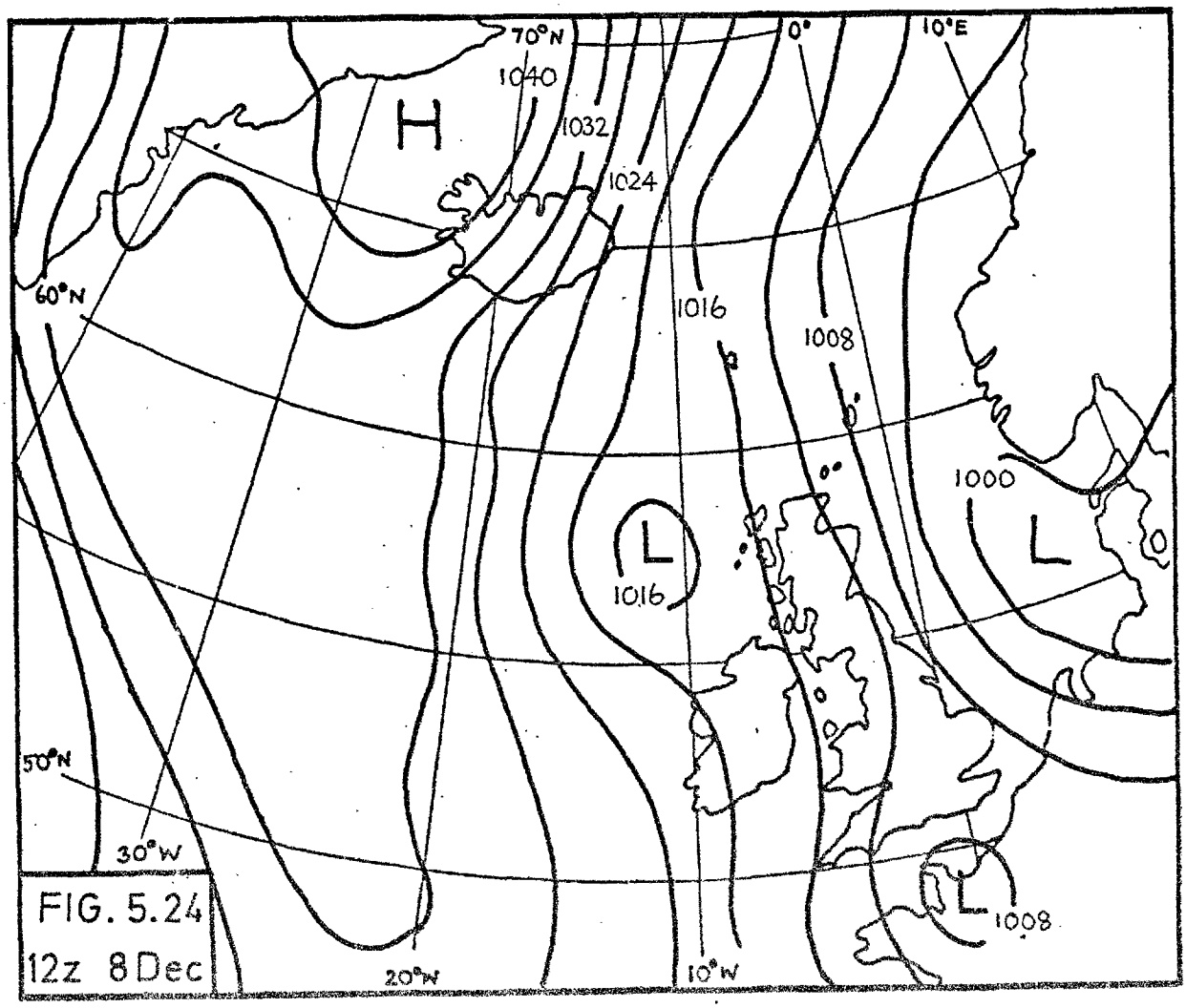


FIG. 5.24
12z 8Dec

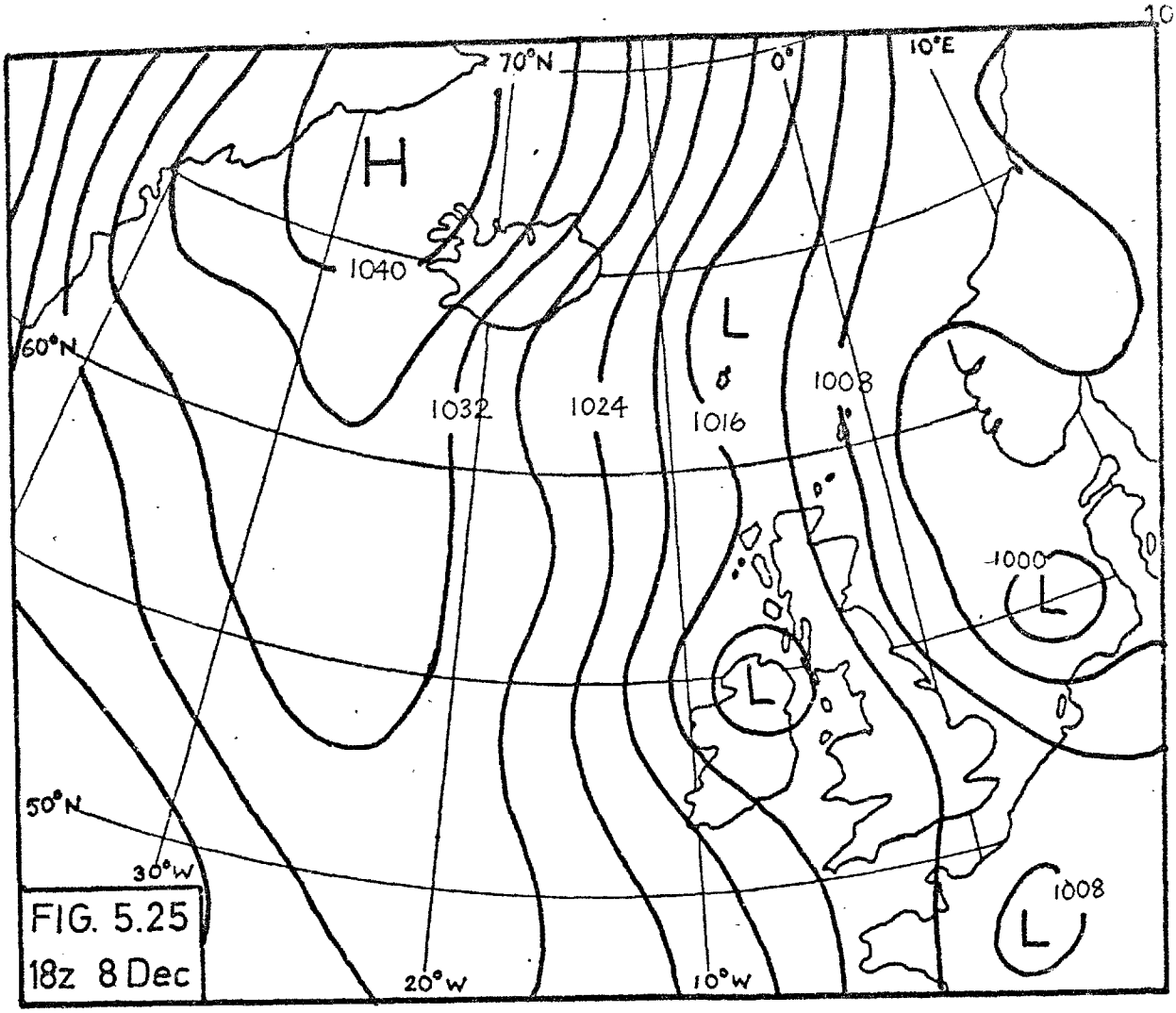


FIG. 5.25
18z 8 Dec

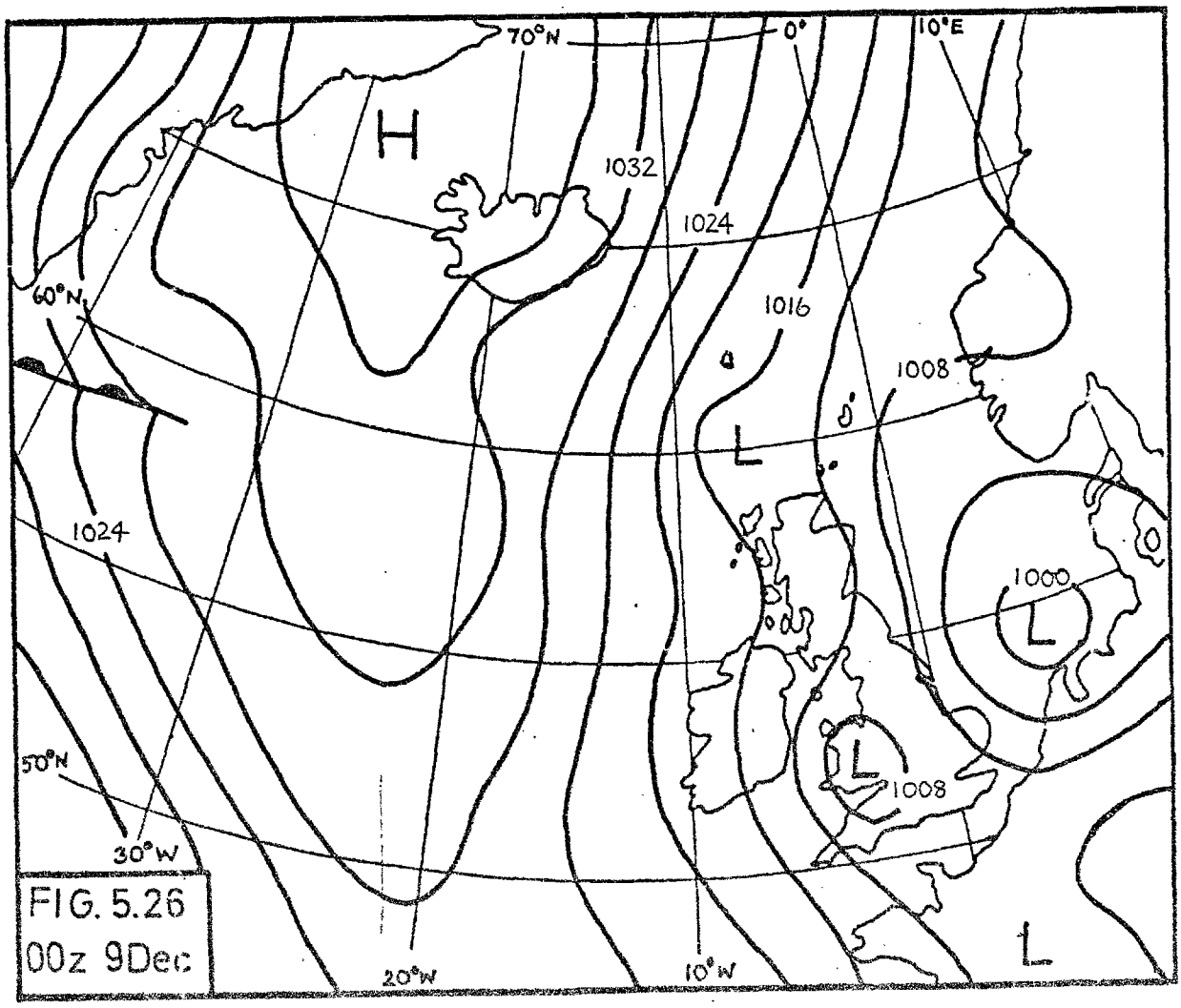


FIG. 5.26
00z 9Dec

References

Ball, F.K. 1960 'Control of inversion height by surface heating', Quart.J.R.Met.Soc., 86, pp.483-494.

Brunt, D. 1944 'Physical and dynamical meteorology', Cambridge University Press.

Burke, C.J. 1945 'Transformation of polar continental air to polar maritime air', J.Met., 2, pp.94-112.

Charney, J.G. and Eliassen, A. 1949 'A numerical method for predicting the perturbations of the middle latitude westerlies', Tellus, 1, No.2, pp.39-54.

Eady, E.T. 1949 'Long waves and cyclone waves', Tellus, 1, No.3, pp.33-52.

George, D.J. 1972 'The snowstorms of 4 March 1970', Weather, 27, pp.96-110.

Goldstein, S. 1938 'Modern developments in fluid dynamics', Vol.2, pp.563-565, Clarendon Press, Oxford.

Green, J.S.A. 1960 'A problem in baroclinic stability', Quart.J.R.Met.Soc., 86, pp.237-251.

Haltiner, G.J. and Caverly, D.E. 1965 'The influence of friction on the growth and structure of baroclinic waves', Quart.J.R.Met.Soc., 91, pp.209-214.

Harley, D.G. 1960 'Frontal contour analysis of a "polar" low', Met.Mag., 89, pp.146-147.

Harrold, T.W. and Browning, K.A. 1969 'The polar low as a baroclinic disturbance', Quart.J.R.Met.Soc., 95, pp.710-723.

Harwood, R.S. 1969 'Vorticity patterns in extra-tropical cyclones', Ph.D. Thesis, London University.

Holopainen, E.O. 1961 'On the effect of friction in baroclinic waves', Tellus, 13, pp.363-367.

Miller, M.J. 1968 'Arctic outbreaks: heat transport and polar lows', M.Sc. Dissertation, London University.

Nitta, T. 1964 'On the development of the relatively small scale cyclone due to the release of latent heat by condensation', J.Met.Soc.Japan, 42, pp.260-267.

Rayleigh, J.W.S.	1945	'The theory of sound', Vol.2, pp.392-394, Dover Publications, New York.
Sheppard, P.A.	1958	'Transfer across the earth's surface and through the air above', Quart.J.R.Met.Soc., 84, pp.205-224.
Stevenson, C.M.	1968	'The snowfalls of early December 1967', Weather, 23, pp.156-162.
Suttie, T.K.	1970	'Portrait of a polar low', Weather, 25, pp.504-506.

Acknowledgements

The author wishes to thank Dr. J.S.A. Green for his advice and encouragement throughout and Miss Marion Street for typing the thesis.

The work was supported by a N.E.R.C. grant.